Universidad de Concepción

Facultad de Ciencias Físicas y Matemáticas

KuPol Spectropolarimeter Calibration

Calibración Espectropolarímetro KuPol

por **Alexandra Andrea Suárez Espinosa**

Tesis presentada a la Facultad de Ciencias Físicas y Matemáticas
de la Universidad de Concepción para optar al grado de
Magíster en Ciencias con mención en Física

Profesor Guía: Rodrigo Reeves Díaz
Profesores comisión: Neil Nagar y Rafael Rodríguez

Concepción, Chile
Abril de 2019

KuPol Spectropolarimeter Calibration
Calibración Espectropolarímetro KuPol

A Víctor y Sandra, por su amor infinito.
A Felipe, por siempre creer en mi.

Agradecimientos

Cuando tomamos un nuevo desafío, muchas veces no dimensionamos lo grandes o complicados que pueden llegar a tornarse, y además, desconocemos lo trascendentales que pueden llegar a ser en nuestras vidas.
Sin duda agradezco a mi familia por su amor infinito, apoyo incondicional, llamadas constantes, innecesarias preocupaciones y fructíferas discusiones. Sin ustedes, nada de lo que soy, tengo y puedo entregar, sería posible.
A dos grandes equipos que fueron un pilar fundamental en el transcurso de este Magíster. Equipo de profesionales de CePIA, gracias por sus discusiones, risas, atenciones, abrazos, conversaciones y ánimos. Sin dudas ustedes hicieron este trabajo más sabroso. Equipo Aster Kimün, grandes mujeres con las que nos arriesgamos a tomar un gran desafío y con las que sin duda, seguiremos creciendo día a día.
También agradezco a mis numerosos y amados amigos. Franki, Juanca, Kudai, Trapo, Seba, Maka, Feña, Katty Vejar, Liszy, Yaris, Flaco, Yessy, Panchito, Anita, Caqui, Naty, Katty Cortés, Nico, Poti, Cata, Bodoque, Alonso, Dani, Phillipe, Pelao, Caddy y Jeanette. Muchísimas gracias por tanto amor, reflexiones, cuidados, apoyo, risas y lindos momentos.
A María Soledad, por mostrarme a la gran mujer que soy y que puedo llegar a ser.
A mis profesores. Ricardo Bustos por su disposición a seguir trabajando juntos. A mi tutor Rodrigo Reeves por las infinitas horas de análisis, preocupaciones, oportunidades, confianza y conversaciones. Gracias por abrir mis ojos, motivarme con los alcances de la instrumentación y el impacto que puede tener la ciencia en la sociedad.
A la Universidad de Concepción por otorgarme una beca para costear parte de mi Magíster.
A Dios y mi China. Gracias por presentarme caminos en los que dejé de intentar hacer mágica la realidad y comencé a hacer real la magia.

Contents

List of Figures

Resumen

Los blazars son un tipo de AGN que corresponden a fuentes de energía altamente variables y compactas, que se caracterizan por la emisión de un chorro que apunta en la dirección de la línea de visión del observador. La emisión de estos chorros se considera uno de los fenómenos más violentos del Universo y es de gran interés para la astronomía extragaláctica. Si bien su estudio es reciente en comparación con otras áreas de investigación, se puede ver un gran progreso dentro de este tema, pero aun así, no existe una claridad y comprensión total sobre los procesos y fenómenos que tienen lugar en ellos y en su entorno, como por ejemplo, la presencia y comportamiento de su campo magnético. Por esta razón, se han desarrollado nuevas tecnologías dentro de varios programas de observación que apuntan al estudio de estos interesantes fenómenos. Un ejemplo de esto, es el programa de monitoreo del telescopio de 40m del Radio Observatorio de Owens Valley (OVRO, según su sigla en inglés), perteneciente al Instituto Tecnológico de California (Caltech), ubicado en Big Pine, California, USA, y que monitorea aproximadamente 1,800 blazars, dos veces por semana.
En esta tesis, se propone un modelo matemático para la calibración en polarización del receptor del telescopio de 40m de OVRO, KuPol. Basándose en cálculo de matrices de transmisión, es posible obtener relaciones que facilitan la descripción y estudio del comportamiento del instrumento, lo cual aporta a la realización de diagnósticos instrumentales a partir del modelo.

Abstract

Blazars are a type of AGN that correspond to highly variable and compact energy sources, which are characterized by the emission of a jet that points to the line of sight of the observer. The emission of these jets is considered one of the most violent phenomena in the Universe and is of great interest for extragalactic astronomy. While its study is recent compared to other areas of research, great progress can be seen in this topic, but even so, there is no clarity and full understanding of the processes and phenomena that take place in them and their environment, for example, the presence and behavior of its magnetic field. For this reason, new technologies have been developed within several observation programs that aim to study these interesting phenomena. An example of this is the monitoring program of the 40m telescope Owens Valley Radio Observatory (OVRO), belonging to California Institute of Technology (Caltech), located in Big Pine, California, USA, and It monitors approximately 1,800 blazars, twice a week.
In this thesis, a mathematical model is proposed for the polarization calibration of the 40m telescope OVRO receiver, KuPol. Based on transmission matrices calculation, it is possible to obtain relations that facilitate the description and study of the instrument behavior, which contributes to the instrumental diagnosis from the model.

Chapter 1

Introduction

Astronomy offers a unique instance for the development of great and varied technology. In particular, blazar offers us an opportunity to study in depth the magnetic fields of the jets that these sources eject. For this purpose, the observation of polarization in astrophysical objects, allows us to measure magnetic fields in their environment or to learn about the physical conditions in the regions where light is scattered into our line of sight. Thus, the development of instruments associated with the study of polarization becomes relevant, and in particular for this thesis, the polarization calibration of an unique spectropolarimeter, such as KuPol.

1.1 Active Galaxy Nuclei

Active galactic nuclei (AGN) house some of the most powerful particle accelerators in the universe. This sources have a strongly non-isotropic radiative output, with a pair of relativistic jets emanating at opposite directions from the central engine [2]. These objects are believed to consist of a supermassive black hole (SMBH) at the center of a galaxy, as shown in figure 1.1. The SMBH supports a complex structure that in some cases can outshine the combined emission of all the stars in the galactic host. A great variety of AGN exist, a small fraction of which are bright radio sources [15].

1.1.1 Blazar

When the observer's line of sight happens to be aligned with the outflow direction, this type of AGN is called blazar [19].

Blazars are broadband sources, emitting brightly over the entire electromagnetic spectrum [9]. Many are bright gamma-ray emitters, with emission extending in some cases to the TeV regime [14]. Furthermore, these sources are strongly variable in all bands, with significant variation

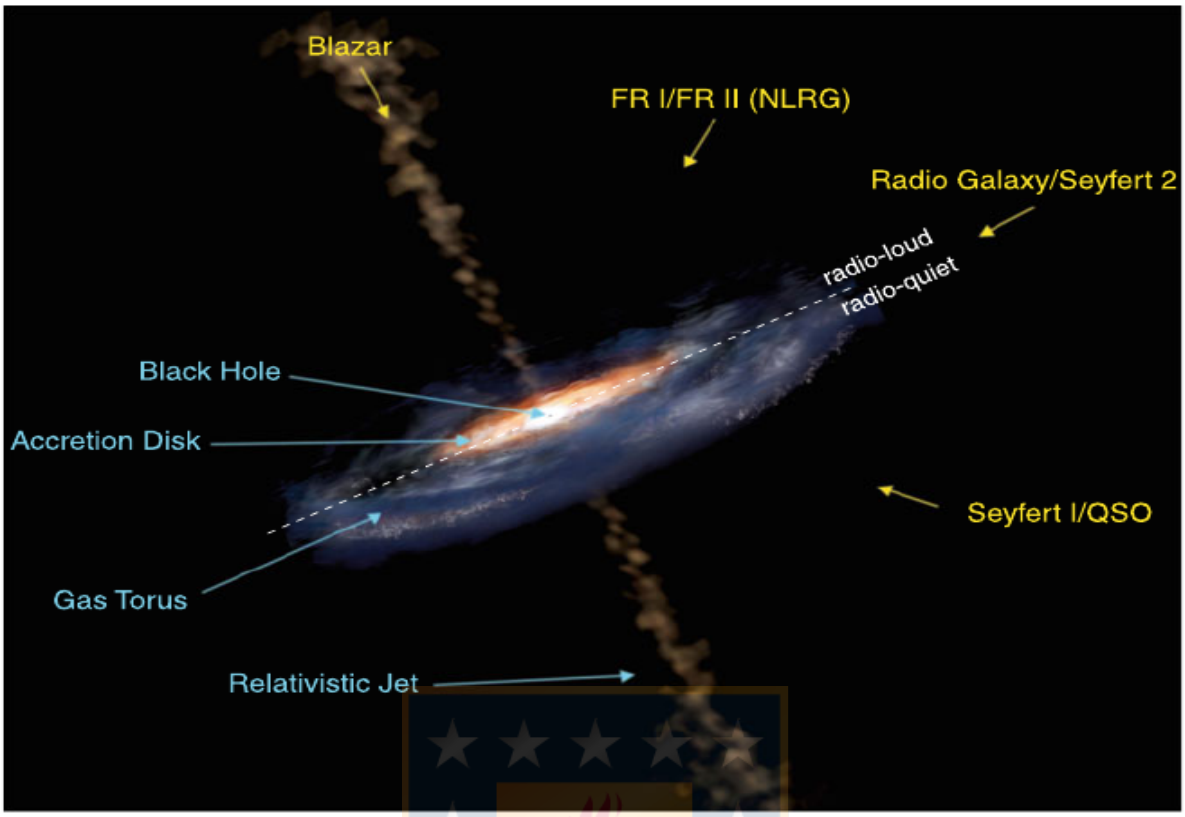

Figure 1.1: Illustration of the viewing angle dependent standard model of AGN. Source: Image produced by Aurore Simonnet, Sonoma State University [4].

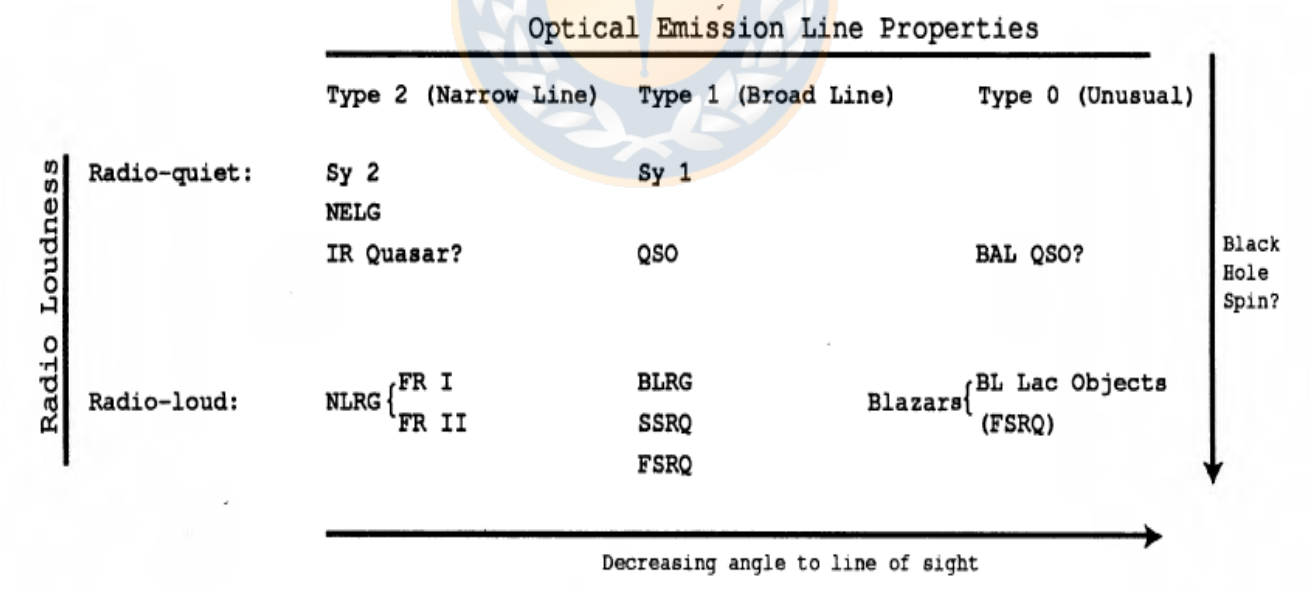

Figure 1.2: AGN taxonomy. Source: Urry & Padovani [19].

on timescales ranging from many years down to a few minutes in some bands [1]. Blazars are some of the most significant sources of extragalactic high-energy emission.

Blazars are widely understood to be the beamed counterparts to the radio galaxies. Unfortunately, AGN taxonomy is complicated by rather frequent changes in terminology, in some cases

to reconcile conventions from different branches of astronomy, and in some reflecting a shift in the physical understanding of the sources. The original definition of the blazar class was rather informal, so there is some variation in use of the term. This is showed in the figure 1.2.

1.1.1.1 Relevance of the polarization study in blazars

Magnetic fields play a critical role in various aspects of the physics of relativistic jets. Dominance of magnetic over rest-mass energy at the base of a jet is required in order to accelerate plasmas almost to the speed of light, the natural velocity of dynamic electromagnetic phenomena. For this reason, the characterization of jet polarization properties provides a powerful diagnostic of jet physics, particularly with respect to magnetic field configuration and particle acceleration. Extragalactic jets generally emit a continuum of radiation from radio through optical, and often into the X-ray regime. Through matched resolution comparisons of flux density measurements at various frequencies, we can glean morphological information about particle acceleration regions and jet energetic structure [12].

1.1.2 Origin of astronomical polarization

Polarization not only arise from propagation, the emission can be intrinsically polarized such as synchrotron. In general, polarization is created or modified, wherever the cylindrical symmetry of the propagating light is broken. This breaking of the symmetry can be due to the change of direction of the light itself or due to the presence of unidirectional magnetic (or electric) fields. The following physical processes are all known to produce and/or modify polarization [16]:

- Anisotropic scattering or reflection of continuum radiation. For instance Rayleigh scattering in the Earth's (or another planet's).
- Anisotropy of line radiation. Here, the emergent polarization depends largely on the quantum numbers of the transition.
- Differential absortion or scattering by magnetically aligned non-spherical dust grains. This creates continuum polarization particularly in the infrered (IR) range and beyond.
- Synchrotron radiation from charged particles in a magnetic field exhibits continuum polarization.
- Magnetic fields also produce line polarization through the Zeeman effect. This line polarization may be modified by magneto-optical effects (i.e. birefringence of the medium due to the magnetic field; the Faraday effect and the Voigt effect).
- Electric fields can produce a similar line polarization (the Stark effect).

- Magnetic fields also modify and despolarize line polarization due to scattering through the Hanle effect.

- Line polarization can also be created when the light is absorbed in a plasma in which atoms are aligned by optical pumping ([11], [10]), or oriented by a magnetic field.

1.2 OVRO and 40m telescope

The Owens Valley Radio Observatory (OVRO) is one of the largest radio observatories in the world operated by universities. It is located near Bishop, California, approximately 400 kilometers north of Los Angeles, USA.
The OVRO telescopes carry out experiments in the field of monitoring of transient star flares, interstellar medium, cosmic microwave background and Blazars jet physics. In this last field, the OVRO 40 meter telescope works. With the aim of doing research, in 2014 a new polarimetric receiver, called KuPol, was installed in the 40m telescope, replacing the previous receiver (Ku-Band). This increased the sensitivity of the telescope and its bandwidth, in addition to allowing polarimetric observations.
Currently the 40m telescope is monitoring flux densities at 15 [GHz] of approximately 1800 blazars twice a week. These measurements are quite interesting, because by correlations in their variability with the measurements of the *Fermi* gamma-ray telescope, it is possible to explain the emission mechanisms in the jets that emerge from these AGNs [20]. The majority of our sources are reasonably bright—more than 50 mJy at 15 GHz so the sensitivity requirements of the program are relatively modest. This has allowed us to optimize for rapid observations and easily repeatable measurements rather than scrabbling for sensitivity at all costs. Still, a full understanding of the behavior of the telescope and receiver and careful measurement and calibration are essential.

1.2.1 40m telescope receiver: KuPol spectropolarimeter

The KuPol instrument is a dual-beam receiver for the 40 m telescope at OVRO. It is, in fact, a hybrid of two separate instruments called the analog and the digital instrument [7].

- **Analog instrument:** The analog instrument is a dual-polarization, beam-differencing radiometer that is designed to produce identical data to the previous Ku-band instrument that KuPol replaces. The purpose of this instrument is to maintain the total intensity data from Ku band receiver.

- **Digital instrument:** The digital instrument is digital spectropolarimeter covering the 13 to 18 GHz band with ~ 8 MHz resolution. The purpose of this instrument is to deliver the Stokes parameters from horns Ant and Ref.

An idea of the KuPol architecture and its general operation is shown in the figure 1.3.

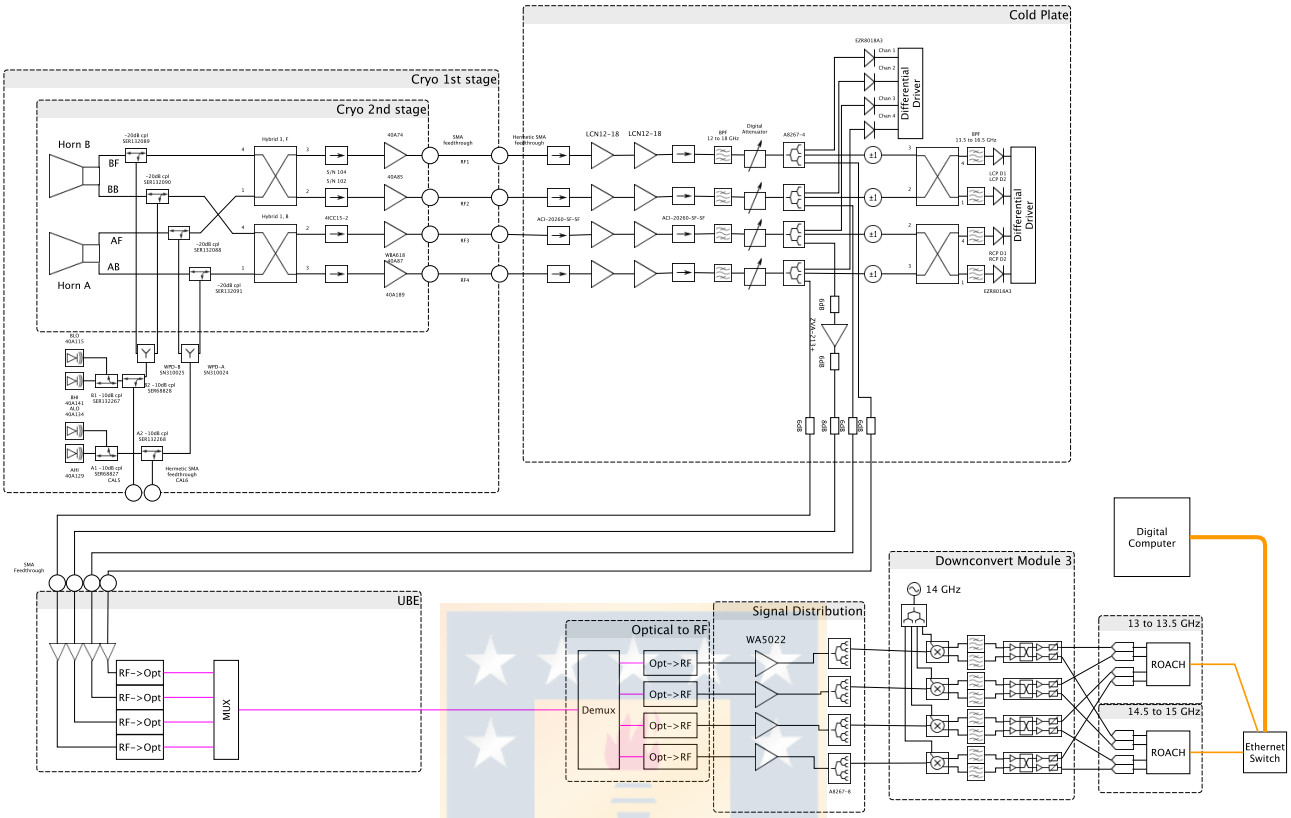

Figure 1.3: System signal diagram, showing only some of the digital hardware. The blocks named as Cryo stages, Cold Plate, UBE, optical to RF, signal distribution, and downconverter represent the analog instrument. The block named as roach represents the digital instrument. Source: KuPol Manual [7].

1.2.1.1 Analog instrument

The RF electronics in the cryostat consists of two circular horns, followed by circular to square waveguide transitions, 90° waveguide phase shifters, and quad-ridge OMTs. These produce circular polarization signals. We then couple noise diode signals into the signal paths using cryogenic directional couplers. These signals are then combined in 180° hybrids to produce sum and difference voltages mixing signals with the same polarization (LCP or RCP). These signals are amplified before exiting the cryostat.

The cold plate houses the remaining RF electronics for the analog receiver, and splits the signal path to send RF1 through RF4 to the RF/optical system. The signals from the cryostat are filtered, amplified, controlled by digital step attenuators, and then split. One part of the split sends the signals to the RF/optical system for the digital instrument, while the other part goes to the remaining part of the analog instrument. There are also some detector diodes at this point in the system to monitor the RF power level in each signal chain.

The remaining part of the analog instrument consists of phase switches, followed by 180°. At the output of the 180° hybrids we have separated the horn polarizations Ant_{RCP}, Ant_{LCP}, Ref_{RCP}, and Ref_{LCP}. These are then filtered by 13.5 to 17 GHz bandpass filters before being sensed by detector diodes. The outputs of the detector diodes are passed to differential driver circuits mounted on the underside of the cold plate.

The third section of the receiver at the prime focus the UBE box. The contents are: UBE frame, RF/optical transmitters, RF amplification, optical mux, USB to serial, USB over fiber hub, power supplies for the above, and 12-fiber optical fiber bundle.

1.2.1.2 Digital instrument

The KuPol digital instrument processes the band between 13 and 18 GHz in 500 MHz wide chunks. The digital stages are:

1. Signal distribution: The four RF channels were converted to optical and multiplexed onto a single optical fiber at the prime focus. The signal distribution crate contains the demultiplexing box, followed by the optical to RF converters. The RF signals cover 13 to 18 GHz, and are amplified and then split 8 ways for distribution.

2. Downconversion: The receiver has 6 downconverter trays. Each tray produces two 500 MHz wide IF bands (the lower sideband and the upper sideband) for each RF input. Each downconverter tray contains four identical sets of downconversion hardware, driven by a common LO signal. This LO signal is generated by a crystal oscillator, amplified to ensure a high enough LO level, then split 4-ways. The downconversion hardware consists of an IQ-mixer, then a sideband-separating board (called a scm), and then a 500 to 1000 MHz IF bandpass filter.

3. Digitization and processing: The four LSB (or USB) outputs from a downconverter tray are connected to a digital processing board. We use ROACH boards from the CASPER collaboration. This digitizes the four IF data streams, and processes them.

4. Data readout and archiving: The control system running on kupolcontrol acquires the data from each ROACH board, timestamps it, and stores it in an archive. In particular, the four channels are passed through a polyphase filter bank (PFB) and then FFT'ed. The PFB/FFT combination improves the spectral response of the instrument. The spectral response of several adjacent frequency bins for a model with 32 total bins. After the FFT step we apply a complex correction independently to each frequency bin. The purpose of this correction is to equalize the path lengths and gains of the four IF channels, so that the sums and differences of the IF data streams will recover the individual antenna polarizations. The coefficients are loaded by the control system from disk. Once the individual antenna polarizations have been recovered, they are passed through a correlation

block to calculate the power in each polarization for each horn, and the Stokes Q and U polarizations of both horns. These data are then passed to an accumulator block. This accumulates a specified number of samples, then writes them to disk [1]. All this process is showed in the figure 1.4.

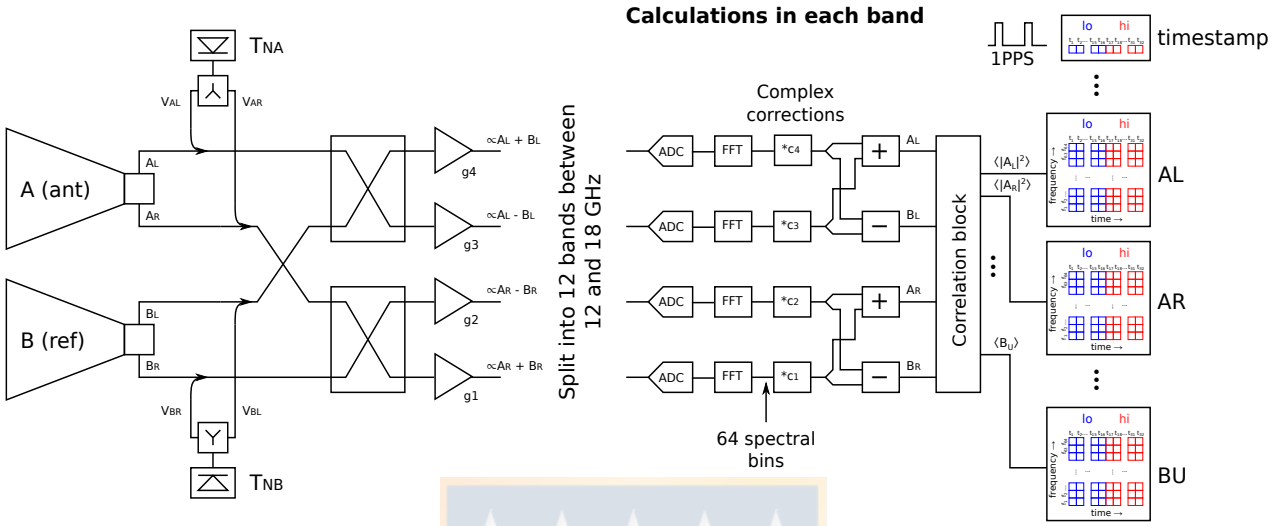

Figure 1.4: Part of analog and digital operation overview.

In the right side, you can see the operation of *data readout and archiving* presented in point 4 of the previous section. Note that the instrument has 12 bands in a bandwidth 12 to 18 GHz. We must mention, that the design and construction of the KuPol instrument includes these characteristics, but due to the high levels of RFI present in OVRO, it was decided to eliminate the first two bands of the instrument, and limit its operation to 13 and 18 GHz. Source: KuPol Manual [7].

1.2.1.3 Instrumental error models for KuPol receiver

Currently the polarization calibration of KuPol receiver is not finished. Within the 40m telescope collaboration there is a proposed method for instrumental calibration and that to date has few results. A general idea of this method, is presented below.

Important coments of the method.

The actual instrumental calibration method for the KuPol receiver is based on Mueller matrix calculus (see the next secctions). From this is possible to describe how the instrument affects the astronomical signal.

The measured Stokes vector in terms of the instrumental Mueller matrix can be expressed by

$$e^{A_{L,R}} = M_{C_{L,R}} M_A M_{par} e^S \tag{1.1}$$

$$e^{B_{L,R}} = M_{C_{L,R}} M_B M_{par} e^S \tag{1.2}$$

[1] To understand in depth the digital model process developed in this stage, it is recommended to see appendix B.

where M_{par} is the Mueller matrix for parallactic angle rotation due to the el/az mount of the 40m telescope, M_A is the Mueller matrix for horn Ant, M_B is the Mueller matrix for horn Ref, and $M_{C_{L,R}}$ is the Mueller matrix that describes the action of the correlation receiver.
Note that M_A and M_B describe the effect of imperfections in the horns, and are in principle different for two horns.

In particular, for the instrument calibration and to contrast this with our model, we are interested in the $M_{C_{L,R}}$ characterization. A deep description of calculus is presented in Appendix D of this thesis, where the method to obtain the *instrument-corrected data streams for horns Ant and Ref* is presented.

For other hand, the Stokes vectors from the KuPoL data channels, for horn Ant and Ref are respectively

$$e^{A_{L,R}} = \begin{bmatrix} A_{L,R} \\ A_Q \\ A_U \\ 0 \end{bmatrix} \tag{1.3}$$

$$e^{B_{L,R}} = \begin{bmatrix} B_{L,R} \\ B_Q \\ B_U \\ 0 \end{bmatrix} \tag{1.4}$$

Here, we treat the intensities recorded in LCP and RCP separately because they are produced by different gain chains, and we have considered that the gain for signals LCP and RCP is the same for horn Ant and Ref.

1.3 Polarization

In general terms, the polarization is a process or state in which rays of light exhibit different properties in different directions, especially the state in which all the vibration takes place in one plane. Several formalism exist to describe polarization, the application of which depending on the polarimetric principle.

1.3.1 A mathematical formulation of polarization

In his remarkable article of 1852 entitled *On the composition and resolution of streams of polarized light from different sources*, George Gabriel Stokes, established an ideal mathematical formalism to describe the state of polarization of any beam of light. In addition, he demonstrated several of the most important properties of polarized light, among which he noted the following:

When any number of independent polarized streams, of given refrangibility, are mixed together, the nature of the mixture is completely determined by the values of four constants, which are certain functions of the intensities of the streams, and of the azimuths and eccentricities of the ellipses by which they are respectively characterized; so that any two groups of polarized streams which furnish the same values for each of these four constants are optically equivalent.
Those four constants that Stokes refers are the *Stokes parameters*. Unfortunately, the usefulness of formalism and the importance of Stokes theorems seem to have been ignored by the scientific community for the next 80 years. In 1929, in a very complete study of the partial polarization of light, the physicist Paul Soleillet described the Stokes parameters and used them everywhere. Interestingly, in the third part of this same article, it is presented a formulation of an anisotropic absorption theory that is nothing else than the construction of a transfer equation for polarized radiation. Unfortunately, this document is still quite unknown by the astrophysical community. Eighteen years later, in 1947, in his famous series of documents on the radiative balance of stellar atmospheres, where Soleillet's work is unknown, the american astrophysicist Subrahmanyan Chandrasekhar, published a summary of Stokes results, emphasizing the importance and the usefulness of the formalism that proved to be especially suitable for the formulation of a radiative transfer equation in a stellar atmosphere.

A year later, in 1948, Hans Mueller, professor of physics at the Massachusetts Institute of Technology, devised a phenomenological approach to describe the transformation of Stokes parameters by means of 4x4 matrices (now known as *Mueller matrices*). Since then, Mueller's approach has been widely used to treat with partially polarized light. A precursor of this formalism can be found in an article by Francis Perrin (1942).

A few years before Mueller's work, between 1941 and 1947, the american physicist Robert Clark Jones presented his formalism to describe totally polarized light and the transformations between any two totally polarized light beams [3].

1.3.2 Theorical background

1.3.2.1 Polarization formalisms

1. **Stokes Parameters**

   The polarization state of a signal is usually described by the Stokes parameters I, Q, U, and V. In particular, I describes the total signal intensity, Q and U describe the linear polarization state, and V describes the circular polarization state.

   The Stokes parameters are a representation of the coherence vector, e (see appendix A.1) in an indeterminate space. Thus, the Stokes vector S, is obtained from the coherence

vector by

$$S = \begin{bmatrix} I \\ Q \\ U \\ V \end{bmatrix} = Te \tag{1.5}$$

where T is a coordinate transformation of the coherence vector to the indeterminate space of Stokes.

If we consider the orthogonal modes of the incident signal, $E_x(t)$ and $E_y(t)$, and if these are represented analytically as complex voltages, we have that for a lineal basis system, the Stokes parameters can be represented according to the modes $E_x(t)$ and $E_y(t)$, as

$$I =< |E_x(t)|^2 > + < |E_y(t)|^2 > \tag{1.6}$$

$$Q =< |E_x(t)|^2 > - < |E_y(t)|^2 > \tag{1.7}$$

$$U =< E_x(t)E_y^*(t) > + < E_x^*(t)E_l(t) >= 2 < Re(E_x(t)E_y^*(t)) > \tag{1.8}$$

$$V = -i[< E_x(t)E_y^*(t) > - < E_x^*(t)E_y(t) >] = 2 < Im(E_x(t)E_y^*(t)) > \tag{1.9}$$

For a orthogonal circular basis, where $\widehat{l} = \frac{1}{\sqrt{2}}(\widehat{x} - i\widehat{y})$ y $\widehat{r} = \frac{1}{\sqrt{2}}(\widehat{x} + i\widehat{y})$ [2], the Stokes parameters are

$$I =< |E_l(t)|^2 > + < |E_r(t)|^2 > \tag{1.10}$$

$$Q =< E_l(t)E_r^*(t) > + < E_l^*(t)E_r(t) >= 2 < Re(E_l(t)E_r^*(t)) > \tag{1.11}$$

$$U = -i[< E_l(t)E_r^*(t) > - < E_l^*(t)E_r(t) >] = -2 < Im(E_l(t)E_r^*(t)) > \tag{1.12}$$

$$V =< |E_l(t)|^2 > - < |E_r(t)|^2 > \tag{1.13}$$

2. **Mueller matrix**

The four Stokes parameters denote the flow of radiant energy in specific vibrations of the electromagnetic field, and all four are expressed in the same units. We write them collectively as a column array of four elements, which is generally known as Stokes vector, where its elements are not all independent, so as a 4-vector it is somewhat limited. When convenient, the vector will be written as an array of rows, but use will always be prioritized as a column matrix.

When the radiation propagates through a certain "volume of space" (which may be empty or contain some medium of material), the polarization of the input and output radiation is represented by the input and output parameters of Stokes. Within the volume, the polarization state can be altered: in general, any elliptical polarization can be transformed

[2]For a better understand the basis change, see appendix A

into some other form of elliptical polarization, or the radiation can be polarized by the medium. This can be represented by a transformation between the input and output Stokes parameters, and in general the transformation is linear. When the input and output Stokes parameters are arranged as 4-vectors, the transformation becomes a M matrix of 4x4, called *Mueller matrix*, which is related to the Stokes parameters as

$$S_{out} = MS_{in} \tag{1.14}$$

where,

$$M = \begin{bmatrix} m_{11} & m_{12} & m_{13} & m_{14} \\ m_{21} & m_{22} & m_{23} & m_{24} \\ m_{31} & m_{32} & m_{33} & m_{34} \\ m_{41} & m_{42} & m_{43} & m_{44} \end{bmatrix} \tag{1.15}$$

Note that:

- M works as the transfer function between S_{out} and S_{in}.
- The matrix elements are just the partial derivatives, for example [6],

$$m_{V,Q} = \frac{\partial V_{out}}{\partial Q_{in}} \tag{1.16}$$

- Since the Stokes parameters are real quantities, the elements of M are all real numbers; $m_{i,j}$ must be positive (I is always positive) and the other elements can be positive or negative.

When the radiation travels through several successive media, the output Stokes vector for a media a is the input Stokes vector for the next media, b, that is,

$$S_{b,out} = M_b S_{b,in} = M_b S_{a,out} = M_b M_a S_{a,in} = MS_{a,in} \tag{1.17}$$

or

$$M = M_b Ma \tag{1.18}$$

where M represents the combined action of the two media a and b; this is the product of the matrix of M_b and M_a (note the order: the first medium traversed comes last in the equation of the matrix). This procedure is widely used in the design of optical instruments and in the representation of the polarized radiation transformations within a multiple or distributed astronomical source of polarized radiation (for example, a stellar or planetary atmosphere). In the radio wave domain, a similar but distinct development has occurred: 4x4 matrices of a slightly different type are used to describe the polarization response of a correlation-type interferometer [18] [5].

3. **Jones matrix**

   When the phase of a polarized signal relative to some other polarized signal is important, the Stokes parameters are no use; they deliberately ignore phase (except in a relative sense within each signal, as needed to specify the state of polarization). However, there are situations (such as when combining the beams of an interferometer) when phase does matter. Under such circumstances, we have to use *Jones vectors and matrices* [18].

   Jones's calculation can not handle partial polarization (mixed states of polarization). There are situations in which the phase is important but the polarization is partial. In such a case, the radiation must be formally separated into two (generally unequal) mutually incoherent polarized components (pure states) of orthogonal polarizations (ie, partial polarization in the input signal and its opposite), treating each separately by calculating Jones and obtaining the final result by incoherent formal recombination of the outputs.

   Note that the relationship between the Mueller and Jones matrices is that each Mueller matrix has its counterpart in Jones.

1.3.2.2 Scattering matrix

Consider an arbitrary network of N ports. The incident wave will be denoted to a port i by V_i^+, the wave reflected by V_i^- and the noise wave produced by the network to this port by c_i. These quantities are related by the Scatering matrix and noise wave vector c, as

$$\begin{bmatrix} V_1^- \\ V_2^- \\ \vdots \\ V_N^- \end{bmatrix} = \begin{bmatrix} S_{11} & S_{12} & \dots & S_{1N} \\ S_{21} & & & \vdots \\ \vdots & & & \\ S_{N1} & \dots & & S_{NN} \end{bmatrix} \begin{bmatrix} V_1^+ \\ V_2^+ \\ \vdots \\ V_N^+ \end{bmatrix} + \begin{bmatrix} c_1 \\ c_2 \\ \vdots \\ c_N \end{bmatrix} \tag{1.19}$$

The Scattering matrix is unitary if the device has no losses and the reciprocal of the network has symmetric Scattering matrices [13] [8].

In the formulation of the Scattering matrix, any component or network of components (excluding the detectors) can be described by a Scattering matrix dependent on the frequency S_ν. The scattering matrix relates the incident, reflected and transmitted waves that travel in transmission lines connected to the N ports of a linear network. This formulation can be extended to optical systems and used to describe instruments that contain optical components, such as lenses or mirrors, and microwave circuit techniques, such as horns, transmission lines, filters, etc. [8]

1.3.3 Polarization study: Polarimetry and spectropolarimetry

Every astronomical object is polarized to some degree. Astronomical polarimetry, by nature, therefore yield more information than imaging and/or spectroscopy alone. Polarization, i.e. the vector properties of (scattered) starlight is particulary dependent on the physical circumstances of the location where the light originated.
Another important and unique capability of polarimetry is the measurement of magnetic fields. Magnetics fields are ubiquitous in astronomical contexts of all scales, but their exact influence on many physical processes is often poorly understood. Only the measurement of magnetic fields through polarimetry allows for the understanding of stars through all stages of their lives, from their formation out of magnetized molecular clouds, to stellar activity during their time on the main sequence, and to their final breaths and their after-life as pulsars or magnetars.

In several ways, astronomical polarimetry is orthogonal to imaging and spectroscopy. Most importantly, polarimetry yields astronomical information that is very complementary. But also, the technical implementation of polarimetry in the optical regime in conjunction with imaging or spectroscopy (spectropolarimetry) and also interferometry (polarimetric interferometry) almost always requires trade-offs on either side [16].

1.4 Objectives of this thesis

1.4.1 General objectives

1. Polarization calibration of the OVRO 40m telescope receiver, KuPol.

1.4.2 Specific objectives

1. To know and to understand the operation of the KuPol receiver.

2. To develop a polarization calibration model for the KuPol receiver.

3. Characterize KuPol receiver parameters from the polarization calibration model.

4. To contrast the results of the calibration model with instrument data.

1.5 Overview of thesis

This thesis is organized as follows. In chapter 1, we have presented the scientific aim and the theoretical tools to achieve this thesis, and a general 40m telescope and its receiver description. In chapter 2, we develop and present the polarization calibration model proposal for KuPol receiver. Chapter 3, we examine an instrumental parameter consideration over the polarization calibration model proposal and from these, we perform instrumental diagnostics such as the isolation. Chapter 4, we will develop an analysis from previous diagnostics for to obtain instrumental parameters. In chapter 5, we present the conclusions of this thesis. Guidelines for future work will also be presented.

Chapter 2

Analytical calibration model proposal for KuPol receiver

Polarimetry is a very challenging technique because the signals to measure are typically very weak ($< 1\%$ of the observed intensity) and because the telescope employed instrumentation introduces spurious polarization. Most polarimeters have calibration optics to determine polarimetric properties downstream from their mounting point. Other calibration techniques include using polarized and unpolarized standard stars, lamps or daytime sky sources. Using a range of techniques, it is possible to remove the instrumental contamination from the observed signals but there are several difficulties. Calibration source brightness, instrument sensitivity, ability to track targets and source availability all limit calibration techniques. Ideally, one would like to have calibration polarizers before the entire optical train covering the full aperture. This would illuminate the optics with a beam identical to that of the science observations but with controlled polarimetric properties [17].

The commissioning, in general terms, corresponds to the stage that follows the installation and testing of the functioning of a service, project or instrument, and which ends when a normal, continuous and optimal operation is achieved. In this process, a severe revision and efforts are made to prevent future defects in the operation of the instrument. In addition, commissioning is the last opportunity to detect and correct design flaws that are impossible to predict.
For us, the commissioning offers a unique opportunity to fully understand the complex operation of the KuPol spectropolarimeter. Within this stage, the polarization calibration of the instrument is important in order to obtain instrument parameters characterization.

2.1 Analytical model description

The proposal (complete) polarization calibration model for KuPoL, propagates the signals that enter for *Ant* and *Ref* horns throughout the instrument. For this, the model uses an abstraction of the instrument, which groups the components into 4 stages that behave like *black boxes* and that contain components that have similar effects on the signal that passes through them. Finally, the model correlates the 4 signals that come out of the last black box and gives the Stokes parameters on orthogonal circular basis for horns *Ant* and *Ref*. For a complete graphic description of this model, see figure 2.3.
We have use the expressions for Stokes Q and U from the *Simulink model* of the receiver (see appendix B) implemented for the digital processing of the signals. Thus, the Stokes parameters calculated for KuPol per horn are

- **Horn Ant**

$$I_A = |A_l|^2 + |A_r|^2 \tag{2.1}$$

$$Q_A = \mathfrak{Re}(A_l)\mathfrak{Re}(A_r) + \mathfrak{Im}(A_l)\mathfrak{Im}(A_r) \tag{2.2}$$

$$U_A = \mathfrak{Re}(A_l)\mathfrak{Im}(A_r) - \mathfrak{Im}(A_l)\mathfrak{Re}(A_r) \tag{2.3}$$

$$V_A = |A_l|^2 - |A_r|^2 \tag{2.4}$$

- **Horn Ref**

$$I_B = |B_l|^2 + |B_r|^2 \tag{2.5}$$

$$Q_B = \mathfrak{Re}(B_l)\mathfrak{Re}(B_r) + \mathfrak{Im}(B_l)\mathfrak{Im}(B_r) \tag{2.6}$$

$$U_B = \mathfrak{Re}(B_l)\mathfrak{Im}(B_r) - \mathfrak{Im}(B_l)\mathfrak{Re}(B_r) \tag{2.7}$$

$$V_B = |B_l|^2 - |B_r|^2 \tag{2.8}$$

Note that $(A, B)_{l,r}$ are the outputs of last black box for our model, $|(A, B)_{l,r}|^2$ are their square modules, and $\mathfrak{Re}(A, B)_{l,r}$ and $\mathfrak{Im}(A, B)_{l,r}$ are their real and imaginary components.

2.1.1 General comments for KuPol proposal polarization calibration model

The proposed calibration model will work making a propagation of the signals that enter by horns *Ant* and *Ref*, until the correlation box named *Stokes* that calculates of Stokes parameters for circular polarization. It is important to note that the signals entering by *Ant* and *Ref* will work separately. After horns, the orthogonal components of the signal, *LCP* and *RCP*, are separated for each horn (called as A_l and A_r for horn *Ant*, and B_l and B_r for horn *Ref*). After

that, the noise diodes (*stage 1*) are injected (one per branch). Then, the signals are mixed in two 180° analog hybrids (*stage 2*) that receive signals with the same polarization from both horns. Then the signals, separated by polarization, enter to the balance corrections boxes (*stage 3*) that contain all the parameters related to the instrument balance. After that, the signals with the same polarization, are mixed in two 180° digital hybrid (*stage 4*) boxes.
The proposed model for the KuPol polarization calibration, will not work based on Mueller matrices as it is usually done for this type of calibration. The 180° analog and digital hybrids (*stages 2 and 4*) mix the signals coming from both horns with the same polarization. We postulate that the non ideal Mueller matrix associated to these component must be a 8x8 matrix as follows

$$M_{hybrid} = \begin{bmatrix} [AA]_{4x4} & [AB]_{4x4} \\ [BA]_{4x4} & [BB]_{4x4} \end{bmatrix} \tag{2.9}$$

where AA and BB are the signals from Ant and Ref respectively, and AB and BA are the mixes of the signals from Ant and Ref produced by the imperfection of the component. Then to simplify the calculations, we have decided do not use Mueller matrices.

2.2 Simplified polarization calibration model

Before we begin to develop the full polarization calibration model for KuPol, we will analyze the signals propagation (A_l, A_r, B_l, and B_r) along the KuPol receiver assumed that the instrument components are perfect (they do not have losses) and the signals that enter the correlation box (*Stokes*) are fully balanced (in amplitude and phase).
Thus, the KuPol receiver is reduced according to the figure 2.1.

The KuPol simplified calibration model we will consider 3 stages:

1. Noise diodes injection.
2. Perfect 180° analog hybrid.
3. Perfect 180° digital hybrid.

To start developing the simplified polarization calibration model, we have that the signals that enter to the KuPol instrument and what are the signals that come out of the horns Ant and Ref [1] are expressed by

1. **Upper branches: Horn Ant signals**
   (a) Branch 1:

$$Ant_{(lcp)} : A_l e^{-i(\omega t + \theta_A + \delta_A)} \tag{2.10}$$

[1] In our model we neglect the effect of the optical train on the signal, since in practice, we will not have access to instrumental data at this place

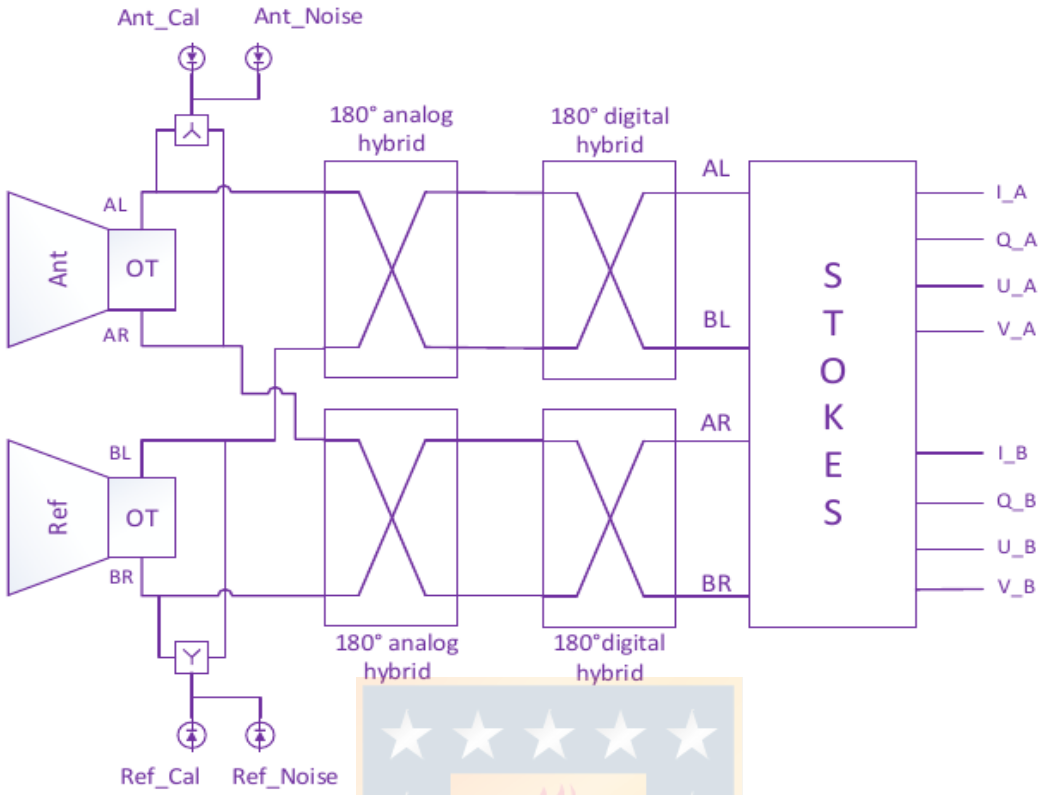

Figure 2.1: Simplified calibration model.
Considers that the instrument is fully balanced and the two hybrids do not have imperfections. The signals that come out of the second hybrid enter the Stokes box where the Stokes parameters are calculated on a circular basis. Source: Own production.

(b) Branch 2:

$$Ant_{(rcp)} : A_r e^{i(\omega t + \theta_A)} \tag{2.11}$$

2. **Lower branches: Horn Ref signals**

(a) Branch 3:

$$Ref_{(lcp)} : B_l e^{-i(\omega t + \theta_B + \delta_B)} \tag{2.12}$$

(b) Branch 4:

$$Ref_{(rcp)} : B_r e^{i(\omega t + \theta_B)} \tag{2.13}$$

Note that ωt is the cosmic signal frecuency, $\theta_{A,B}$ is the cosmic signal phase, and $\delta_{A,B}$ is the phase difference between LCP and RCP branches per horn.

In the following sections we will propagate the previous signals along the instrument according to the figure 2.1.

2.2.1 Stage 1: Noise diodes (nd)

Each noise diodes signals are injected into LCP and RCP branches per horn (one per branch; see relations (2.10) to (2.13)).

1. **Upper branches: Horn Ant**

   (a) Branch 1:

$$E_{l,out}^{nd,A} = A_l e^{-i(\omega t+\theta_A+\delta_A)} + V_A \tag{2.14}$$

   (b) Branch 2:

$$E_{r,out}^{nd,A} = A_r e^{i(\omega t+\theta_A)} + V_A \tag{2.15}$$

2. **Lower branches: Horn Ref**

   (a) Branch 3:

$$E_{l,out}^{nd,B} = B_l e^{-i(\omega t+\theta_B+\delta_B)} + V_B \tag{2.16}$$

   (b) Branch 4:

$$E_{r,out}^{nd,B} = B_r e^{i(\omega t+\theta_B)} + V_B \tag{2.17}$$

Note that $V_{A,B}$ are the noise diode voltage injected into Ant and Ref branches respectively. KuPol instrument has 4 noise diodes that are injected after horns Ant and Ref. Two of these diodes are injected on horn Ant signals and two on horn Ref signals. On one side, we have to $NOISE$ diode that provides a noise temperature comparable to the system temperature and on the other hand, the CAL diode provides a noise temperature comparable to the antenna temperature of the astronomical sources we are observing [15].

2.2.2 Stage 2: 180° analog hybrid (ah)

The perfect 180° analog hybrid effect on the signal is given by the Scattering matrix for a 180° ideal hybrid [8] as

$$S_{180}^{ideal} = \frac{1}{\sqrt{2}} \begin{bmatrix} 0 & 1 & 1 & 0 \\ 1 & 0 & 0 & -1 \\ 1 & 0 & 0 & 1 \\ 0 & -1 & 1 & 0 \end{bmatrix} \tag{2.18}$$

Considering that the hybrid corresponds to a four ports network, and that ports 1 and 4 are the inputs and ports 2 and 3 are the outputs, the output signals from the 180° analog hybrid are

$$(Output)_2 = \frac{1}{\sqrt{2}}[(Input)_1 + (Input)_4] \tag{2.19}$$

$$(Output)_3 = \frac{1}{\sqrt{2}}[(Input)_1 - (Input)_4] \tag{2.20}$$

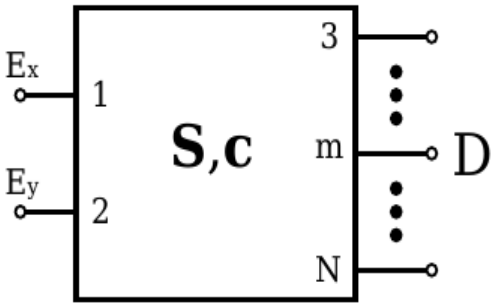

Figure 2.2: Arbitrary receiver.
The linear polarization orthogonal voltajes are $E_x(t)$ y $E_y(t)$ in the ports 1 and 2 respectively. In the ports 3 to N are the output ports. Note that for our analysis the ports 1 and 4 are the inputs and 2 and 3 are the outputs. Source: O. King, et al. [8].

If we use relations (2.19) and (2.20), to obtain the 180° analog hybrid output, and we remember that for our work, the two upper branches of figure 1.3 are called 1 and 2 (LCP polarization) and that the two lower branches are called 3 and 4 (RCP polarization), the 180° analog hybrids outputs are

1. **Upper branches: LCP**

   (a) Branch 1:

$$E_{l,out}^{ah,1} = \frac{1}{\sqrt{2}}[(A_l e^{-i(\omega_A t+\theta_A+\delta_A)} + V_A) + (B_l e^{-i(\omega_B t+\theta_B+\delta_B)} + V_B)] \tag{2.21}$$

   (b) Branch 2:

$$E_{l,out}^{ah,2} = \frac{1}{\sqrt{2}}[(A_l e^{-i(\omega_A t+\theta_A+\delta_A)} + V_A) - (B_l e^{-i(\omega_B t+\theta_B+\delta_B)} + V_B)] \tag{2.22}$$

2. **Lower branches: RCP**

   (a) Branch 3:

$$E_{r,out}^{ah,3} = \frac{1}{\sqrt{2}}[(A_r e^{i(\omega_A t+\theta_A)} + V_A) + (B_r e^{i(\omega_B t+\theta_B)} + V_B)] \tag{2.23}$$

   (b) Branch 4:

$$E_{r,out}^{ah,4} = \frac{1}{\sqrt{2}}[(A_r e^{i(\omega_A t+\theta_A)} + V_A) - (B_r e^{i(\omega_B t+\theta_B)} + V_B)] \tag{2.24}$$

The instrument applies a temporal averaging over the signals before the digital hybrid imple-

mentation [2]. In particular $A_{l,r}e^{i\omega t}$ and $B_{l,r}e^{i\omega t}$ will be 1. Thus, the signals that enter to the next stage for the *simplified model* are

1. **Upper branches: LCP**

   (a) Branch 1:

$$E_{l,out}^{ah,1} = \frac{1}{\sqrt{2}}[(A_l e^{-i(\theta_A+\delta_A)} + V_A) + (B_l e^{-i(\theta_B+\delta_B)} + V_B)] \tag{2.25}$$

   (b) Branch 2:

$$E_{l,out}^{ah,2} = \frac{1}{\sqrt{2}}[(A_l e^{-i(\theta_A+\delta_A)} + V_A) - (B_l e^{-i(\theta_B+\delta_B)} + V_B)] \tag{2.26}$$

2. **Lower branches: RCP**

   (a) Branch 3:

$$E_{r,out}^{ah,3} = \frac{1}{\sqrt{2}}[(A_r e^{i\theta_A} + V_A) + (B_r e^{i\theta_B} + V_B)] \tag{2.27}$$

   (b) Branch 4:

$$E_{r,out}^{ah,4} = \frac{1}{\sqrt{2}}[(A_r e^{i\theta_A} + V_A) - (B_r e^{i\theta_B} + V_B)] \tag{2.28}$$

2.2.3 Stage 3: 180° digital hybrid (dh)

Using relations (2.19) and (2.20) that correspond to the output signals from a perfect 180° hybrid and taking into account that the signals that enter to this stage are the signals that come out of the previous section, the outputs signals from the 180° digital hybrid for KuPol are

1. **Upper branches: LCP**

   (a) Branch 1:

$$\begin{aligned} E_{l,out}^{dh,1} &= \frac{1}{2}[(A_l e^{-i(\theta_A+\delta_A)} + V_A + B_l e^{-i(\theta_B+\delta_B)} + V_B) \\ &\quad + (A_l e^{-i(\theta_A+\delta_A)} + V_A - B_l e^{-i(\theta_B+\delta_B)} - V_B)] \\ &= A_l e^{-i(\theta_A+\delta_A)} + V_A \end{aligned} \tag{2.29}$$

[2] For this, $< e^{i\omega t} >= 1$. Note that $< ... >$ symbol denotes temporal averages.

(b) Branch 2:

$$\begin{aligned} E_{l,out}^{dh,2} &= \frac{1}{2}[(A_l e^{-i(\theta_A+\delta_A)} + V_A + B_l e^{-i(\theta_B+\delta_B)} + V_B) \\ &- (A_l e^{-i(\theta_A+\delta_A)} + V_A - B_l e^{-i(\theta_B+\delta_B)} - V_B)] \\ &= B_l e^{-i(\theta_B+\delta_B)} + V_B \end{aligned} \tag{2.30}$$

2. **Lower branches: RCP**

(a) Branch 3:

$$\begin{aligned} E_{r,out}^{dh,3} &= \frac{1}{2}[(A_r e^{i\theta_A} + V_A + B_r e^{i\theta_B} + V_B) \\ &+ (A_r e^{i\theta_A} + V_A - B_r e^{i\theta_B} - V_B)] \\ &= A_r e^{i\theta_A} + V_A \end{aligned} \tag{2.31}$$

(b) Branch 4:

$$\begin{aligned} E_{r,out}^{dh,4} &= \frac{1}{2}[(A_r e^{i\theta_A} + V_A + B_r e^{i\theta_B} + V_B) \\ &- (A_r e^{i\theta_A} + V_A - B_r e^{i\theta_B} - V_B)] \\ &= B_r e^{i\theta_B} + V_B \end{aligned} \tag{2.32}$$

2.2.4 Stokes parameter for KuPol receiver from simplified calibration model

In the previous section, we obtained the 180° digital hybrid outputs. To calculate the Stokes parameters for the simplified model, we will use the (2.1) to (2.8) relations, that give us the Stokes parameters relations on a circular basis. To obtain this, we need to identify the real and imaginary components, and the square modules of the previous digital hybrid outputs.

2.2.4.1 Real and imaginary components 180° digital hybrid outputs

Using the Euler's formula for the complex analysis, the *real* and *imaginary* components outputs from 180° digital hybrid are

1. **Upper branches: LCP**

(a) Branch 1:

$$\begin{aligned} E_{l,out}^{dh,1} &= A_l e^{-i(\theta_A+\delta_A)} + V_A \\ &= (A_l cos(\theta_A+\delta_A) + V_A) - i(A_l sin(\theta_A+\delta_A)) \end{aligned} \tag{2.33}$$

(b) Branch 2:

$$\begin{aligned} E_{l,out}^{dh,2} &= B_l e^{-i(\theta_B+\delta_B)} + V_B \\ &= (B_l cos(\theta_B+\delta_B) + V_B) - i(B_l sin(\theta_B+\delta_B)) \end{aligned} \tag{2.34}$$

2. **Lower branches: RCP**

(a) Branch 3:

$$\begin{aligned} E_{r,out}^{dh,3} &= A_r e^{i\theta_A} + V_A \\ &= (A_r cos(\theta_A) + V_A) + i(A_r sin(\theta_A)) \end{aligned} \tag{2.35}$$

(b) Branch 4:

$$\begin{aligned} E_{r,out}^{dh,4} &= B_r e^{i\theta_B} + V_B \\ &= (B_r cos(\theta_B) + V_B) + i(B_r sin(\theta_B)) \end{aligned} \tag{2.36}$$

2.2.4.2 Square modules 180° digital hybrid outputs

Taking the square modules of the 180° digital hybrid outputs, we have

1. **Upper branches: LCP**

(a) Branch 1:

$$\begin{aligned} |E_{l,out}^{dh,1}|^2 &= (A_l cos(\theta_A+\delta_A) + V_A)^2 + (A_l sin(\theta_A+\delta_A))^2 \\ &= (V_A)^2 + (A_l)^2 \end{aligned} \tag{2.37}$$

(b) Branch 2:

$$\begin{aligned} |E_{l,out}^{dh,2}|^2 &= (B_l cos(\theta_B+\delta_B) + V_B)^2 + (B_l sin(\theta_B+\delta_B))^2 \\ &= (V_B)^2 + (B_l)^2 \end{aligned} \tag{2.38}$$

2. **Lower branches: RCP**

(a) Branch 3:

$$\begin{aligned} |E_{r,out}^{dh,3}|^2 &= (A_r cos(\theta_A) + V_A)^2 + (A_r sin(\theta_A))^2 \\ &= (V_A)^2 + (A_r)^2 \end{aligned} \tag{2.39}$$

(b) Branch 4:

$$\begin{aligned} |E_{r,out}^{dh,4}|^2 &= (B_r cos(\theta_B) + V_B)^2 + (B_r sin(\theta_B))^2 \\ &= (V_B)^2 + (B_r)^2 \end{aligned} \tag{2.40}$$

Note that in relations (2.37) - (2.40), uncorrelated terms have been eliminated.

2.2.4.3 Stokes parameters calculation from simplified calibration model

Considering sections 2.2.4.1 and 2.2.4.2, the Stokes parameters for KuPol receiver from the simplified model, for horns *Ant* and Ref, are

- **Horn Ant**

$$I_A = |E_l^A|^2 + |E_r^A|^2 = (A_l)^2 + (A_r)^2 + 2V_A^2 \tag{2.41}$$

$$Q_A = \mathfrak{Re}(E_l^A)\mathfrak{Re}(E_r^A) + \mathfrak{Im}(E_l^A)\mathfrak{Im}(E_r^A) = A_l A_r cos(2\theta_A + \delta_A) + V_A^2 \tag{2.42}$$

$$U_A = \mathfrak{Re}(E_l^A)\mathfrak{Im}(E_r^A) - \mathfrak{Im}(E_l^A)\mathfrak{Re}(E_r^A) = A_l A_r sin(2\theta_A + \delta_A) \tag{2.43}$$

$$V_A = |E_l^A|^2 - |E_r^A|^2 = (A_l)^2 - (A_r)^2 \tag{2.44}$$

- **Horn Ref**

$$I_B = |E_l^B|^2 + |E_r^B|^2 = (B_l)^2 + (B_r)^2 + 2V_B^2 \tag{2.45}$$

$$Q_B = \mathfrak{Re}(E_l^B)\mathfrak{Re}(E_r^B) + \mathfrak{Im}(E_l^B)\mathfrak{Im}(E_r^B) = B_l B_r cos(2\theta_B + \delta_B) + V_B^2 \tag{2.46}$$

$$U_B = \mathfrak{Re}(E_l^B)\mathfrak{Im}(E_r^B) - \mathfrak{Im}(E_l^B)\mathfrak{Re}(E_r^B) = B_l B_r sin(2\theta_B + \delta_B) \tag{2.47}$$

$$V_B = |E_l^B|^2 - |E_r^B|^2 = (B_l)^2 - (B_r)^2 \tag{2.48}$$

Note that:

- In relations (2.41) - (2.48), uncorrelated terms have been eliminated. Here we have assumed that the horn *Ant* and Ref voltages (A_l, A_r, B_l, and B_r) and the noise diode voltages ($V_{A,B}$) are uncorrelated. Hence terms like $< A_l * B_l >$, $< A_r * V_A >$, or $< B_r * V_B >$[3] are equal to zero.
- The relations (2.41) - (2.48) are the Stokes parameters for the ideal KuPol instrument.

[3]Note that $< ... >$ denotes temporal averages.

2.3 Complete polarization calibration model for KuPol receiver

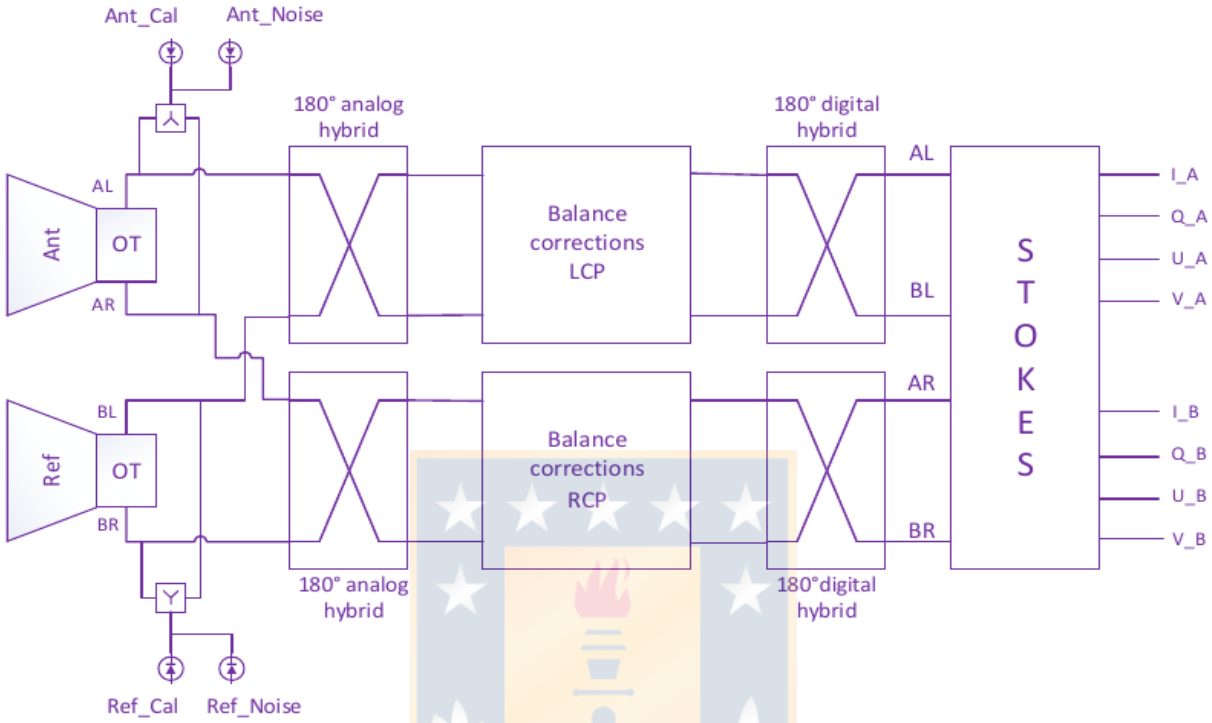

Figure 2.3: Complete polarization calibration model.
Source: Own production.

As shown in the figure 2.2, the KuPol calibration model will work considering a 4 stages through which the signals that enter the instrument will be propagated.

1. **Stage 1: Noise diodes** that are injected into the system in each polarization branch after horns Ant and Ref.

2. **Stage 2:** 180° **analog hybrid** that combines the signals with the same polarization from Ant and Ref.

3. **Stage 3: Instrumental balance corrections parameters** that contains the total balance instrument parameters (for amplitude and phase) between branches with same polarization and between branches with different polarization. This stage considers the balance from the analog instrument and the complex corrections coefficients from digital instrument. In this stage, the instrument gain terms (complex) are incorporated.

4. **Stage 4:** 180° **digital hybrid** that combines the signal with the same polarization in the digital instrument. It is important to note that for our work, we will consider this implementation as perfect.

After stage 4, the signals that come out of the digital hybrid enter the *Stokes box* where the Stokes parameters are calculated.
It is important to note that in the *complete model*, we will consider all the instrumental imperfections.

2.3.1 Stage 1: Noise Diode (nd)

KuPol instrument has 4 noise diodes that are injected after horns Ant and Ref. Two of these diodes are injected on horn Ant signals and two on horn Ref signals. On one side, we have to $NOISE$ diode that provides a noise temperature comparable to the system temperature and on the other hand, the CAL diode provides a noise temperature comparable to the antenna temperature of the astronomical sources we are observing [15]. Note that the $NOISE$ diode is ~ 1000 times stronger than CAL.
The effect that the noise diodes have on the signals that enter to the horns is adding their voltage on the input signal.

1. **Upper branches: Horn Ant**

$$\begin{bmatrix} E^{nd,A}_{l,out} \\ E^{nd,A}_{r,out} \end{bmatrix} = \begin{bmatrix} A_l e^{-i(\omega t+\theta_A+\delta_A)} \\ A_r e^{i(\omega t+\theta_A)} \end{bmatrix} + \begin{bmatrix} V_A e^{i(\omega t+\gamma^A_l)} \\ V_A e^{i(\omega t+\gamma^A_r)} \end{bmatrix} \tag{2.49}$$

$$\begin{aligned} \Longrightarrow E^{nd,A}_{l,out} &= A_l e^{-i(\omega t+\theta_A+\delta_A)} + V_A e^{i(\omega t+\gamma^A_l)} \\ \Longrightarrow E^{nd,A}_{r,out} &= A_r e^{i(\omega t+\theta_A)} + V_A e^{i(\omega t+\gamma^A_r)} \end{aligned} \tag{2.50}$$

2. **Lower branches: Horn Ref**

$$\begin{bmatrix} E^{nd,B}_{l,out} \\ E^{nd,B}_{r,out} \end{bmatrix} = \begin{bmatrix} B_l e^{-i(\omega t+\theta_B+\delta_B)} \\ B_r e^{i(\omega t+\theta_B)} \end{bmatrix} + \begin{bmatrix} V_B e^{i(\omega t+\gamma^B_l)} \\ V_B e^{i(\omega t+\gamma^B_r)} \end{bmatrix} \tag{2.51}$$

$$\begin{aligned} \Longrightarrow E^{nd,B}_{l,out} &= B_l e^{-i(\omega t+\theta_B+\delta_B)} + V_B e^{i(\omega t+\gamma^B_l)} \\ \Longrightarrow E^{nd,B}_{r,out} &= B_r e^{i(\omega t+\theta_B)} + V_B e^{i(\omega t+\gamma^B_r)} \end{aligned} \tag{2.52}$$

Note that in $A_{l,r}e^{i\omega t}$ and $B_{l,r}e^{i\omega t}$, ωt is the cosmic signal frecuency, $\theta_{A,B}$ is the cosmic signal phase, $\delta_{A,B}$ is the phase difference between LCP and RCP branches per horn. On the other hand, in $V_A e^{i(\omega t+\gamma^A_{l,r})}$ and $V_B e^{i(\omega t+\gamma^B_{l,r})}$, $V_{A,B}$ are the noise diode voltage injected into Ant and Ref branches, and $\gamma^{A,B}_{l,r}$ are the phase which the noise diodes signal are injected on the branch.

2.3.2 Stage 2: 180° analog hybrid (ah)

General scattering matrix of a reciprocal four-port network matched at all ports has the following form:

$$[S] = \begin{bmatrix} 0 & S_{12} & S_{13} & S_{14} \\ S_{12} & 0 & S_{23} & S_{24} \\ S_{13} & S_{23} & 0 & S_{34} \\ S_{14} & S_{24} & S_{34} & 0 \end{bmatrix} \tag{2.53}$$

Further simplification can be made by choosing the phase references on three of the four ports. Thus, we choose $S_{12} = S_{34} = \alpha$, $S_{13} = \beta e^{j\theta}$, and $S_{24} = \beta e^{j\phi}$, where α and β are real, and θ and ϕ are phase constants to be determined (one of which we are still free to choose).
If we consider a relation between the output ports (2 and 3 for four-port network), there is a relation between the phase constants as $\theta + \phi = \pi \pm 2n\pi$.
Then, considering the previous relation and replacing in (2.53),

$$[S] = \begin{bmatrix} 0 & \alpha & \beta e^{i\theta} & 0 \\ \alpha & 0 & 0 & \beta e^{i\phi} \\ \beta e^{i\theta} & 0 & 0 & \alpha \\ 0 & \beta e^{i\phi} & \alpha & 0 \end{bmatrix} \tag{2.54}$$

If we ignore integer multiples of 2π, there are a particular choices that commonly occur in practice, which coincide with the 180° hybrid as an antisymmetric coupler: $\theta = 0$, $\phi = \pi$. Also, now we consider that $\theta + \phi = \pi + \Delta\phi$. The phases of the terms having amplitude β are chosen to be 180° apart. Then the scattering matrix has the following form:

$$[S] = \begin{bmatrix} 0 & \alpha & \beta & 0 \\ \alpha & 0 & 0 & -\beta e^{i\Delta\phi} \\ \beta & 0 & 0 & \alpha \\ 0 & -\beta e^{i\Delta\phi} & \alpha & 0 \end{bmatrix} \tag{2.55}$$

Note that these two couplers differ only in the choice of reference planes. In addition, the amplitudes α and β are not independent. So, $\alpha^2 + \beta^2 = 1$. Thus, apart from phase references, an ideal four-port directional coupler has only one degree of freedom, leading to two possible configurations [13].
On the other hand, for to characterize the hybrid effect, we will use the scattering matrix for a 180° non ideal hybrid from [8]:

$$S_{180} = \frac{1}{\sqrt{2}} \begin{bmatrix} 0 & \sqrt{1+\delta_{180}} & \sqrt{1-\delta_{180}}e^{-i\phi_\Sigma} & 0 \\ \sqrt{1+\delta_{180}} & 0 & 0 & -\sqrt{1-\delta_{180}}e^{-i\phi_\Delta} \\ \sqrt{1-\delta_{180}}e^{-i\phi_\Sigma} & 0 & 0 & \sqrt{1+\delta_{180}} \\ 0 & -\sqrt{1-\delta_{180}}e^{-i\phi_\Delta} & \sqrt{1+\delta_{180}} & 0 \end{bmatrix} \tag{2.56}$$

where δ_{180} is the amplitude imbalance of the hybrid, ϕ_Σ indicates the phase error in the operation sum, and ϕ_Δ indicates the phase error in the operation subtraction.
Note that:

1. (2.53) corresponds to the scattering 180° perfect hybrid matrix if $\delta_{180} = \phi_\Sigma = \phi_\Delta = 0$.
2. If we compare (2.55) and (2.56), we note that: $\alpha = \sqrt{1+\delta_{180}}$ and $\beta = \sqrt{1-\delta_{180}}$.
3. If we compare (2.55) and (2.56), we note that exist a relation between ϕ_Σ and ϕ_Δ. This relation is given by the phase difference $\Delta\phi$ from element S_{24} of (2.55).

Thus, the scatering matrix proposed for our non ideal analog 180° hybrid is,

$$S_{180} = \frac{1}{\sqrt{2}} \begin{bmatrix} 0 & \sqrt{1+\delta_{180}} & \sqrt{1-\delta_{180}} & 0 \\ \sqrt{1+\delta_{180}} & 0 & 0 & -\sqrt{1-\delta_{180}}e^{i\Delta\phi} \\ \sqrt{1-\delta_{180}} & 0 & 0 & \sqrt{1+\delta_{180}} \\ 0 & -\sqrt{1-\delta_{180}}e^{i\Delta\phi} & \sqrt{1+\delta_{180}} & 0 \end{bmatrix} \tag{2.57}$$

From figure 2.2. and considering that the ports 1 and 2 correspond to the inputs, and the ports 3 and 4 are the outputs, we obtain that the relations that describe the hybrid outputs signals from (2.57) are

$$(Output)_3 = \frac{1}{\sqrt{2}}[\sqrt{1-\delta_{180}}(Input)_1 + \sqrt{1+\delta_{180}}(Input)_4] \tag{2.58}$$

$$(Output)_2 = \frac{1}{\sqrt{2}}[\sqrt{1+\delta_{180}}(Input)_1 - \sqrt{1-\delta_{180}}e^{i\Delta\phi}(Input)_4] \tag{2.59}$$

Thus, using (2.58) and (2.59), we have that the output hybrid signals are:

1. **Upper branches: LCP**

   (a) Branch 1:

$$\begin{aligned} E_{l,out}^{ah,1} = \frac{1}{\sqrt{2}}[&\sqrt{1-\delta_{180}}(A_l e^{-i(\omega t+\theta_A+\delta_A)} + V_A e^{i(\omega t+\gamma_l^A)}) \\ &+ \sqrt{1+\delta_{180}}(B_l e^{-i(\omega t+\theta_B+\delta_B)} + V_B e^{i(\omega t+\gamma_l^B)})] \end{aligned} \tag{2.60}$$

   (b) Branch 2:

$$\begin{aligned} E_{l,out}^{ah,2} = \frac{1}{\sqrt{2}}[&\sqrt{1+\delta_{180}}(A_l e^{-i(\omega t+\theta_A+\delta_A)} + V_A e^{i(\omega t+\gamma_l^A)}) \\ &- \sqrt{1-\delta_{180}}e^{i\Delta\phi_l}(B_l e^{-i(\omega t+\theta_B+\delta_B)} + V_B e^{i(\omega t+\gamma_l^B)})] \end{aligned} \tag{2.61}$$

2. **Lower branches: RCP**

(a) Branch 3:

$$E_{l,out}^{ah,3} = \frac{1}{\sqrt{2}}[\sqrt{1-\delta_{180}}(A_r e^{i(\omega t+\theta_A)} + V_A e^{i(\omega t+\gamma_r^A)}) + \sqrt{1+\delta_{180}}(B_r e^{i(\omega t+\theta_B)} + V_B e^{i(\omega t+\gamma_r^B)})] \tag{2.62}$$

(b) Branch 4:

$$E_{l,out}^{ah,4} = \frac{1}{\sqrt{2}}[\sqrt{1+\delta_{180}}(A_r e^{i(\omega t+\theta_A)} + V_A e^{i(\omega t+\gamma_r^A)}) - \sqrt{1-\delta_{180}}e^{i\Delta\phi_r}(B_r e^{i(\omega t+\theta_B)} + V_B e^{i(\omega t+\gamma_r^B)})] \tag{2.63}$$

The $\Delta\phi_{l,r}$ are the difference phase for LCP and RCP polarizations branches. Remember that KuPol has two 180° analog hybrid (see figure 2.3.).

2.3.3 Stage 3: Instrumental balance corrections parameters (bc)

We propose that in this stage, a series of parameters will be presented and these will give us evidence of instrumental imbalance. This parameters will contribute to its correction.
The balance corrections parameters for branches with the same polarization are α_{lcp}, α_{rcp}, β_{lcp}, and β_{rcp}, and for branches with the different polarization are α_{rl} and β_{rl}.
On the other hand, usually antenna feeds measure the components of the incident radiation along two orthogonal polarization states by two separate feeds. The signals from the two feeds travel through essentially independent paths till the correlator. However, due to mechanical imperfections in the feed or imperfections in the electronics, the two signals can leak into each other at various points in the signal chain. This is the *polarization leakage* that α_{rl} and β_{rl} represent.
The instrument gain terms are incorpored. Note that the gain is complex as $g_j = |g_j|e^{i\phi_j}$, where j is the number branch.

1. **Upper branches: LCP**

(a) Branch 1:

$$\begin{aligned} E_{l,out}^{bc,1} &= g_1 E_{l,out}^{ah,1} \\ &= \frac{g_1}{\sqrt{2}}[\sqrt{1-\delta_{180}}(A_l e^{-i(\omega t+\theta_A+\delta_A)} + V_A e^{i(\omega t+\gamma_l^A)})) \\ &+ \sqrt{1+\delta_{180}}(B_l e^{-i(\omega t+\theta_B+\delta_B)} + V_B e^{i(\omega t+\gamma_l^B)})] \end{aligned} \tag{2.64}$$

(b) Branch 2:

$$\begin{aligned} E_{l,out}^{bc,2} &= g_1\alpha_{lcp}e^{i\beta_{lcp}}E_{l,out}^{ah,2} \\ &= \frac{g_1\alpha_{lcp}e^{i\beta_{lcp}}}{\sqrt{2}}[\sqrt{1+\delta_{180}}(A_l e^{-i(\omega t+\theta_A+\delta_A)} + V_A e^{i(\omega t+\gamma_l^A)})) \\ &- \sqrt{1-\delta_{180}}e^{i\Delta\phi_l}(B_l e^{-i(\omega t+\theta_B+\delta_B)} + V_B e^{i(\omega t+\gamma_l^B)}))] \end{aligned} \tag{2.65}$$

2. **Lower branches: RCP**

(a) Branch 3:

$$\begin{aligned} E_{r,out}^{bc,3} &= g_3\alpha_{rl}e^{i\beta_{rl}}E_{r,out}^{ah,3} \\ &= \frac{g_3\alpha_{rl}e^{i\beta_{rl}}}{\sqrt{2}}[\sqrt{1-\delta_{180}}(A_r e^{i(\omega t+\theta_A)} + V_A e^{i(\omega t+\gamma_r^A)})) \\ &+ \sqrt{1+\delta_{180}}(B_r e^{i(\omega t+\theta_B)} + V_B e^{i(\omega t+\gamma_r^B)})] \end{aligned} \tag{2.66}$$

(b) Branch 4:

$$\begin{aligned} E_{r,out}^{bc,4} &= g_3(\alpha_{rl}e^{i\beta_{rl}})(\alpha_{rcp}e^{i\beta_{rcp}})E_{r,out}^{ah,4} \\ &= \frac{g_3\alpha_{rl}e^{i\beta_{rl}}\alpha_{rcp}e^{i\beta_{rcp}}}{\sqrt{2}}[\sqrt{1+\delta_{180}}(A_r e^{i(\omega t+\theta_A)} + V_A e^{i(\omega t+\gamma_r^A)})) \\ &- \sqrt{1-\delta_{180}}e^{i\Delta\phi_r}(B_r e^{i(\omega t+\theta_B)} + V_B e^{i(\omega t+\gamma_r^B)})] \end{aligned} \tag{2.67}$$

The instrument applies a temporal averaging over the signals before the digital hybrid implementation [4]. In particular $A_{l,r}e^{i\omega t}$ and $B_{l,r}e^{i\omega t}$ will be 1. Thus, the signals that enter to the next stage for the *complete model* are

1. **Upper branches: LCP**

(a) Branch 1:

$$E_{l,out}^{ah,1} = \frac{g_1}{\sqrt{2}}[\sqrt{1-\delta_{180}}(A_l e^{-i(\theta_A+\delta_A)} + V_A) + \sqrt{1+\delta_{180}}(B_l e^{-i(\theta_B+\delta_B)} + V_B)] \tag{2.68}$$

(b) Branch 2:

$$E_{l,out}^{ah,2} = \frac{g_1\alpha_{lcp}e^{i\beta_{lcp}}}{\sqrt{2}}[\sqrt{1+\delta_{180}}(A_l e^{-i(\theta_A+\delta_A)}+V_A) - \sqrt{1-\delta_{180}}e^{i\Delta\phi_l}(B_l e^{-i(\theta_B+\delta_B)}+V_B)] \tag{2.69}$$

2. **Lower branches: RCP**

[4] For this, $< e^{i\omega t} >= 1$. Note that $< ... >$ symbol denotes temporal averages.

(a) Branch 3:

$$E_{l,out}^{ah,3} = \frac{g_3 \alpha_{rl} e^{i\beta_{rl}}}{\sqrt{2}} [\sqrt{1-\delta_{180}}(A_r e^{i\theta_A} + V_A) + \sqrt{1+\delta_{180}}(B_r e^{i\theta_B} + V_B)] \tag{2.70}$$

(b) Branch 4:

$$E_{l,out}^{ah,4} = \frac{g_3 \alpha_{rl} e^{i\beta_{rl}} \alpha_{rcp} e^{i\beta_{rcp}}}{\sqrt{2}} [\sqrt{1+\delta_{180}}(A_r e^{i\theta_A} + V_A) - \sqrt{1-\delta_{180}} e^{i\Delta\phi_r}(B_r e^{i\theta_B} + V_B)] \tag{2.71}$$

2.3.4 Stage 4: 180° digital hybrid (dh)

The 180° digital hybrid effect on the signal is given by the Scattering matrix for a 180° ideal hybrid [8] as

$$S_{180} = \frac{1}{\sqrt{2}} \begin{bmatrix} 0 & 1 & 1 & 0 \\ 1 & 0 & 0 & -1 \\ 1 & 0 & 0 & 1 \\ 0 & -1 & 1 & 0 \end{bmatrix} \tag{2.72}$$

Using (2.19) and (2.20), we have that the digital hybrid outputs are:

1. **Upper branches: LCP**

(a) Branch 1:

$$\begin{aligned} E_{l,out}^{dh,1} &= \frac{1}{\sqrt{2}}[E_{l,out}^{bc,1} + E_{l,out}^{bc,2}] \\ &= \frac{g_1}{2}[(A_l e^{-i(\theta_A+\delta_A)} + V_A)(\sqrt{1-\delta_{180}} + \alpha_{lcp} e^{i\beta_{lcp}} \sqrt{1+\delta_{180}}) \\ &+ (B_l e^{-i(\theta_B+\delta_B)} + V_B)(\sqrt{1+\delta_{180}} - \alpha_{lcp} \sqrt{1-\delta_{180}} e^{i(\Delta\phi_l+\beta_{lcp})}] \end{aligned} \tag{2.73}$$

(b) Branch 2:

$$\begin{aligned} E_{l,out}^{dh,2} &= \frac{1}{\sqrt{2}}[E_{l,out}^{bc,1} - E_{l,out}^{bc,2}] \\ &= \frac{g_1}{2}[(A_l e^{-i(\theta_A+\delta_A)} + V_A)(\sqrt{1-\delta_{180}} - \alpha_{lcp} e^{i\beta_{lcp}} \sqrt{1+\delta_{180}}) \\ &+ (B_l e^{-i(\theta_B+\delta_B)} + V_B)(\sqrt{1+\delta_{180}} + \alpha_{lcp} \sqrt{1-\delta_{180}} e^{i(\Delta\phi_l+\beta_{lcp})})] \end{aligned} \tag{2.74}$$

2. **Lower branches: RCP**

(a) Branch 3:

$$\begin{aligned} E_{r,out}^{dh,3} &= \frac{1}{\sqrt{2}}[E_{r,out}^{bc,3} + E_{r,out}^{bc,4}] \\ &= \frac{g_3\alpha_{rl}e^{i\beta_{rl}}}{2}[(A_r e^{i\theta_A} + V_A)(\sqrt{1-\delta_{180}} + \alpha_{rcp}e^{i\beta_{rcp}}\sqrt{1+\delta_{180}}) \\ &+ (B_r e^{i\theta_B} + V_B)(\sqrt{1+\delta_{180}} - \alpha_{rcp}\sqrt{1-\delta_{180}}e^{i(\Delta\phi_r+\beta_{rcp})})] \end{aligned} \tag{2.75}$$

(b) Branch 4:

$$\begin{aligned} E_{r,out}^{dh,4} &= \frac{1}{\sqrt{2}}[E_{r,out}^{bc,3} - E_{r,out}^{bc,4}] \\ &= \frac{g_3\alpha_{rl}e^{i\beta_{rl}}}{2}[(A_r e^{i\theta_A} + V_A)(\sqrt{1-\delta_{180}} - \alpha_{rcp}e^{i\beta_{rcp}}\sqrt{1+\delta_{180}}) \\ &+ (B_r e^{i\theta_B} + V_B)(\sqrt{1+\delta_{180}} + \alpha_{rcp}\sqrt{1-\delta_{180}}e^{i(\Delta\phi_r+\beta_{rcp})})] \end{aligned} \tag{2.76}$$

Note that the digital hybrid will acts on the signals with same polarization, that is, it mixes the signals of branches 1 and 2, and those of branches 3 and 4.

2.3.5 Stokes parameters for KuPol receiver from complete calibration model

To calculate the new Stokes parameters, we will use the (2.1) to (2.8) relations, that give us the Stokes parameters relations on a circular basis. For to obtain this, we need to identify the real and imaginary components, and the square modules of the previous digital hybrid outputs.

2.3.5.1 Real and imaginary components 180° digital hybrid outputs

Using the Euler's formula for the complex analysis, the components real and imaginary outputs from 180° digital hybrid are

1. **Uper branches: LCP**

$$
\begin{aligned}
E_{l,out}^{dh,1} &= \mathfrak{Re}(E_{l,out}^{dh,1}) + i\mathfrak{Im}(E_{l,out}^{dh,1}) \\
&= \frac{g_1}{2}[[A_l(\sqrt{1-\delta_{180}}cos(\theta_A+\delta_A) + \sqrt{1+\delta_{180}}\alpha_{lcp}cos(\theta_A+\delta_A-\beta_{lcp})) \\
&+ V_A(\sqrt{1-\delta_{180}} + \sqrt{1+\delta_{180}}\alpha_{lcp}cos(\beta_{lcp})) \\
&+ B_l(\sqrt{1+\delta_{180}}cos(\theta_B+\delta_B) - \sqrt{1-\delta_{180}}\alpha_{lcp}cos(\theta_B+\delta_B-\Delta\phi_l-\beta_{lcp})) \\
&+ V_B(\sqrt{1+\delta_{180}} - \sqrt{1-\delta_{180}}\alpha_{lcp}cos(\Delta\phi_l+\beta_{lcp}))] \\
&- i[A_l(\sqrt{1-\delta_{180}}sin(\theta_A+\delta_A) + \sqrt{1+\delta_{180}}\alpha_{lcp}sin(\theta_A+\delta_A-\beta_{lcp})) \\
&- V_A\sqrt{1+\delta_{180}}\alpha_{lcp}sin(\beta_{lcp}) \\
&+ B_l(\sqrt{1+\delta_{180}}sin(\theta_B+\delta_B) - \sqrt{1-\delta_{180}}\alpha_{lcp}sin(\theta_B+\delta_B-\Delta\phi_l-\beta_{lcp})) \\
&+ V_B\sqrt{1-\delta_{180}}\alpha_{lcp}sin(\Delta\phi_l+\beta_{lcp})]]
\end{aligned}
\tag{2.77}
$$

$$
\begin{aligned}
E_{l,out}^{dh,2} &= \mathfrak{Re}(E_{l,out}^{dh,2}) + i\mathfrak{Im}(E_{l,out}^{dh,2}) \\
&= \frac{g_1}{2}[[A_l(\sqrt{1-\delta_{180}}cos(\theta_A+\delta_A) - \sqrt{1+\delta_{180}}\alpha_{lcp}cos(\theta_A+\delta_A-\beta_{lcp})) \\
&+ V_A(\sqrt{1-\delta_{180}} - \sqrt{1+\delta_{180}}\alpha_{lcp}cos(\beta_{lcp})) \\
&+ B_l(\sqrt{1+\delta_{180}}cos(\theta_B+\delta_B) + \sqrt{1-\delta_{180}}\alpha_{lcp}cos(\theta_B+\delta_B-\Delta\phi_l-\beta_{lcp})) \\
&+ V_B(\sqrt{1+\delta_{180}} + \sqrt{1-\delta_{180}}\alpha_{lcp}cos(\Delta\phi_l+\beta_{lcp}))] \\
&- i[A_l(\sqrt{1-\delta_{180}}sin(\theta_A+\delta_A) - \sqrt{1+\delta_{180}}\alpha_{lcp}sin(\theta_A+\delta_A-\beta_{lcp})) \\
&+ V_A\sqrt{1+\delta_{180}}\alpha_{lcp}sin(\beta_{lcp}) \\
&+ B_l(\sqrt{1+\delta_{180}}sin(\theta_B+\delta_B) + \sqrt{1-\delta_{180}}\alpha_{lcp}sin(\theta_B+\delta_B-\Delta\phi_l-\beta_{lcp})) \\
&- V_B\sqrt{1-\delta_{180}}\alpha_{lcp}sin(\Delta\phi_l+\beta_{lcp})]]
\end{aligned}
\tag{2.78}
$$

2. **Lower branches: RCP**

$$
\begin{aligned}
E_{r,out}^{dh,3} &= \mathfrak{Re}(E_{r,out}^{dh,3}) + i\mathfrak{Im}(E_{r,out}^{dh,3}) \\
&= \frac{g_3\alpha_{rl}}{2}[[A_r(\sqrt{1-\delta_{180}}cos(\theta_A+\beta_{rl}) + \sqrt{1+\delta_{180}}\alpha_{rcp}cos(\theta_A+\beta_{rl}+\beta_{rcp})) \\
&+ V_A(\sqrt{1-\delta_{180}}cos(\beta_{rl}) + \sqrt{1+\delta_{180}}\alpha_{rcp}cos(\beta_{rl}+\beta_{rcp})) \\
&+ B_r(\sqrt{1+\delta_{180}}cos(\theta_B+\beta_{rl}) - \sqrt{1-\delta_{180}}\alpha_{rcp}cos(\theta_B+\beta_{rl}+\Delta\phi_r+\beta_{rcp})) \\
&+ V_B(\sqrt{1+\delta_{180}}cos(\beta_{rl}) - \sqrt{1-\delta_{180}}\alpha_{rcp}cos(\beta_{rl}+\Delta\phi_r+\beta_{rcp}))] \\
&+ i[A_r(\sqrt{1-\delta_{180}}sin(\theta_A+\beta_{rl}) + \sqrt{1+\delta_{180}}\alpha_{rcp}sin(\theta_A+\beta_{rl}+\beta_{rcp})) \\
&+ V_A(\sqrt{1-\delta_{180}}sin(\beta_{rl}) + \sqrt{1+\delta_{180}}\alpha_{rcp}sin(\beta_{rl}+\beta_{rcp})) \\
&+ B_r(\sqrt{1+\delta_{180}}sin(\theta_B+\beta_{rl}) - \sqrt{1-\delta_{180}}\alpha_{rcp}sin(\theta_B+\beta_{rl}+\Delta\phi_r+\beta_{rcp})) \\
&+ V_B(\sqrt{1+\delta_{180}}sin(\beta_{rl}) - \sqrt{1-\delta_{180}}\alpha_{rcp}sin(\beta_{rl}+\Delta\phi_r+\beta_{rcp})]]
\end{aligned}
\tag{2.79}
$$

$$
\begin{aligned}
E_{r,out}^{dh,4} &= \mathfrak{Re}(E_{r,out}^{dh,4}) + i\mathfrak{Im}(E_{r,out}^{dh,4}) \\
&= \frac{g_3\alpha_{rl}}{2}[[A_r(\sqrt{1-\delta_{180}}cos(\theta_A+\beta_{rl}) - \sqrt{1+\delta_{180}}\alpha_{rcp}cos(\theta_A+\beta_{rl}+\beta_{rcp})) \\
&+ V_A(\sqrt{1-\delta_{180}}cos(\beta_{rl}) - \sqrt{1+\delta_{180}}\alpha_{rcp}cos(\beta_{rl}+\beta_{rcp})) \\
&+ B_r(\sqrt{1+\delta_{180}}cos(\theta_B+\beta_{rl}) + \sqrt{1-\delta_{180}}\alpha_{rcp}cos(\theta_B+\beta_{rl}+\Delta\phi_r+\beta_{rcp})) \\
&+ V_B(\sqrt{1+\delta_{180}}cos(\beta_{rl}) + \sqrt{1-\delta_{180}}\alpha_{rcp}cos(\beta_{rl}+\Delta\phi_r+\beta_{rcp}))] \\
&+ i[A_r(\sqrt{1-\delta_{180}}sin(\theta_A+\beta_{rl}) - \sqrt{1+\delta_{180}}\alpha_{rcp}sin(\theta_A+\beta_{rl}+\beta_{rcp})) \\
&+ V_A(\sqrt{1-\delta_{180}}sin(\beta_{rl}) - \sqrt{1+\delta_{180}}\alpha_{rcp}sin(\beta_{rl}+\beta_{rcp})) \\
&+ B_r(\sqrt{1+\delta_{180}}sin(\theta_B+\beta_{rl}) + \sqrt{1-\delta_{180}}\alpha_{rcp}sin(\theta_B+\beta_{rl}+\Delta\phi_r+\beta_{rcp})) \\
&+ V_B(\sqrt{1+\delta_{180}}sin(\beta_{rl}) + \sqrt{1-\delta_{180}}\alpha_{rcp}sin(\beta_{rl}+\Delta\phi_r+\beta_{rcp}))]]
\end{aligned}
\tag{2.80}
$$

2.3.5.2 Square modules 180° digital hybrid outputs

Taking the square modules of the relations for the 180° digital hybrid outputs, we have

1. **Upper branches: LCP**

$$
\begin{aligned}
|E_{l,out}^{dh,1}|^2 &= \frac{|g_1|^2}{4}[((A_l)^2+(V_A)^2) \\
&((\sqrt{1-\delta_{180}})^2 + (\alpha_{lcp}\sqrt{1+\delta_{180}})^2 + 2\alpha_{lcp}\sqrt{1+\delta_{180}}\sqrt{1-\delta_{180}}cos(\beta_{lcp})) \\
&+ ((B_l)^2+(V_B)^2) \\
&((\sqrt{1+\delta_{180}})^2 + (\alpha_{lcp}\sqrt{1-\delta_{180}})^2 - 2\alpha_{lcp}\sqrt{1+\delta_{180}}\sqrt{1-\delta_{180}}cos(\Delta\phi_l+\beta_{lcp}))]
\end{aligned}
\tag{2.81}
$$

$$
\begin{aligned}
|E_{l,out}^{dh,2}|^2 &= \frac{|g_1|^2}{4}[((A_l)^2+(V_A)^2) \\
&((\sqrt{1-\delta_{180}})^2 + (\alpha_{lcp}\sqrt{1+\delta_{180}})^2 - 2\alpha_{lcp}\sqrt{1+\delta_{180}}\sqrt{1-\delta_{180}}cos(\beta_{lcp})) \\
&+ ((B_l)^2+(V_B)^2) \\
&((\sqrt{1+\delta_{180}})^2 + (\alpha_{lcp}\sqrt{1-\delta_{180}})^2 + 2\alpha_{lcp}\sqrt{1+\delta_{180}}\sqrt{1-\delta_{180}}cos(\Delta\phi_l+\beta_{lcp}))]
\end{aligned}
\tag{2.82}
$$

2. **Lower branches: RCP**

$$
\begin{aligned}
|E_{r,out}^{dh,3}|^2 &= \frac{|g_3|^2\alpha_{rl}^2}{4}[((A_r)^2+(V_A)^2) \\
&((\sqrt{1-\delta_{180}})^2 + (\alpha_{rcp}\sqrt{1+\delta_{180}})^2 + 2\alpha_{rcp}\sqrt{1+\delta_{180}}\sqrt{1-\delta_{180}}cos(\beta_{rcp})) \\
&+ ((B_r)^2+(V_B)^2) \\
&((\sqrt{1+\delta_{180}})^2 + (\alpha_{rcp}\sqrt{1-\delta_{180}})^2 - 2\alpha_{rcp}\sqrt{1+\delta_{180}}\sqrt{1-\delta_{180}}cos(\Delta\phi_r+\beta_{rcp}))]
\end{aligned}
\tag{2.83}
$$

$$
\begin{aligned}
|E_{r,out}^{dh,4}|^2 &= \frac{|g_3|^2\alpha_{rl}^2}{4}[((A_r)^2+(V_A)^2) \\
&((\sqrt{1-\delta_{180}})^2 + (\alpha_{rcp}\sqrt{1+\delta_{180}})^2 - 2\alpha_{rcp}\sqrt{1+\delta_{180}}\sqrt{1-\delta_{180}}cos(\beta_{rcp})) \\
&+ ((B_r)^2+(V_B)^2) \\
&((\sqrt{1+\delta_{180}})^2 + (\alpha_{rcp}\sqrt{1-\delta_{180}})^2 + 2\alpha_{rcp}\sqrt{1+\delta_{180}}\sqrt{1-\delta_{180}}cos(\Delta\phi_r+\beta_{rcp}))]
\end{aligned}
\tag{2.84}
$$

Note that in relations (2.81) to (2.84), uncorrelated terms have been eliminated. Here we have assumed that the horn *Ant* and *Ref* voltages (for both polarizations) and the noise diode voltages ($V_{A,B}$) are uncorrelated. Hence terms like $< A_l * B_l >$, $< A_r * V_A >$, or $< B_r * V_B >$[5] are equal to zero.

2.3.5.3 Stokes parameters calculation from complete calibration model

Considering the previous sections and taking the relations of Stokes parameters for circular basis, the Stokes parameters for KuPol receiver from the *complete model* are

- **Horn Ant.**

$$
\begin{aligned}
I_A = \frac{1}{4}[&|g_1|^2[((A_l)^2 + (V_A)^2) \\
&((\sqrt{1-\delta_{180}})^2 + (\alpha_{lcp}\sqrt{1+\delta_{180}})^2 + 2\alpha_{lcp}\sqrt{1+\delta_{180}}\sqrt{1-\delta_{180}}cos(\beta_{lcp})) \\
&+ ((B_l)^2 + (V_B)^2) \\
&((\sqrt{1+\delta_{180}})^2 + (\alpha_{lcp}\sqrt{1-\delta_{180}})^2 - 2\alpha_{lcp}\sqrt{1+\delta_{180}}\sqrt{1-\delta_{180}}cos(\Delta\phi_l + \beta_{lcp}))] \\
&+ |g_3|^2\alpha_{rl}^2[((A_r)^2 + (V_A)^2) \\
&((\sqrt{1-\delta_{180}})^2 + (\alpha_{rcp}\sqrt{1+\delta_{180}})^2 + 2\alpha_{rcp}\sqrt{1+\delta_{180}}\sqrt{1-\delta_{180}}cos(\beta_{rcp})) \\
&+ ((B_r)^2 + (V_B)^2) \\
&((\sqrt{1+\delta_{180}})^2 + (\alpha_{rcp}\sqrt{1-\delta_{180}})^2 - 2\alpha_{rcp}\sqrt{1+\delta_{180}}\sqrt{1-\delta_{180}}cos(\Delta\phi_r + \beta_{rcp}))]]
\end{aligned}
\tag{2.85}
$$

$$
\begin{aligned}
Q_A = \frac{g_1 g_3 \alpha_{rl}}{2}&[[A_l(\sqrt{1-\delta_{180}}cos(\theta_A + \delta_A) + \sqrt{1+\delta_{180}}\alpha_{lcp}cos(\theta_A + \delta_A - \beta_{lcp})) \\
&+ V_A(\sqrt{1-\delta_{180}} + \sqrt{1+\delta_{180}}\alpha_{lcp}cos(\beta_{lcp})) \\
&+ B_l(\sqrt{1+\delta_{180}}cos(\theta_B + \delta_B) - \sqrt{1-\delta_{180}}\alpha_{lcp}cos(\theta_B + \delta_B - \Delta\phi_l - \beta_{lcp})) \\
&+ V_B(\sqrt{1+\delta_{180}} - \sqrt{1-\delta_{180}}\alpha_{lcp}cos(\Delta\phi_l + \beta_{lcp}))] \\
&* [A_r(\sqrt{1-\delta_{180}}cos(\theta_A + \beta_{rl}) + \sqrt{1+\delta_{180}}\alpha_{rcp}cos(\theta_A + \beta_{rl} + \beta_{rcp})) \\
&+ V_A(\sqrt{1-\delta_{180}}cos(\beta_{rl}) + \sqrt{1+\delta_{180}}\alpha_{rcp}cos(\beta_{rl} + \beta_{rcp})) \\
&+ B_r(\sqrt{1+\delta_{180}}cos(\theta_B + \beta_{rl}) - \sqrt{1-\delta_{180}}\alpha_{rcp}cos(\theta_B + \beta_{rl} + \Delta\phi_l + \beta_{rcp})) \\
&+ V_B(\sqrt{1+\delta_{180}}cos(\beta_{rl}) - \sqrt{1-\delta_{180}}\alpha_{rcp}cos(\beta_{rl} + \Delta\phi_l + \beta_{rcp}))] \\
&- [A_l(\sqrt{1-\delta_{180}}sin(\theta_A + \delta_A) + \sqrt{1+\delta_{180}}\alpha_{lcp}sin(\theta_A + \delta_A - \beta_{lcp})) \\
&- V_A\sqrt{1+\delta_{180}}\alpha_{lcp}sin(\beta_{lcp}) \\
&+ B_l(\sqrt{1+\delta_{180}}sin(\theta_B + \delta_B) - \sqrt{1-\delta_{180}}\alpha_{lcp}sin(\theta_B + \delta_B - \Delta\phi_r - \beta_{lcp})) \\
&+ V_B\sqrt{1-\delta_{180}}\alpha_{lcp}sin(\Delta\phi_r + \beta_{lcp})] \\
&* [A_r(\sqrt{1-\delta_{180}}sin(\theta_A + \beta_{rl}) + \sqrt{1+\delta_{180}}\alpha_{rcp}sin(\theta_A + \beta_{rl} + \beta_{rcp})) \\
&+ V_A(\sqrt{1-\delta_{180}}sin(\beta_{rl}) + \sqrt{1+\delta_{180}}\alpha_{rcp}sin(\beta_{rl} + \beta_{rcp})) \\
&+ B_r(\sqrt{1+\delta_{180}}sin(\theta_B + \beta_{rl}) - \sqrt{1-\delta_{180}}\alpha_{rcp}sin(\theta_B + \beta_{rl} + \Delta\phi_r + \beta_{rcp})) \\
&+ V_B(\sqrt{1+\delta_{180}}sin(\beta_{rl}) - \sqrt{1-\delta_{180}}\alpha_{rcp}sin(\beta_{rl} + \Delta\phi_r + \beta_{rcp}))]]
\end{aligned}
\tag{2.86}
$$

[5] Note that $< ... >$ denotes temporal averages.

$$
\begin{aligned}
U_A = \frac{g_1 g_3 \alpha_{rl}}{2}[&[A_l(\sqrt{1-\delta_{180}}cos(\theta_A+\delta_A)+\sqrt{1+\delta_{180}}\alpha_{lcp}cos(\theta_A+\delta_A-\beta_{lcp}))\\
&+V_A(\sqrt{1-\delta_{180}}+\sqrt{1+\delta_{180}}\alpha_{lcp}cos(\beta_{lcp}))\\
&+B_l(\sqrt{1+\delta_{180}}cos(\theta_B+\delta_B)-\sqrt{1-\delta_{180}}\alpha_{lcp}cos(\theta_B+\delta_B-\Delta\phi_l-\beta_{lcp}))\\
&+V_B(\sqrt{1+\delta_{180}}-\sqrt{1-\delta_{180}}\alpha_{lcp}cos(\Delta\phi_l+\beta_{lcp}))]\\
&*[A_r(\sqrt{1-\delta_{180}}sin(\theta_A+\beta_{rl})+\sqrt{1+\delta_{180}}\alpha_{rcp}sin(\theta_A+\beta_{rl}+\beta_{rcp}))\\
&+V_A(\sqrt{1-\delta_{180}}sin(\beta_{rl})+\sqrt{1+\delta_{180}}\alpha_{rcp}sin(\beta_{rl}+\beta_{rcp}))\\
&+B_r(\sqrt{1+\delta_{180}}sin(\theta_B+\beta_{rl})-\sqrt{1-\delta_{180}}\alpha_{rcp}sin(\theta_B+\beta_{rl}+\Delta\phi_l+\beta_{rcp}))\\
&+V_B(\sqrt{1+\delta_{180}}sin(\beta_{rl})-\sqrt{1-\delta_{180}}\alpha_{rcp}sin(\beta_{rl}+\Delta\phi_l+\beta_{rcp})]\\
&+[A_l(\sqrt{1-\delta_{180}}sin(\theta_A+\delta_A)+\sqrt{1+\delta_{180}}\alpha_{lcp}sin(\theta_A+\delta_A-\beta_{lcp}))\\
&-V_A\sqrt{1+\delta_{180}}\alpha_{lcp}sin(\beta_{lcp})\\
&+B_l(\sqrt{1+\delta_{180}}sin(\theta_B+\delta_B)-\sqrt{1-\delta_{180}}\alpha_{lcp}sin(\theta_B+\delta_B-\Delta\phi_r-\beta_{lcp}))\\
&+V_B\sqrt{1-\delta_{180}}\alpha_{lcp}sin(\Delta\phi_r+\beta_{lcp})]\\
&*[A_r(\sqrt{1-\delta_{180}}cos(\theta_A+\beta_{rl})-\sqrt{1+\delta_{180}}\alpha_{rcp}cos(\theta_A+\beta_{rl}+\beta_{rcp}))\\
&+V_A(\sqrt{1-\delta_{180}}cos(\beta_{rl})-\sqrt{1+\delta_{180}}\alpha_{rcp}cos(\beta_{rl}+\beta_{rcp}))\\
&+B_r(\sqrt{1+\delta_{180}}cos(\theta_B+\beta_{rl})+\sqrt{1-\delta_{180}}\alpha_{rcp}cos(\theta_B+\beta_{rl}+\Delta\phi_r+\beta_{rcp}))\\
&+V_B(\sqrt{1+\delta_{180}}cos(\beta_{rl})+\sqrt{1-\delta_{180}}\alpha_{rcp}cos(\beta_{rl}+\Delta\phi_r+\beta_{rcp}))]]
\end{aligned}
\tag{2.87}
$$

$$
\begin{aligned}
V_A = \frac{1}{4}[&|g_1|^2[((A_l)^2+(V_A)^2)\\
&((\sqrt{1-\delta_{180}})^2+(\alpha_{lcp}\sqrt{1+\delta_{180}})^2+2\alpha_{lcp}\sqrt{1+\delta_{180}}\sqrt{1-\delta_{180}}cos(\beta_{lcp}))\\
&+((B_l)^2+(V_B)^2)\\
&((\sqrt{1+\delta_{180}})^2+(\alpha_{lcp}\sqrt{1-\delta_{180}})^2-2\alpha_{lcp}\sqrt{1+\delta_{180}}\sqrt{1-\delta_{180}}cos(\Delta\phi_l+\beta_{lcp}))]\\
&-|g_3|^2\alpha_{rl}^2[((A_r)^2+(V_A)^2)\\
&((\sqrt{1-\delta_{180}})^2+(\alpha_{rcp}\sqrt{1+\delta_{180}})^2+2\alpha_{rcp}\sqrt{1+\delta_{180}}\sqrt{1-\delta_{180}}cos(\beta_{rcp}))\\
&+((B_r)^2+(V_B)^2)\\
&((\sqrt{1+\delta_{180}})^2+(\alpha_{rcp}\sqrt{1-\delta_{180}})^2-2\alpha_{rcp}\sqrt{1+\delta_{180}}\sqrt{1-\delta_{180}}cos(\Delta\phi_r+\beta_{rcp}))]]
\end{aligned}
\tag{2.88}
$$

- **Horn Ref.**

$$
\begin{aligned}
I_B = \frac{1}{4}[&|g_1|^2[((A_l)^2+(V_A)^2)\\
&((\sqrt{1-\delta_{180}})^2+(\alpha_{lcp}\sqrt{1+\delta_{180}})^2-2\alpha_{lcp}\sqrt{1+\delta_{180}}\sqrt{1-\delta_{180}}cos(\beta_{lcp}))\\
&+((B_l)^2+(V_B)^2)\\
&((\sqrt{1+\delta_{180}})^2+(\alpha_{lcp}\sqrt{1-\delta_{180}})^2+2\alpha_{lcp}\sqrt{1+\delta_{180}}\sqrt{1-\delta_{180}}cos(\Delta\phi_l+\beta_{lcp}))]\\
&+|g_3|^2\alpha_{rl}^2[((A_r)^2+(V_A)^2)\\
&((\sqrt{1-\delta_{180}})^2+(\alpha_{rcp}\sqrt{1+\delta_{180}})^2-2\alpha_{rcp}\sqrt{1+\delta_{180}}\sqrt{1-\delta_{180}}cos(\beta_{rcp}))\\
&+((B_r)^2+(V_B)^2)\\
&((\sqrt{1+\delta_{180}})^2+(\alpha_{rcp}\sqrt{1-\delta_{180}})^2+2\alpha_{rcp}\sqrt{1+\delta_{180}}\sqrt{1-\delta_{180}}cos(\Delta\phi_r+\beta_{rcp}))]]
\end{aligned}
\tag{2.89}
$$

$$
\begin{aligned}
Q_B = \frac{g_1 g_3 \alpha_{rl}}{2} & [[A_l(\sqrt{1-\delta_{180}} cos(\theta_A + \delta_A) - \sqrt{1+\delta_{180}} \alpha_{lcp} cos(\theta_A + \delta_A - \beta_{lcp})) \\
& + V_A(\sqrt{1-\delta_{180}} - \sqrt{1+\delta_{180}} \alpha_{lcp} cos(\beta_{lcp})) \\
& + B_l(\sqrt{1+\delta_{180}} cos(\theta_B + \delta_B) + \sqrt{1-\delta_{180}} \alpha_{lcp} cos(\theta_B + \delta_B - \Delta\phi_l - \beta_{lcp})) \\
& + V_B(\sqrt{1+\delta_{180}} + \sqrt{1-\delta_{180}} \alpha_{lcp} cos(\Delta\phi_l + \beta_{lcp}))] \\
& * [A_r(\sqrt{1-\delta_{180}} cos(\theta_A + \beta_{rl}) - \sqrt{1+\delta_{180}} \alpha_{rcp} cos(\theta_A + \beta_{rl} + \beta_{rcp})) \\
& + V_A(\sqrt{1-\delta_{180}} cos(\beta_{rl}) - \sqrt{1+\delta_{180}} \alpha_{rcp} cos(\beta_{rl} + \beta_{rcp})) \\
& + B_r(\sqrt{1+\delta_{180}} cos(\theta_B + \beta_{rl}) + \sqrt{1-\delta_{180}} \alpha_{rcp} cos(\theta_B + \beta_{rl} + \Delta\phi_l + \beta_{rcp})) \\
& + V_B(\sqrt{1+\delta_{180}} cos(\beta_{rl}) + \sqrt{1-\delta_{180}} \alpha_{rcp} cos(\beta_{rl} + \Delta\phi_l + \beta_{rcp}))] \\
& - [A_l(\sqrt{1-\delta_{180}} sin(\theta_A + \delta_A) - \sqrt{1+\delta_{180}} \alpha_{lcp} sin(\theta_A + \delta_A - \beta_{lcp})) \\
& + V_A \sqrt{1+\delta_{180}} \alpha_{lcp} sin(\beta_{lcp}) \\
& + B_l(\sqrt{1+\delta_{180}} sin(\theta_B + \delta_B) + \sqrt{1-\delta_{180}} \alpha_{lcp} sin(\theta_B + \delta_B - \Delta\phi_r - \beta_{lcp})) \\
& - V_B \sqrt{1-\delta_{180}} \alpha_{lcp} sin(\Delta\phi_r + \beta_{lcp})] \\
& * [A_r(\sqrt{1-\delta_{180}} sin(\theta_A + \beta_{rl}) - \sqrt{1+\delta_{180}} \alpha_{rcp} sin(\theta_A + \beta_{rl} + \beta_{rcp})) \\
& + V_A(\sqrt{1-\delta_{180}} sin(\beta_{rl}) - \sqrt{1+\delta_{180}} \alpha_{rcp} sin(\beta_{rl} + \beta_{rcp})) \\
& + B_r(\sqrt{1+\delta_{180}} sin(\theta_B + \beta_{rl}) + \sqrt{1-\delta_{180}} \alpha_{rcp} sin(\theta_B + \beta_{rl} + \Delta\phi_r + \beta_{rcp})) \\
& + V_B(\sqrt{1+\delta_{180}} sin(\beta_{rl}) + \sqrt{1-\delta_{180}} \alpha_{rcp} sin(\beta_{rl} + \Delta\phi_r + \beta_{rcp}))]]
\end{aligned}
\tag{2.90}
$$

$$
\begin{aligned}
U_B = \frac{g_1 g_3 \alpha_{rl}}{2} & [[A_l(\sqrt{1-\delta_{180}} cos(\theta_A + \delta_A) - \sqrt{1+\delta_{180}} \alpha_{lcp} cos(\theta_A + \delta_A - \beta_{lcp})) \\
& + V_A(\sqrt{1-\delta_{180}} - \sqrt{1+\delta_{180}} \alpha_{lcp} cos(\beta_{lcp})) \\
& + B_l(\sqrt{1+\delta_{180}} cos(\theta_B + \delta_B) + \sqrt{1-\delta_{180}} \alpha_{lcp} cos(\theta_B + \delta_B - \Delta\phi_l - \beta_{lcp})) \\
& + V_B(\sqrt{1+\delta_{180}} + \sqrt{1-\delta_{180}} \alpha_{lcp} cos(\Delta\phi_l + \beta_{lcp}))] \\
& * [A_r(\sqrt{1-\delta_{180}} sin(\theta_A + \beta_{rl}) - \sqrt{1+\delta_{180}} \alpha_{rcp} sin(\theta_A + \beta_{rl} + \beta_{rcp})) \\
& + V_A(\sqrt{1-\delta_{180}} sin(\beta_{rl}) - \sqrt{1+\delta_{180}} \alpha_{rcp} sin(\beta_{rl} + \beta_{rcp})) \\
& + B_r(\sqrt{1+\delta_{180}} sin(\theta_B + \beta_{rl}) + \sqrt{1-\delta_{180}} \alpha_{rcp} sin(\theta_B + \beta_{rl} + \Delta\phi_l + \beta_{rcp})) \\
& + V_B(\sqrt{1+\delta_{180}} sin(\beta_{rl}) + \sqrt{1-\delta_{180}} \alpha_{rcp} sin(\beta_{rl} + \Delta\phi_l + \beta_{rcp})] \\
& + [A_l(\sqrt{1-\delta_{180}} sin(\theta_A + \delta_A) - \sqrt{1+\delta_{180}} \alpha_{lcp} sin(\theta_A + \delta_A - \beta_{lcp})) \\
& + V_A \sqrt{1+\delta_{180}} \alpha_{lcp} sin(\beta_{lcp}) \\
& + B_l(\sqrt{1+\delta_{180}} sin(\theta_B + \delta_B) + \sqrt{1-\delta_{180}} \alpha_{lcp} sin(\theta_B + \delta_B - \Delta\phi_r - \beta_{lcp})) \\
& - V_B \sqrt{1-\delta_{180}} \alpha_{lcp} sin(\Delta\phi_r + \beta_{lcp})] \\
& * [A_r(\sqrt{1-\delta_{180}} cos(\theta_A + \beta_{rl}) - \sqrt{1+\delta_{180}} \alpha_{rcp} cos(\theta_A + \beta_{rl} + \beta_{rcp})) \\
& + V_A(\sqrt{1-\delta_{180}} cos(\beta_{rl}) - \sqrt{1+\delta_{180}} \alpha_{rcp} cos(\beta_{rl} + \beta_{rcp})) \\
& + B_r(\sqrt{1+\delta_{180}} cos(\theta_B + \beta_{rl}) + \sqrt{1-\delta_{180}} \alpha_{rcp} cos(\theta_B + \beta_{rl} + \Delta\phi_r + \beta_{rcp})) \\
& + V_B(\sqrt{1+\delta_{180}} cos(\beta_{rl}) + \sqrt{1-\delta_{180}} \alpha_{rcp} cos(\beta_{rl} + \Delta\phi_r + \beta_{rcp}))]]
\end{aligned}
\tag{2.91}
$$

$$
\begin{aligned}
V_B = \frac{1}{4}[&|g_1|^2[((A_l)^2 + (V_A)^2) \\
&((\sqrt{1-\delta_{180}})^2 + (\alpha_{lcp}\sqrt{1+\delta_{180}})^2 - 2\alpha_{lcp}\sqrt{1+\delta_{180}}\sqrt{1-\delta_{180}}cos(\beta_{lcp})) \\
&+ ((B_l)^2 + (V_B)^2) \\
&((\sqrt{1+\delta_{180}})^2 + (\alpha_{lcp}\sqrt{1-\delta_{180}})^2 + 2\alpha_{lcp}\sqrt{1+\delta_{180}}\sqrt{1-\delta_{180}}cos(\Delta\phi_l + \beta_{lcp}))] \\
&- |g_3|^2\alpha_{rl}^2[((A_r)^2 + (V_A)^2) \\
&((\sqrt{1-\delta_{180}})^2 + (\alpha_{rcp}\sqrt{1+\delta_{180}})^2 - 2\alpha_{rcp}\sqrt{1+\delta_{180}}\sqrt{1-\delta_{180}}cos(\beta_{rcp})) \\
&+ ((B_r)^2 + (V_B)^2) \\
&((\sqrt{1+\delta_{180}})^2 + (\alpha_{rcp}\sqrt{1-\delta_{180}})^2 + 2\alpha_{rcp}\sqrt{1+\delta_{180}}\sqrt{1-\delta_{180}}cos(\Delta\phi_r + \beta_{rcp}))]]
\end{aligned}
\tag{2.92}
$$

Note that in relations (2.85) to (2.92), uncorrelated terms have been eliminated. Here we have assumed that the horn Ant and Ref voltages (for both polarizations) and the noise diode voltages ($V_{A,B}$) are uncorrelated. Hence terms like $< A_l * B_l >$, $< A_r * V_A >$, or $< B_r * V_B >$[6] are equal to zero.

Thus, the instrumental Stokes parameters obtained from the complete analytical calibration model and that represent the real operation of the KuPol receiver are the relation (2.85) to (2.92).

[6]Note that $< ... >$ denotes temporal averages.

Chapter 3

Instrumental considerations and diagnosis

The analytical model developed in chapter 2, gives us the opportunity to identify a serie of instrumental parameters that will contribute to the KuPol calibration.
The next diagnosis and considerations will be applicated to the *complete model* presented in the section 2.3.

3.1 Instrumental parameters considerations

3.1.1 180° analog hybrid considerations

In this seccion we will take into account the analyzes presented in appendix C of this thesis, which presents a balance analysis of the four 180° hybrid that were fabricated and are present in the analog instrument of Kupol.
From the figure C.1 we can be seen that the balance parameter for amplitude (δ_{180}) and for phase ($\Delta\phi$). If we consider the results between 13 and 18 GHz, and we assume that the highest gain hybrids have been located in the cryogenic stage and that the worst gain have been located in the cold plate stage (see figure 1.3), the hybrids 1 and 4 will be considered for our analysis. Then, we can consider that $\sim \delta_{180} = 0$ for hybrid 1 and 4.
For the phase balance parameter ($\Delta\phi_{l,r}$), we can not have an approximation since it varies for hybrid 1 and 4. To obtain this parameter, other analyzes are necessary.
Thus, considering the figure 2.1, where ports 1 and 2 correspond to the inputs, and the ports 3 and 4 are the outputs, we obtain that the relations that describe the hybrid outputs signals

from (2.58) and (2.59) are

$$(Output)_3 = \frac{1}{\sqrt{2}}[(Input)_1 + (Input)_4] \tag{3.1}$$

$$(Output)_2 = \frac{1}{\sqrt{2}}[(Input)_1 - e^{\Delta\phi}(Input)_4] \tag{3.2}$$

Now, if we use relations (3.1) and (3.2), for to obtain the 180° analog hybrid output, and we remember that for our work with the instrument, the two upper branches of figure 1.3 are called 1 and 2 (LCP polarization) and that the two lower branches are called 3 and 4 (RCP polarization), the analog hybrids outputs are

1. **Upper branches: LCP**

   (a) Branch 1:

$$E_{l,out}^{ah,1} = \frac{1}{\sqrt{2}}[(A_l e^{-i(\omega t+\theta_A+\delta_A)} + V_A e^{i(\omega t+\gamma_l^A)}) + (B_l e^{-i(\omega t+\theta_B+\delta_B)} + V_B e^{i(\omega t+\gamma_l^B)})] \tag{3.3}$$

   (b) Branch 2:

$$E_{l,out}^{ah,2} = \frac{1}{\sqrt{2}}[(A_l e^{-i(\omega t+\theta_A+\delta_A)} + V_A e^{i(\omega t+\gamma_l^A)}) - e^{i\Delta\phi_l}(B_l e^{-i(\omega t+\theta_B+\delta_B)} + V_B e^{i(\omega t+\gamma_l^B)})] \tag{3.4}$$

2. **Lower branches: RCP**

   (a) Branch 3:

$$E_{l,out}^{ah,3} = \frac{1}{\sqrt{2}}[(A_r e^{i(\omega t+\theta_A)} + V_A e^{i(\omega t+\gamma_r^A)}) + (B_r e^{i(\omega t+\theta_B)} + V_B e^{i(\omega t+\gamma_r^B)})] \tag{3.5}$$

   (b) Branch 4:

$$E_{l,out}^{ah,4} = \frac{1}{\sqrt{2}}[(A_r e^{i(\omega t+\theta_A)} + V_A e^{i(\omega t+\gamma_r^A)}) - e^{i\Delta\phi_r}(B_r e^{i(\omega t+\theta_B)} + V_B e^{i(\omega t+\gamma_r^B)})] \tag{3.6}$$

Remember that KuPol has two 180° analog hybrid. Then $\Delta\phi_l$ corresponds to the phase difference for LCP polarization branches and $\Delta\phi_r$ corresponds to the phase difference for RCP polarization branches.

3.1.2 Instrumental balance corrections parameters (bc)

Taking the same parameters and considerations from 2.3.3 section and now, taking into account that the signals that enter to this stage are the signals that come out of the previous section

((3.3) to (3.6)), the outputs signals from the instrument balance stage are

1. **Upper branches: LCP**

   (a) Branch 1:

$$\begin{aligned} E_{l,out}^{ah,1} &= g_1 E_{l,out}^{ah,1} \\ &= \frac{g_1}{\sqrt{2}}[(A_l e^{-i(\omega t+\theta_A+\delta_A)} + V_A e^{i(\omega t+\gamma_l^A)}) + (B_l e^{-i(\omega t+\theta_B+\delta_B)} + V_B e^{i(\omega t+\gamma_l^B)})] \end{aligned} \tag{3.7}$$

   (b) Branch 2:

$$\begin{aligned} E_{l,out}^{ah,2} &= g_1 \alpha_{lcp} e^{i\beta_{lcp}} E_{l,out}^{ah,2} \\ &= \frac{g_1 \alpha_{lcp} e^{i\beta_{lcp}}}{\sqrt{2}}[(A_l e^{-i(\omega t+\theta_A+\delta_A)} + V_A e^{i(\omega t+\gamma_l^A)}) - e^{i\Delta\phi_l}(B_l e^{-i(\omega t+\theta_B+\delta_B)} + V_B e^{i(\omega t+\gamma_l^B)})] \end{aligned} \tag{3.8}$$

2. **Lower branches: RCP**

   (a) Branch 3:

$$\begin{aligned} E_{l,out}^{ah,3} &= g_3 \alpha_{rl} e^{i\beta_{rl}} E_{r,out}^{ah,3} \\ &= \frac{g_3 \alpha_{rl} e^{i\beta_{rl}}}{\sqrt{2}}[(A_r e^{i(\omega t+\theta_A)} + V_A e^{i(\omega t+\gamma_r^A)}) + (B_r e^{i(\omega t+\theta_B)} + V_B e^{i(\omega t+\gamma_r^B)})] \end{aligned} \tag{3.9}$$

   (b) Branch 4:

$$\begin{aligned} E_{l,out}^{ah,4} &= g_3(\alpha_{rl} e^{i\beta_{rl}})(\alpha_{rcp} e^{i\beta_{rcp}}) E_{r,out}^{ah,4} \\ &= \frac{g_3 \alpha_{rl} e^{i\beta_{rl}} \alpha_{rcp} e^{i\beta_{rcp}}}{\sqrt{2}}[(A_r e^{i(\omega t+\theta_A)} + V_A e^{i(\omega t+\gamma_r^A)}) - e^{i\Delta\phi_r}(B_r e^{i(\omega t+\theta_B)} + V_B e^{i(\omega t+\gamma_r^B)})] \end{aligned} \tag{3.10}$$

The instrument applies a temporal averaging over the signals before the digital hybrid implementation [1]. In particular $A_{l,r}e^{i\omega t}$ and $B_{l,r}e^{i\omega t}$ will be 1. Thus, the signals that enter to the next stages for the *complete model* will be

1. **Upper branches: LCP**

   (a) Branch 1:

$$E_{l,out}^{bc,1} = \frac{g_1}{\sqrt{2}}[(A_l e^{-i(\theta_A+\delta_A)} + V_A) + (B_l e^{-i(\theta_B+\delta_B)} + V_B)] \tag{3.11}$$

[1] For this, $< e^{i\omega t} >= 1$. Note that $< ... >$ symbol denotes temporal averages.

(b) Branch 2:

$$\begin{aligned} E^{bc,2}_{l,out} &= g_1\alpha_{lcp}e^{i\beta_{lcp}}E^{ah,2}_{l,out} \\ &= \frac{g_1\alpha_{lcp}e^{i\beta_{lcp}}}{\sqrt{2}}[(A_l e^{-i(\theta_A+\delta_A)}+V_A)-e^{i\Delta\phi_l}(B_l e^{-i(\theta_B+\delta_B)}+V_B)] \end{aligned} \tag{3.12}$$

2. **Lower branches: RCP**

(a) Branch 3:

$$\begin{aligned} E^{bc,3}_{r,out} &= g_3\alpha_{rl}e^{i\beta_{rl}}E^{ah,3}_{r,out} \\ &= \frac{g_3\alpha_{rl}e^{i\beta_{rl}}}{\sqrt{2}}[(A_r e^{i\theta_A}+V_A)+(B_r e^{i\theta_B}+V_B)] \end{aligned} \tag{3.13}$$

(b) Branch 4:

$$\begin{aligned} E^{bc,4}_{r,out} &= g_3(\alpha_{rl}e^{i\beta_{rl}})(\alpha_{rcp}e^{i\beta_{rcp}})E^{ah,4}_{r,out} \\ &= \frac{g_3\alpha_{rl}e^{i\beta_{rl}}\alpha_{rcp}e^{i\beta_{rcp}}}{\sqrt{2}}[(A_r e^{i\theta_A}+V_A)-e^{i\Delta\phi_r}(B_r e^{i\theta_B}+V_B)] \end{aligned} \tag{3.14}$$

3.1.3 180° digital hybrid (dh)

Using relations (2.19) and (2.20) that correspond to the output signals from a perfect 180° hybrid, and taking into account that the signals that enter to this stage are the signals that come out of the previous section ((3.11) to (3.14)), the new outputs signals from the 180° digital hybrid for KuPol are

1. **Upper branches: LCP**

(a) Branch 1:

$$\begin{aligned} E^{dh,1}_{l,out} &= \frac{1}{\sqrt{2}}[E^{bc,1}_{l,out}+E^{bc,2}_{l,out}] \\ &= \frac{g_1}{2}[(A_l e^{-i(\theta_A+\delta_A)}+V_A)(1+\alpha_{lcp}e^{i\beta_{lcp}}) \\ &+ (B_l e^{-i(\theta_B+\delta_B)}+V_B)(1-\alpha_{lcp}e^{i(\Delta\phi_l+\beta_{lcp})})] \end{aligned} \tag{3.15}$$

(b) Branch 2:

$$\begin{aligned} E_{l,out}^{dh,2} &= \frac{1}{\sqrt{2}}[E_{l,out}^{bc,1} - E_{l,out}^{bc,2}] \\ &= \frac{g_1}{2}[(A_l e^{-i(\theta_A+\delta_A)} + V_A)(1 - \alpha_{lcp} e^{i\beta_{lcp}}) \\ &+ (B_l e^{-i(\theta_B+\delta_B)} + V_B)(1 + \alpha_{lcp} e^{i(\Delta\phi_l+\beta_{lcp})})] \end{aligned} \tag{3.16}$$

2. **Lower branches: RCP**

(a) Branch 3:

$$\begin{aligned} E_{r,out}^{dh,3} &= \frac{1}{\sqrt{2}}[E_{r,out}^{bc,3} + E_{r,out}^{bc,4}] \\ &= \frac{g_3\alpha_{rl}e^{i\beta_{rl}}}{2}[(A_r e^{i\theta_A} + V_A)(1 + \alpha_{rcp} e^{i\beta_{rcp}}) \\ &+ (B_r e^{i\theta_B} + V_B)(1 - \alpha_{rcp} e^{i(\Delta\phi_r+\beta_{rcp})})] \end{aligned} \tag{3.17}$$

(b) Branch 4:

$$\begin{aligned} E_{r,out}^{dh,4} &= \frac{1}{\sqrt{2}}[E_{r,out}^{bc,3} - E_{r,out}^{bc,4}] \\ &= \frac{g_3\alpha_{rl}e^{i\beta_{rl}}}{2}[(A_r e^{i\theta_A} + V_A)(1 - \alpha_{rcp} e^{i\beta_{rcp}}) \\ &+ (B_r e^{i\theta_B} + V_B)(1 + \alpha_{rcp} e^{i(\Delta\phi_r+\beta_{rcp})})] \end{aligned} \tag{3.18}$$

3.1.4 Stokes parameters for KuPol receiver considering $\delta_{180} = 0$

In the previous section, we obtained the new outputs for the 180° digital hybrid from the analyzes presented in appendix C, which it was concluded that $\delta_{180} = 0$.
To calculate the new Stokes parameters, we will use the (2.1) to (2.8) relations, that give us the Stokes parameters relations on a circular basis. For to obtain this, we need to identify the real and imaginary components, and the square modules of the previous digital hybrid outputs.

3.1.4.1 Real and imaginary components 180° digital hybrid outputs when $\delta_{180} = 0$

Using the Euler's formula for the complex analysis, the new outputs signals from 180° digital hybrid when $\delta_{180} = 0$ (see relation (3.15) to (3.18)) are:

1. **Uper branches: LCP**

$$\begin{aligned}
E^{dh,1}_{l,out} &= \mathfrak{Re}(E^{dh,1}_{l,out}) + i\mathfrak{Im}(E^{dh,1}_{l,out}) \\
&= \frac{|g_1|}{2}[[A_l(cos(\theta_A+\delta_A)+\alpha_{lcp}cos(\theta_A+\delta_A-\beta_{lcp}))+V_A(1+\alpha_{lcp}cos(\beta_{lcp})) \\
&+ B_l(cos(\theta_B+\delta_B)-\alpha_{lcp}cos(\theta_B+\delta_B-\Delta\phi_l-\beta_{lcp}))+V_B(1-\alpha_{lcp}cos(\Delta\phi_l+\beta_{lcp}))] \\
&- i[A_l(sin(\theta_A+\delta_A)+\alpha_{lcp}sin(\theta_A+\delta_A-\beta_{lcp}))-V_A\alpha_{lcp}sin(\beta_{lcp}) \\
&+ B_l(sin(\theta_B+\delta_B)-\alpha_{lcp}sin(\theta_B+\delta_B-\Delta\phi_l-\beta_{lcp}))+V_B\alpha_{lcp}sin(\Delta\phi_l+\beta_{lcp})]]
\end{aligned} \tag{3.19}$$

$$\begin{aligned}
E^{dh,2}_{l,out} &= \mathfrak{Re}(E^{dh,2}_{l,out}) + i\mathfrak{Im}(E^{dh,2}_{l,out}) \\
&= \frac{|g_1|}{2}[[A_l(cos(\theta_A+\delta_A)-\alpha_{lcp}cos(\theta_A+\delta_A-\beta_{lcp}))+V_A(1-\alpha_{lcp}cos(\beta_{lcp})) \\
&+ B_l(cos(\theta_B+\delta_B)+\alpha_{lcp}cos(\theta_B+\delta_B-\Delta\phi_l-\beta_{lcp}))+V_B(1+\alpha_{lcp}cos(\Delta\phi_l+\beta_{lcp}))] \\
&- i[A_l(sin(\theta_A+\delta_A)-\alpha_{lcp}sin(\theta_A+\delta_A-\beta_{lcp}))+V_A\alpha_{lcp}sin(\beta_{lcp}) \\
&+ B_l(sin(\theta_B+\delta_B)+\alpha_{lcp}sin(\theta_B+\delta_B-\Delta\phi_l-\beta_{lcp}))-V_B\alpha_{lcp}sin(\Delta\phi_l+\beta_{lcp})]]
\end{aligned} \tag{3.20}$$

2. **Lower branches: RCP**

$$\begin{aligned}
E^{dh,3}_{r,out} &= \mathfrak{Re}(E^{dh,3}_{r,out}) + i\mathfrak{Im}(E^{dh,3}_{r,out}) \\
&= \frac{|g_3|\alpha_{rl}}{2}[[A_r(cos(\theta_A+\beta_{rl})+\alpha_{rcp}cos(\theta_A+\beta_{rl}+\beta_{rcp})) \\
&+ V_A(cos(\beta_{rl})+\alpha_{rcp}cos(\beta_{rl}+\beta_{rcp})) \\
&+ B_r(cos(\theta_B+\beta_{rl})-\alpha_{rcp}cos(\theta_B+\beta_{rl}+\Delta\phi_r+\beta_{rcp})) \\
&+ V_B(cos(\beta_{rl})-\alpha_{rcp}cos(\beta_{rl}+\Delta\phi_r+\beta_{rcp}))] \\
&+ i[A_r(sin(\theta_A+\beta_{rl})+\alpha_{rcp}sin(\theta_A+\beta_{rl}+\beta_{rcp})) \\
&+ V_A(sin(\beta_{rl})+\alpha_{rcp}sin(\beta_{rl}+\beta_{rcp})) \\
&+ B_r(sin(\theta_B+\beta_{rl})-\alpha_{rcp}sin(\theta_B+\beta_{rl}+\Delta\phi_r+\beta_{rcp})) \\
&+ V_B(sin(\beta_{rl})-\alpha_{rcp}sin(\beta_{rl}+\Delta\phi_r+\beta_{rcp}))]]
\end{aligned} \tag{3.21}$$

$$\begin{aligned}
E^{dh,4}_{r,out} &= \mathfrak{Re}(E^{dh,4}_{r,out}) + i\mathfrak{Im}(E^{dh,4}_{r,out}) \\
&= \frac{|g_3|\alpha_{rl}}{2}[[A_r(cos(\theta_A+\beta_{rl})-\alpha_{rcp}cos(\theta_A+\beta_{rl}+\beta_{rcp})) \\
&+ V_A(cos(\beta_{rl})-\sqrt{1+\delta_{180}}\alpha_{rcp}cos(\beta_{rl}+\beta_{rcp})) \\
&+ B_r(cos(\theta_B+\beta_{rl})+\alpha_{rcp}cos(\theta_B+\beta_{rl}+\Delta\phi_r+\beta_{rcp})) \\
&+ V_B(cos(\beta_{rl})+\alpha_{rcp}cos(\beta_{rl}+\Delta\phi_r+\beta_{rcp}))] \\
&+ i[A_r(sin(\theta_A+\beta_{rl})-\alpha_{rcp}sin(\theta_A+\beta_{rl}+\beta_{rcp})) \\
&+ V_A(sin(\beta_{rl})-\alpha_{rcp}sin(\beta_{rl}+\beta_{rcp})) \\
&+ B_r(sin(\theta_B+\beta_{rl})+\alpha_{rcp}sin(\theta_B+\beta_{rl}+\Delta\phi_r+\beta_{rcp})) \\
&+ V_B(sin(\beta_{rl})+\alpha_{rcp}sin(\beta_{rl}+\Delta\phi_r+\beta_{rcp}))]]
\end{aligned} \tag{3.22}$$

3.1.4.2 Square modules 180° digital hybrid outputs when $\delta_{180} = 0$

Taking the square modules of the new relations for the 180° digital hybrid outputs, we have

1. **Upper branches: LCP**

$$\begin{aligned}|E_{l,out}^{dh,1}|^2 = \frac{|g_1|^2}{4}[&((A_l)^2 + (V_A)^2)(1 + \alpha_{lcp}^2 + 2\alpha_{lcp}cos(\beta_{lcp})) \\ &+ ((B_l)^2 + (V_B)^2)(1 + \alpha_{lcp}^2 - 2\alpha_{lcp}cos(\Delta\phi_l + \beta_{lcp}))]\end{aligned} \tag{3.23}$$

$$\begin{aligned}|E_{l,out}^{dh,2}|^2 = \frac{|g_1|^2}{4}[&((A_l)^2 + (V_A)^2)(1 + \alpha_{lcp}^2 - 2\alpha_{lcp}cos(\beta_{lcp})) \\ &+ ((B_l)^2 + (V_B)^2)(1 + \alpha_{lcp}^2 + 2\alpha_{lcp}cos(\Delta\phi_l + \beta_{lcp}))]\end{aligned} \tag{3.24}$$

2. **Lower branches: RCP**

$$\begin{aligned}|E_{r,out}^{dh,3}|^2 = \frac{|g_3|^2\alpha_{rl}^2}{4}[&((A_r)^2 + (V_A)^2)(1 + \alpha_{rcp}^2 + 2\alpha_{rcp}cos(\beta_{rcp})) \\ &+ ((B_r)^2 + (V_B)^2)(1 + \alpha_{rcp}^2 - 2\alpha_{rcp}cos(\Delta\phi_r + \beta_{rcp}))]\end{aligned} \tag{3.25}$$

$$\begin{aligned}|E_{r,out}^{dh,4}|^2 = \frac{|g_3|^2\alpha_{rl}^2}{4}[&((A_r)^2 + (V_A)^2)(1 + \alpha_{rcp}^2 - 2\alpha_{rcp}cos(\beta_{rcp})) \\ &+ ((B_r)^2 + (V_B)^2)(1 + \alpha_{rcp}^2 + 2\alpha_{rcp}cos(\Delta\phi_r + \beta_{rcp}))]\end{aligned} \tag{3.26}$$

Note that in relations (3.23) to (3.26), uncorrelated terms have been eliminated. Here we have assumed that the horn Ant and Ref voltages (for both polarizations) and the noise diode voltages ($V_{A,B}$) are uncorrelated. Hence terms like $< A_l * B_l >$, $< A_r * V_A >$, or $< B_r * V_B >$[2] are equal to zero.

3.1.4.3 Stokes parameters calculation from complete calibration model when $\delta_{180} = 0$

Considering that KuPol 180° analog hybrids are balanced in amplitude ($\delta_{180} = 0$) and taking the relations of Stokes parameters for circular basis, the new Stokes parameters for KuPol receiver are

- **Horn Ant.**

$$\begin{aligned}I_A = \frac{1}{4}[&|g_1|^2[((A_l)^2 + (V_A)^2)(1 + \alpha_{lcp}^2 + 2\alpha_{lcp}cos(\beta_{lcp})) \\ &+ ((B_l)^2 + (V_B)^2)(1 + \alpha_{lcp}^2 - 2\alpha_{lcp}cos(\Delta\phi_l + \beta_{lcp}))] \\ &+ |g_3|^2\alpha_{rl}^2[((A_r)^2 + (V_A)^2)(1 + \alpha_{rcp}^2 + 2\alpha_{rcp}cos(\beta_{rcp})) \\ &+ ((B_r)^2 + (V_B)^2)(1 + \alpha_{rcp}^2 - 2\alpha_{rcp}cos(\Delta\phi_r + \beta_{rcp}))]]\end{aligned} \tag{3.27}$$

[2]Note that $< ... >$ denotes temporal averages.

$$
\begin{aligned}
Q_A = \frac{|g_1||g_3|\alpha_{rl}}{2}[&[A_l(cos(\theta_A+\delta_A)+\alpha_{lcp}cos(\theta_A+\delta_A-\beta_{lcp}))+V_A(1+\alpha_{lcp}cos(\beta_{lcp}))\\
&+B_l(cos(\theta_B+\delta_B)-\alpha_{lcp}cos(\theta_B+\delta_B-\Delta\phi_l-\beta_{lcp}))+V_B(1-\alpha_{lcp}cos(\Delta\phi_l+\beta_{lcp}))]\\
&*[A_r(cos(\theta_A+\beta_{rl})+\alpha_{rcp}cos(\theta_A+\beta_{rl}+\beta_{rcp}))+V_A(cos(\beta_{rl})+\alpha_{rcp}cos(\beta_{rl}+\beta_{rcp}))\\
&+B_r(cos(\theta_B+\beta_{rl})-\alpha_{rcp}cos(\theta_B+\beta_{rl}+\Delta\phi_l+\beta_{rcp}))\\
&+V_B(cos(\beta_{rl})-\alpha_{rcp}cos(\beta_{rl}+\Delta\phi_l+\beta_{rcp}))]\\
&-[A_l(sin(\theta_A+\delta_A)+\alpha_{lcp}sin(\theta_A+\delta_A-\beta_{lcp}))-V_A\alpha_{lcp}sin(\beta_{lcp})\\
&+B_l(sin(\theta_B+\delta_B)-\alpha_{lcp}sin(\theta_B+\delta_B-\Delta\phi_r-\beta_{lcp}))+V_B\alpha_{lcp}sin(\Delta\phi_r+\beta_{lcp})]\\
&*[A_r(sin(\theta_A+\beta_{rl})+\alpha_{rcp}sin(\theta_A+\beta_{rl}+\beta_{rcp}))+V_A(sin(\beta_{rl})+\alpha_{rcp}sin(\beta_{rl}+\beta_{rcp}))\\
&+B_r(sin(\theta_B+\beta_{rl})-\alpha_{rcp}sin(\theta_B+\beta_{rl}+\Delta\phi_r+\beta_{rcp}))\\
&+V_B(sin(\beta_{rl})-\alpha_{rcp}sin(\beta_{rl}+\Delta\phi_r+\beta_{rcp})]]
\end{aligned}
\tag{3.28}
$$

$$
\begin{aligned}
U_A = \frac{|g_1||g_3|\alpha_{rl}}{2}[&[A_l(cos(\theta_A+\delta_A)+\alpha_{lcp}cos(\theta_A+\delta_A-\beta_{lcp}))+V_A(1+\alpha_{lcp}cos(\beta_{lcp}))\\
&+B_l(cos(\theta_B+\delta_B)-\alpha_{lcp}cos(\theta_B+\delta_B-\Delta\phi_l-\beta_{lcp}))+V_B(1-\alpha_{lcp}cos(\Delta\phi_l+\beta_{lcp}))]\\
&*[A_r(sin(\theta_A+\beta_{rl})+\alpha_{rcp}sin(\theta_A+\beta_{rl}+\beta_{rcp}))+V_A(sin(\beta_{rl})+\alpha_{rcp}sin(\beta_{rl}+\beta_{rcp}))\\
&+B_r(sin(\theta_B+\beta_{rl})-\alpha_{rcp}sin(\theta_B+\beta_{rl}+\Delta\phi_l+\beta_{rcp}))\\
&+V_B(sin(\beta_{rl})-\alpha_{rcp}sin(\beta_{rl}+\Delta\phi_l+\beta_{rcp})]\\
&+[A_l(sin(\theta_A+\delta_A)+\alpha_{lcp}sin(\theta_A+\delta_A-\beta_{lcp}))-V_A\alpha_{lcp}sin(\beta_{lcp})\\
&+B_l(sin(\theta_B+\delta_B)-\alpha_{lcp}sin(\theta_B+\delta_B-\Delta\phi_r-\beta_{lcp}))+V_B\alpha_{lcp}sin(\Delta\phi_r+\beta_{lcp})]\\
&*[A_r(cos(\theta_A+\beta_{rl})-\alpha_{rcp}cos(\theta_A+\beta_{rl}+\beta_{rcp}))+V_A(cos(\beta_{rl})-\alpha_{rcp}cos(\beta_{rl}+\beta_{rcp}))\\
&+B_r(cos(\theta_B+\beta_{rl})+\alpha_{rcp}cos(\theta_B+\beta_{rl}+\Delta\phi_r+\beta_{rcp}))\\
&+V_B(cos(\beta_{rl})+\alpha_{rcp}cos(\beta_{rl}+\Delta\phi_r+\beta_{rcp}))]]
\end{aligned}
\tag{3.29}
$$

$$
\begin{aligned}
V_A = \frac{1}{4}[&|g_1|^2[((A_l)^2+(V_A)^2)(1+\alpha_{lcp}^2+2\alpha_{lcp}cos(\beta_{lcp}))\\
&+((B_l)^2+(V_B)^2)(1+\alpha_{lcp}^2-2\alpha_{lcp}cos(\Delta\phi_l+\beta_{lcp}))]\\
&-|g_3|^2\alpha_{rl}^2[((A_r)^2+(V_A)^2)(1+\alpha_{rcp}^2+2\alpha_{rcp}cos(\beta_{rcp}))\\
&+((B_r)^2+(V_B)^2)(1+\alpha_{rcp}^2-2\alpha_{rcp}cos(\Delta\phi_r+\beta_{rcp}))]]
\end{aligned}
\tag{3.30}
$$

- **Horn Ref.**

$$
\begin{aligned}
I_B = \frac{1}{4}[&|g_1|^2[((A_l)^2+(V_A)^2)(1+\alpha_{lcp}^2-2\alpha_{lcp}cos(\beta_{lcp}))\\
&+((B_l)^2+(V_B)^2)(1+\alpha_{lcp}^2+2\alpha_{lcp}cos(\Delta\phi_l+\beta_{lcp}))]\\
&+|g_3|^2\alpha_{rl}^2[((A_r)^2+(V_A)^2)(1+(\alpha_{rcp}^2-2\alpha_{rcp}cos(\beta_{rcp}))\\
&+((B_r)^2+(V_B)^2)(1+\alpha_{rcp}^2+2\alpha_{rcp}cos(\Delta\phi_r+\beta_{rcp}))]]
\end{aligned}
\tag{3.31}
$$

$$
\begin{aligned}
Q_B = \frac{|g_1||g_3|\alpha_{rl}}{2}[&[A_l(cos(\theta_A+\delta_A)-\alpha_{lcp}cos(\theta_A+\delta_A-\beta_{lcp}))+V_A(1-\alpha_{lcp}cos(\beta_{lcp}))\\
&+B_l(cos(\theta_B+\delta_B)+\alpha_{lcp}cos(\theta_B+\delta_B-\Delta\phi_l-\beta_{lcp}))+V_B(1+\alpha_{lcp}cos(\Delta\phi_l+\beta_{lcp}))]\\
&*[A_r(cos(\theta_A+\beta_{rl})-\alpha_{rcp}cos(\theta_A+\beta_{rl}+\beta_{rcp}))+V_A(cos(\beta_{rl})-\alpha_{rcp}cos(\beta_{rl}+\beta_{rcp}))\\
&+B_r(cos(\theta_B+\beta_{rl})+\alpha_{rcp}cos(\theta_B+\beta_{rl}+\Delta\phi_l+\beta_{rcp}))\\
&+V_B(cos(\beta_{rl})+\alpha_{rcp}cos(\beta_{rl}+\Delta\phi_l+\beta_{rcp}))]\\
&-[A_l(sin(\theta_A+\delta_A)-\alpha_{lcp}sin(\theta_A+\delta_A-\beta_{lcp}))+V_A\alpha_{lcp}sin(\beta_{lcp})\\
&+B_l(sin(\theta_B+\delta_B)+\alpha_{lcp}sin(\theta_B+\delta_B-\Delta\phi_r-\beta_{lcp}))-V_B\alpha_{lcp}sin(\Delta\phi_r+\beta_{lcp})]\\
&*[A_r(sin(\theta_A+\beta_{rl})-\alpha_{rcp}sin(\theta_A+\beta_{rl}+\beta_{rcp}))+V_A(sin(\beta_{rl})-\alpha_{rcp}sin(\beta_{rl}+\beta_{rcp}))\\
&+B_r(sin(\theta_B+\beta_{rl})+\alpha_{rcp}sin(\theta_B+\beta_{rl}+\Delta\phi_r+\beta_{rcp}))\\
&+V_B(sin(\beta_{rl})+\alpha_{rcp}sin(\beta_{rl}+\Delta\phi_r+\beta_{rcp}))]]
\end{aligned}
\tag{3.32}
$$

$$
\begin{aligned}
U_B = \frac{|g_1||g_3|\alpha_{rl}}{2}[&[A_l(cos(\theta_A+\delta_A)-\alpha_{lcp}cos(\theta_A+\delta_A-\beta_{lcp}))+V_A(1-\alpha_{lcp}cos(\beta_{lcp}))\\
&+B_l(cos(\theta_B+\delta_B)+\alpha_{lcp}cos(\theta_B+\delta_B-\Delta\phi_l-\beta_{lcp}))+V_B(1+\alpha_{lcp}cos(\Delta\phi_l+\beta_{lcp}))]\\
&*[A_r(sin(\theta_A+\beta_{rl})-\alpha_{rcp}sin(\theta_A+\beta_{rl}+\beta_{rcp}))+V_A(sin(\beta_{rl})-\alpha_{rcp}sin(\beta_{rl}+\beta_{rcp}))\\
&+B_r(sin(\theta_B+\beta_{rl})+\alpha_{rcp}sin(\theta_B+\beta_{rl}+\Delta\phi_l+\beta_{rcp}))\\
&+V_B(sin(\beta_{rl})+\alpha_{rcp}sin(\beta_{rl}+\Delta\phi_l+\beta_{rcp})]\\
&+[A_l(sin(\theta_A+\delta_A)-\alpha_{lcp}sin(\theta_A+\delta_A-\beta_{lcp}))+V_A\alpha_{lcp}sin(\beta_{lcp})\\
&+B_l(sin(\theta_B+\delta_B)+\alpha_{lcp}sin(\theta_B+\delta_B-\Delta\phi_r-\beta_{lcp}))-V_B\alpha_{lcp}sin(\Delta\phi_r+\beta_{lcp})]\\
&*[A_r(cos(\theta_A+\beta_{rl})-\alpha_{rcp}cos(\theta_A+\beta_{rl}+\beta_{rcp}))+V_A(cos(\beta_{rl})-\alpha_{rcp}cos(\beta_{rl}+\beta_{rcp}))\\
&+B_r(cos(\theta_B+\beta_{rl})+\alpha_{rcp}cos(\theta_B+\beta_{rl}+\Delta\phi_r+\beta_{rcp}))\\
&+V_B(cos(\beta_{rl})+\alpha_{rcp}cos(\beta_{rl}+\Delta\phi_r+\beta_{rcp}))]]
\end{aligned}
\tag{3.33}
$$

$$
\begin{aligned}
V_B = \frac{1}{4}[&|g_1|^2[((A_l)^2+(V_A)^2)(1+\alpha_{lcp}^2-2\alpha_{lcp}cos(\beta_{lcp}))\\
&+((B_l)^2+(V_B)^2)(1+\alpha_{lcp}^2+2\alpha_{lcp}cos(\Delta\phi_l+\beta_{lcp}))]\\
&-|g_3|^2\alpha_{rl}^2[((A_r)^2+(V_A)^2)(1+\alpha_{rcp}^2-2\alpha_{rcp}cos(\beta_{rcp}))\\
&+((B_r)^2+(V_B)^2)(1+\alpha_{rcp}^2+2\alpha_{rcp}cos(\Delta\phi_r+\beta_{rcp}))]]
\end{aligned}
\tag{3.34}
$$

Note that in relations (3.27) to (3.34), uncorrelated terms have been eliminated.Here we have assumed that the horn Ant and Ref voltages (for both polarizations) and the noise diode voltages ($V_{A,B}$) are uncorrelated. Hence terms like $< A_l * B_l >$, $< A_r * V_A >$, or $< B_r * V_B >$[3] are equal to zero.

Thus, the instrumental Stokes parameters obtained from the complete analytical calibration model when the analog hybrids are balanced in amplitude ($\delta_{180} = 0$) and that represent the real operation of the KuPol receiver are the relation (3.27) to (3.34).

[3]Note that $< ... >$ denotes temporal averages.

3.1.5 Reduction of Stokes parameters from diodes injection

For the next considerations, we will take into account only the $NOISE$ diode these provide a comparable temperature to the system temperature.
If we consider that $NOISE$ diode, located at the output of each horn, are injected (or not injected) to the system, the new square modules of 180° digital hybrid outputs (relations (3.23) to (3.26)) and the new Stokes parameters for the *complete model* calibration (relations (3.27) to (3.34)), are reduced to the relations that are presented in the following sections.

For the next sections, note that $V_A = V_B = ON$ indicates that $NOISE$ diode was injected on horn Ant branch or horn Ref branch. For other hand, $V_A = V_B = OFF$ indicates that $NOISE$ diode is in state OFF in both branches.

3.1.5.1 Square modules relations for 180° digital hybrid outputs from diodes injection when $\delta_{180} = 0$

1. V_A **ON;** V_B **OFF**
   $NOISE$ diode state ON on horn Ant branch and state OFF on horn Ref branch.

   (a) **Upper branches: LCP**

$$|E_{l,out}^{dh,1}|^2 = \frac{|g_1|^2}{4}((A_l)^2 + (V_A)^2)(1 + \alpha_{lcp}^2 + 2\alpha_{lcp}cos(\beta_{lcp})) \tag{3.35}$$

$$|E_{l,out}^{dh,2}|^2 = \frac{|g_1|^2}{4}((A_l)^2 + (V_A)^2)(1 + \alpha_{lcp}^2 - 2\alpha_{lcp}cos(\beta_{lcp})) \tag{3.36}$$

   (b) **Lower branches: RCP**

$$|E_{r,out}^{dh,3}|^2 = \frac{|g_3|^2\alpha_{rl}^2}{4}((A_r)^2 + (V_A)^2)(1 + \alpha_{rcp}^2 + 2\alpha_{rcp}cos(\beta_{rcp})) \tag{3.37}$$

$$|E_{r,out}^{dh,4}|^2 = \frac{|g_3|^2\alpha_{rl}^2}{4}((A_r)^2 + (V_A)^2)(1 + \alpha_{rcp}^2 - 2\alpha_{rcp}cos(\beta_{rcp})) \tag{3.38}$$

2. V_A **OFF;** V_B **ON**
   $NOISE$ diode state OFF on horn Ant branch and state ON on horn Ref branch.

   (a) **Upper branches: LCP**

$$|E_{l,out}^{dh,1}|^2 = \frac{|g_1|^2}{4}((B_l)^2 + (V_B)^2)(1 + \alpha_{lcp}^2 - 2\alpha_{lcp}cos(\Delta\phi_l + \beta_{lcp})) \tag{3.39}$$

$$|E_{l,out}^{dh,2}|^2 = \frac{|g_1|^2}{4}((B_l)^2 + (V_B)^2)(1 + \alpha_{lcp}^2 + 2\alpha_{lcp}cos(\Delta\phi_l + \beta_{lcp})) \tag{3.40}$$

   (b) **Lower branches: RCP**

$$|E_{r,out}^{dh,3}|^2 = \frac{|g_3|^2\alpha_{rl}^2}{4}((B_r)^2 + (V_B)^2)(1 + \alpha_{rcp}^2 - 2\alpha_{rcp}cos(\Delta\phi_r + \beta_{rcp})) \tag{3.41}$$

$$|E_{r,out}^{dh,4}|^2 = \frac{|g_3|^2\alpha_{rl}^2}{4}((B_r)^2 + (V_B)^2)(1 + \alpha_{rcp}^2 + 2\alpha_{rcp}cos(\Delta\phi_r + \beta_{rcp})) \tag{3.42}$$

3. V_A **OFF;** V_B **OFF**

   $NOISE$ diode state OFF on horn Ant branch and state OFF on horn Ref branch.

   (a) **Upper branches: LCP**

$$|E_{l,out}^{dh,1}|^2 = \frac{|g_1|^2}{4}[(A_l)^2(1 + \alpha_{lcp}^2 + 2\alpha_{lcp}cos(\beta_{lcp})) + (B_l)^2(1 + \alpha_{lcp}^2 - 2\alpha_{lcp}cos(\Delta\phi_l + \beta_{lcp}))] \tag{3.43}$$

$$|E_{l,out}^{dh,2}|^2 = \frac{|g_1|^2}{4}[(A_l)^2(1 + \alpha_{lcp}^2 - 2\alpha_{lcp}cos(\beta_{lcp})) + (B_l)^2(1 + \alpha_{lcp}^2 + 2\alpha_{lcp}cos(\Delta\phi_l + \beta_{lcp}))] \tag{3.44}$$

   (b) **Lower branches: RCP**

$$\begin{aligned}|E_{r,out}^{dh,3}|^2 = \frac{|g_3|^2\alpha_{rl}^2}{4}&[(A_r)^2(1 + \alpha_{rcp}^2 + 2\alpha_{rcp}cos(\beta_{rcp}))\\ &+ (B_r)^2(1 + \alpha_{rcp}^2 - 2\alpha_{rcp}cos(\Delta\phi_r + \beta_{rcp}))]\end{aligned} \tag{3.45}$$

$$\begin{aligned}|E_{r,out}^{dh,4}|^2 = \frac{|g_3|^2\alpha_{rl}^2}{4}&[(A_r)^2(1 + \alpha_{rcp}^2 - 2\alpha_{rcp}cos(\beta_{rcp}))\\ &+ (B_r)^2(1 + \alpha_{rcp}^2 + 2\alpha_{rcp}cos(\Delta\phi_r + \beta_{rcp}))]\end{aligned} \tag{3.46}$$

3.1.5.2 Stokes parameters reduction from diodes injection when $\delta_{180} = 0$

1. V_A **ON;** V_B **OFF**

   $NOISE$ diode state ON on horn Ant branch and state OFF on horn Ref branch.

   - **Horn Ant.**

$$\begin{aligned}I_A = \frac{1}{4}&[|g_1|^2((A_l)^2 + (V_A)^2)(1 + \alpha_{lcp}^2 + 2\alpha_{lcp}cos(\beta_{lcp}))\\ &+ |g_3|^2\alpha_{rl}^2((A_r)^2 + (V_A)^2)(1 + \alpha_{rcp}^2 + 2\alpha_{rcp}cos(\beta_{rcp}))]\end{aligned} \tag{3.47}$$

$$\begin{aligned}Q_A = \frac{|g_1||g_3|\alpha_{rl}}{2}&[[A_l(cos(\theta_A + \delta_A) + \alpha_{lcp}cos(\theta_A + \delta_A - \beta_{lcp})) + V_A(1 + \alpha_{lcp}cos(\beta_{lcp}))]\\ &* [A_r(cos(\theta_A + \beta_{rl}) + \alpha_{rcp}cos(\theta_A + \beta_{rl} + \beta_{rcp})) + V_A(cos(\beta_{rl}) + \alpha_{rcp}cos(\beta_{rl} + \beta_{rcp}))]\\ &- [A_l(sin(\theta_A + \delta_A) + \alpha_{lcp}sin(\theta_A + \delta_A - \beta_{lcp})) - V_A\alpha_{lcp}sin(\beta_{lcp})]\\ &* [A_r(sin(\theta_A + \beta_{rl}) + \alpha_{rcp}sin(\theta_A + \beta_{rl} + \beta_{rcp})) + V_A(sin(\beta_{rl}) + \alpha_{rcp}sin(\beta_{rl} + \beta_{rcp}))]]\end{aligned} \tag{3.48}$$

$$\begin{aligned}U_A = \frac{|g_1||g_3|\alpha_{rl}}{2}&[[A_l(cos(\theta_A + \delta_A) + \alpha_{lcp}cos(\theta_A + \delta_A - \beta_{lcp})) + V_A(1 + \alpha_{lcp}cos(\beta_{lcp}))]\\ &* [A_r(sin(\theta_A + \beta_{rl}) + \alpha_{rcp}sin(\theta_A + \beta_{rl} + \beta_{rcp})) + V_A(sin(\beta_{rl}) + \alpha_{rcp}sin(\beta_{rl} + \beta_{rcp}))]\\ &+ [A_l(sin(\theta_A + \delta_A) + \alpha_{lcp}sin(\theta_A + \delta_A - \beta_{lcp})) - V_A\alpha_{lcp}sin(\beta_{lcp})\\ &* [A_r(cos(\theta_A + \beta_{rl}) - \alpha_{rcp}cos(\theta_A + \beta_{rl} + \beta_{rcp})) + V_A(cos(\beta_{rl}) - \alpha_{rcp}cos(\beta_{rl} + \beta_{rcp}))]]\end{aligned} \tag{3.49}$$

$$\begin{aligned}V_A = \frac{1}{4}&[|g_1|^2((A_l)^2 + (V_A)^2)(1 + \alpha_{lcp}^2 + 2\alpha_{lcp}cos(\beta_{lcp}))\\ &- |g_3|^2\alpha_{rl}^2((A_r)^2 + (V_A)^2)(1 + \alpha_{rcp}^2 + 2\alpha_{rcp}cos(\beta_{rcp}))]\end{aligned} \tag{3.50}$$

- **Horn Ref.**

$$\begin{aligned} I_B = \frac{1}{4}[&|g_1|^2((A_l)^2 + (V_A)^2)(1 + \alpha_{lcp}^2 - 2\alpha_{lcp}cos(\beta_{lcp})) \\ &+ |g_3|^2\alpha_{rl}^2((A_r)^2 + (V_A)^2)(1 + \alpha_{rcp}^2 - 2\alpha_{rcp}cos(\beta_{rcp}))] \end{aligned} \tag{3.51}$$

$$\begin{aligned} Q_B = \frac{|g_1||g_3|\alpha_{rl}}{2}&[[A_l(cos(\theta_A + \delta_A) - \alpha_{lcp}cos(\theta_A + \delta_A - \beta_{lcp})) + V_A(1 - \alpha_{lcp}cos(\beta_{lcp}))] \\ &* [A_r(cos(\theta_A + \beta_{rl}) - \alpha_{rcp}cos(\theta_A + \beta_{rl} + \beta_{rcp})) + V_A(cos(\beta_{rl}) - \alpha_{rcp}cos(\beta_{rl} + \beta_{rcp}))] \\ &- [A_l(sin(\theta_A + \delta_A) - \alpha_{lcp}sin(\theta_A + \delta_A - \beta_{lcp})) + V_A\alpha_{lcp}sin(\beta_{lcp})] \\ &* [A_r(sin(\theta_A + \beta_{rl}) - \alpha_{rcp}sin(\theta_A + \beta_{rl} + \beta_{rcp})) + V_A(sin(\beta_{rl}) - \alpha_{rcp}sin(\beta_{rl} + \beta_{rcp}))]] \end{aligned} \tag{3.52}$$

$$\begin{aligned} U_B = \frac{|g_1||g_3|\alpha_{rl}}{2}&[[A_l(cos(\theta_A + \delta_A) - \alpha_{lcp}cos(\theta_A + \delta_A - \beta_{lcp})) + V_A(1 - \alpha_{lcp}cos(\beta_{lcp}))] \\ &* [A_r(sin(\theta_A + \beta_{rl}) - \alpha_{rcp}sin(\theta_A + \beta_{rl} + \beta_{rcp})) + V_A(sin(\beta_{rl}) - \alpha_{rcp}sin(\beta_{rl} + \beta_{rcp}))] \\ &+ [A_l(sin(\theta_A + \delta_A) - \alpha_{lcp}sin(\theta_A + \delta_A - \beta_{lcp})) + V_A\alpha_{lcp}sin(\beta_{lcp})] \\ &* [A_r(cos(\theta_A + \beta_{rl}) - \alpha_{rcp}cos(\theta_A + \beta_{rl} + \beta_{rcp})) + V_A(cos(\beta_{rl}) - \alpha_{rcp}cos(\beta_{rl} + \beta_{rcp}))]] \end{aligned} \tag{3.53}$$

$$\begin{aligned} V_B = \frac{1}{4}[&|g_1|^2((A_l)^2 + (V_A)^2)(1 + \alpha_{lcp}^2 - 2\alpha_{lcp}cos(\beta_{lcp})) \\ &- |g_3|^2\alpha_{rl}^2((A_r)^2 + (V_A)^2)(1 + \alpha_{rcp}^2 - 2\alpha_{rcp}cos(\beta_{rcp}))] \end{aligned} \tag{3.54}$$

2. V_A **OFF;** V_B **ON**
   $NOISE$ diode state OFF on horn Ant branch and state ON on horn Ref branch.

- **Horn Ant.**

$$\begin{aligned} I_A = \frac{1}{4}[&|g_1|^2((B_l)^2 + (V_B)^2)(1 + \alpha_{lcp}^2 - 2\alpha_{lcp}cos(\Delta\phi_l + \beta_{lcp})) \\ &+ |g_3|^2\alpha_{rl}^2((B_r)^2 + (V_B)^2)(1 + \alpha_{rcp}^2 - 2\alpha_{rcp}cos(\Delta\phi_r + \beta_{rcp}))] \end{aligned} \tag{3.55}$$

$$\begin{aligned} Q_A = \frac{|g_1||g_3|\alpha_{rl}}{2}&[B_l(cos(\theta_B + \delta_B) - \alpha_{lcp}cos(\theta_B + \delta_B - \Delta\phi_l - \beta_{lcp})) \\ &+ V_B(1 - \alpha_{lcp}cos(\Delta\phi_l + \beta_{lcp}))] \\ &* [B_r(cos(\theta_B + \beta_{rl}) - \alpha_{rcp}cos(\theta_B + \beta_{rl} + \Delta\phi_l + \beta_{rcp})) \\ &+ V_B(cos(\beta_{rl}) - \alpha_{rcp}cos(\beta_{rl} + \Delta\phi_l + \beta_{rcp}))] \\ &- [B_l(sin(\theta_B + \delta_B) - \alpha_{lcp}sin(\theta_B + \delta_B - \Delta\phi_r - \beta_{lcp})) \\ &+ V_B\alpha_{lcp}sin(\Delta\phi_r + \beta_{lcp})] \\ &* [B_r(sin(\theta_B + \beta_{rl}) - \alpha_{rcp}sin(\theta_B + \beta_{rl} + \Delta\phi_r + \beta_{rcp})) \\ &+ V_B(sin(\beta_{rl}) - \alpha_{rcp}sin(\beta_{rl} + \Delta\phi_r + \beta_{rcp}))] \end{aligned} \tag{3.56}$$

$$
\begin{aligned}
U_A = \frac{|g_1||g_3|\alpha_{rl}}{2}[&[B_l(cos(\theta_B+\delta_B) - \alpha_{lcp}cos(\theta_B+\delta_B-\Delta\phi_l-\beta_{lcp}))\\
&+ V_B(1-\alpha_{lcp}cos(\Delta\phi_l+\beta_{lcp}))]\\
&* [B_r(sin(\theta_B+\beta_{rl}) - \alpha_{rcp}sin(\theta_B+\beta_{rl}+\Delta\phi_l+\beta_{rcp}))\\
&+ V_B(sin(\beta_{rl}) - \alpha_{rcp}sin(\beta_{rl}+\Delta\phi_l+\beta_{rcp})]\\
&+ [B_l(sin(\theta_B+\delta_B) - \alpha_{lcp}sin(\theta_B+\delta_B-\Delta\phi_r-\beta_{lcp}))\\
&+ V_B\alpha_{lcp}sin(\Delta\phi_r+\beta_{lcp})]\\
&* [B_r(cos(\theta_B+\beta_{rl}) + \alpha_{rcp}cos(\theta_B+\beta_{rl}+\Delta\phi_r+\beta_{rcp}))\\
&+ V_B(cos(\beta_{rl}) + \alpha_{rcp}cos(\beta_{rl}+\Delta\phi_r+\beta_{rcp}))]]
\end{aligned}
\tag{3.57}
$$

$$
\begin{aligned}
V_A = \frac{1}{4}[&|g_1|^2((B_l)^2+(V_B)^2)(1+\alpha_{lcp}^2 - 2\alpha_{lcp}cos(\Delta\phi_l+\beta_{lcp}))\\
&- |g_3|^2\alpha_{rl}^2((B_r)^2+(V_B)^2)(1+\alpha_{rcp}^2 - 2\alpha_{rcp}cos(\Delta\phi_r+\beta_{rcp}))]
\end{aligned}
\tag{3.58}
$$

- **Horn Ref.**

$$
\begin{aligned}
I_B = \frac{1}{4}[&|g_1|^2((B_l)^2+(V_B)^2)(1+\alpha_{lcp}^2 + 2\alpha_{lcp}cos(\Delta\phi_l+\beta_{lcp}))]\\
&+ |g_3|^2\alpha_{rl}^2((B_r)^2+(V_B)^2)(1+\alpha_{rcp}^2 + 2\alpha_{rcp}cos(\Delta\phi_r+\beta_{rcp}))]
\end{aligned}
\tag{3.59}
$$

$$
\begin{aligned}
Q_B = \frac{|g_1||g_3|\alpha_{rl}}{2}[&[B_l(cos(\theta_B+\delta_B) + \alpha_{lcp}cos(\theta_B+\delta_B-\Delta\phi_l-\beta_{lcp}))\\
&+ V_B(1+\alpha_{lcp}cos(\Delta\phi_l+\beta_{lcp}))]\\
&* [B_r(cos(\theta_B+\beta_{rl}) + \alpha_{rcp}cos(\theta_B+\beta_{rl}+\Delta\phi_l+\beta_{rcp}))\\
&+ V_B(cos(\beta_{rl}) + \alpha_{rcp}cos(\beta_{rl}+\Delta\phi_l+\beta_{rcp}))]\\
&- [B_l(sin(\theta_B+\delta_B) + \alpha_{lcp}sin(\theta_B+\delta_B-\Delta\phi_r-\beta_{lcp}))\\
&- V_B\alpha_{lcp}sin(\Delta\phi_r+\beta_{lcp})]\\
&* [B_r(sin(\theta_B+\beta_{rl}) + \alpha_{rcp}sin(\theta_B+\beta_{rl}+\Delta\phi_r+\beta_{rcp}))\\
&+ V_B(sin(\beta_{rl}) + \alpha_{rcp}sin(\beta_{rl}+\Delta\phi_r+\beta_{rcp})]]
\end{aligned}
\tag{3.60}
$$

$$
\begin{aligned}
U_B = \frac{|g_1||g_3|\alpha_{rl}}{2}[&[B_l(cos(\theta_B+\delta_B) + \alpha_{lcp}cos(\theta_B+\delta_B-\Delta\phi_l-\beta_{lcp}))\\
&+ V_B(1+\alpha_{lcp}cos(\Delta\phi_l+\beta_{lcp}))]\\
&* [B_r(sin(\theta_B+\beta_{rl}) + \alpha_{rcp}sin(\theta_B+\beta_{rl}+\Delta\phi_l+\beta_{rcp}))\\
&+ V_B(sin(\beta_{rl}) + \alpha_{rcp}sin(\beta_{rl}+\Delta\phi_l+\beta_{rcp})]\\
&+ [B_l(sin(\theta_B+\delta_B) + \alpha_{lcp}sin(\theta_B+\delta_B-\Delta\phi_r-\beta_{lcp}))\\
&- V_B\alpha_{lcp}sin(\Delta\phi_r+\beta_{lcp})]\\
&* [B_r(cos(\theta_B+\beta_{rl}) + \alpha_{rcp}cos(\theta_B+\beta_{rl}+\Delta\phi_r+\beta_{rcp}))\\
&+ V_B(cos(\beta_{rl}) + \alpha_{rcp}cos(\beta_{rl}+\Delta\phi_r+\beta_{rcp}))]]
\end{aligned}
\tag{3.61}
$$

$$
\begin{aligned}
V_B = \frac{1}{4}[&|g_1|^2((B_l)^2+(V_B)^2)(1+\alpha_{lcp}^2 + 2\alpha_{lcp}cos(\Delta\phi_l+\beta_{lcp}))]\\
&- |g_3|^2\alpha_{rl}^2((B_r)^2+(V_B)^2)(1+\alpha_{rcp}^2 + 2\alpha_{rcp}cos(\Delta\phi_r+\beta_{rcp}))]]
\end{aligned}
\tag{3.62}
$$

3. V_A **OFF;** V_B **OFF**

$NOISE$ diode state OFF on horn Ant branch and state OFF on horn Ref branch.

- **Horn Ant.**

$$I_A = \frac{1}{4}[|g_1|^2[A_l^2(1+\alpha_{lcp}^2+2\alpha_{lcp}cos(\beta_{lcp}))+B_l^2(1+\alpha_{lcp}^2-2\alpha_{lcp}cos(\Delta\phi_l+\beta_{lcp}))] + |g_3|^2\alpha_{rl}^2[A_r^2(1+\alpha_{rcp}^2+2\alpha_{rcp}cos(\beta_{rcp}))+B_r^2(1+\alpha_{rcp}^2-2\alpha_{rcp}cos(\Delta\phi_r+\beta_{rcp}))]] \tag{3.63}$$

$$\begin{aligned} Q_A = \frac{|g_1||g_3|\alpha_{rl}}{2}[&[A_l(cos(\theta_A+\delta_A)+\alpha_{lcp}cos(\theta_A+\delta_A-\beta_{lcp})) \\ &+B_l(cos(\theta_B+\delta_B)-\alpha_{lcp}cos(\theta_B+\delta_B-\Delta\phi_l-\beta_{lcp}))] \\ &*[A_r(cos(\theta_A+\beta_{rl})+\alpha_{rcp}cos(\theta_A+\beta_{rl}+\beta_{rcp})) \\ &+B_r(cos(\theta_B+\beta_{rl})-\alpha_{rcp}cos(\theta_B+\beta_{rl}+\Delta\phi_l+\beta_{rcp}))] \\ &-[A_l(sin(\theta_A+\delta_A)+\alpha_{lcp}sin(\theta_A+\delta_A-\beta_{lcp})) \\ &+B_l(sin(\theta_B+\delta_B)-\alpha_{lcp}sin(\theta_B+\delta_B-\Delta\phi_r-\beta_{lcp}))] \\ &*[A_r(sin(\theta_A+\beta_{rl})+\alpha_{rcp}sin(\theta_A+\beta_{rl}+\beta_{rcp})) \\ &+B_r(sin(\theta_B+\beta_{rl})-\alpha_{rcp}sin(\theta_B+\beta_{rl}+\Delta\phi_r+\beta_{rcp}))]] \end{aligned} \tag{3.64}$$

$$\begin{aligned} U_A = \frac{|g_1||g_3|\alpha_{rl}}{2}[&[A_l(cos(\theta_A+\delta_A)+\alpha_{lcp}cos(\theta_A+\delta_A-\beta_{lcp})) \\ &+B_l(cos(\theta_B+\delta_B)-\alpha_{lcp}cos(\theta_B+\delta_B-\Delta\phi_l-\beta_{lcp}))] \\ &*[A_r(sin(\theta_A+\beta_{rl})+\alpha_{rcp}sin(\theta_A+\beta_{rl}+\beta_{rcp})) \\ &+B_r(sin(\theta_B+\beta_{rl})-\alpha_{rcp}sin(\theta_B+\beta_{rl}+\Delta\phi_l+\beta_{rcp}))] \\ &+[A_l(sin(\theta_A+\delta_A)+\alpha_{lcp}sin(\theta_A+\delta_A-\beta_{lcp})) \\ &+B_l(sin(\theta_B+\delta_B)-\alpha_{lcp}sin(\theta_B+\delta_B-\Delta\phi_r-\beta_{lcp}))] \\ &*[A_r(cos(\theta_A+\beta_{rl})-\alpha_{rcp}cos(\theta_A+\beta_{rl}+\beta_{rcp})) \\ &+B_r(cos(\theta_B+\beta_{rl})+\alpha_{rcp}cos(\theta_B+\beta_{rl}+\Delta\phi_r+\beta_{rcp}))]] \end{aligned} \tag{3.65}$$

$$V_A = \frac{1}{4}[|g_1|^2[A_l^2(1+\alpha_{lcp}^2+2\alpha_{lcp}cos(\beta_{lcp}))+B_l^2(1+\alpha_{lcp}^2-2\alpha_{lcp}cos(\Delta\phi_l+\beta_{lcp}))] - |g_3|^2\alpha_{rl}^2[A_r^2(1+\alpha_{rcp}^2+2\alpha_{rcp}cos(\beta_{rcp}))+B_r^2(1+\alpha_{rcp}^2-2\alpha_{rcp}cos(\Delta\phi_r+\beta_{rcp}))]] \tag{3.66}$$

- **Horn Ref.**

$$I_B = \frac{1}{4}[|g_1|^2[A_l^2(1+\alpha_{lcp}^2-2\alpha_{lcp}cos(\beta_{lcp}))+B_l^2(1+\alpha_{lcp}^2+2\alpha_{lcp}cos(\Delta\phi_l+\beta_{lcp}))] + |g_3|^2\alpha_{rl}^2[A_r^2(1+(\alpha_{rcp}^2-2\alpha_{rcp}cos(\beta_{rcp}))+B_r^2(1+\alpha_{rcp}^2+2\alpha_{rcp}cos(\Delta\phi_r+\beta_{rcp}))]] \tag{3.67}$$

$$
\begin{aligned}
Q_B = \frac{|g_1||g_3|\alpha_{rl}}{2}[&[A_l(cos(\theta_A+\delta_A)-\alpha_{lcp}cos(\theta_A+\delta_A-\beta_{lcp}))\\
&+B_l(cos(\theta_B+\delta_B)+\alpha_{lcp}cos(\theta_B+\delta_B-\Delta\phi_l-\beta_{lcp}))]\\
&*[A_r(cos(\theta_A+\beta_{rl})-\alpha_{rcp}cos(\theta_A+\beta_{rl}+\beta_{rcp}))\\
&+B_r(cos(\theta_B+\beta_{rl})+\alpha_{rcp}cos(\theta_B+\beta_{rl}+\Delta\phi_l+\beta_{rcp}))]\\
&-[A_l(sin(\theta_A+\delta_A)-\alpha_{lcp}sin(\theta_A+\delta_A-\beta_{lcp}))\\
&+B_l(sin(\theta_B+\delta_B)+\alpha_{lcp}sin(\theta_B+\delta_B-\Delta\phi_r-\beta_{lcp}))]\\
&*[A_r(sin(\theta_A+\beta_{rl})-\alpha_{rcp}sin(\theta_A+\beta_{rl}+\beta_{rcp}))\\
&+B_r(sin(\theta_B+\beta_{rl})+\alpha_{rcp}sin(\theta_B+\beta_{rl}+\Delta\phi_r+\beta_{rcp}))]]
\end{aligned}
\tag{3.68}
$$

$$
\begin{aligned}
U_B = \frac{|g_1||g_3|\alpha_{rl}}{2}[&[A_l(cos(\theta_A+\delta_A)-\alpha_{lcp}cos(\theta_A+\delta_A-\beta_{lcp}))\\
&+B_l(cos(\theta_B+\delta_B)+\alpha_{lcp}cos(\theta_B+\delta_B-\Delta\phi_l-\beta_{lcp}))]\\
&*[A_r(sin(\theta_A+\beta_{rl})-\alpha_{rcp}sin(\theta_A+\beta_{rl}+\beta_{rcp}))\\
&+B_r(sin(\theta_B+\beta_{rl})+\alpha_{rcp}sin(\theta_B+\beta_{rl}+\Delta\phi_l+\beta_{rcp}))]\\
&+[A_l(sin(\theta_A+\delta_A)-\alpha_{lcp}sin(\theta_A+\delta_A-\beta_{lcp}))\\
&+B_l(sin(\theta_B+\delta_B)+\alpha_{lcp}sin(\theta_B+\delta_B-\Delta\phi_r-\beta_{lcp}))]\\
&*[A_r(cos(\theta_A+\beta_{rl})-\alpha_{rcp}cos(\theta_A+\beta_{rl}+\beta_{rcp}))\\
&+B_r(cos(\theta_B+\beta_{rl})+\alpha_{rcp}cos(\theta_B+\beta_{rl}+\Delta\phi_r+\beta_{rcp}))]]
\end{aligned}
\tag{3.69}
$$

$$
\begin{aligned}
V_B = \frac{1}{4}[&|g_1|^2[A_l^2(1+\alpha_{lcp}^2-2\alpha_{lcp}cos(\beta_{lcp}))+B_l^2(1+\alpha_{lcp}^2+2\alpha_{lcp}cos(\Delta\phi_l+\beta_{lcp}))]\\
&-|g_3|^2\alpha_{rl}^2[A_r^2(1+\alpha_{rcp}^2-2\alpha_{rcp}cos(\beta_{rcp}))+B_r^2(1+\alpha_{rcp}^2+2\alpha_{rcp}cos(\Delta\phi_r+\beta_{rcp}))]]
\end{aligned}
\tag{3.70}
$$

3.2 Diagnostics from analytical calibration model

3.2.1 Isolation parameter

In this section we will analyze the receiver balance through the digital backend looking at the isolation between horns when the noise source is fired in either one of them.

To analize the instrumental isolation parameter between A and B beams (γ), it is neccesary to consider the CAL procedure[4], the diode on and off states, polarization (LCP or RCP), and band number.

The numerical relation for the instrumental isolation parameter is

$$
\boxed{\gamma = \frac{(|A|^2(on)-|A|^2(off))-(|B|^2(on)-|B|^2(off))}{(|A|^2(on)-|A|^2(off))+(|B|^2(on)-|B|^2(off))}}
\tag{3.71}
$$

[4]Note that the output of the CAL and NOISE diodes is measured via the CAL procedure.

It is important to note:

- The perfect value for instrumental isolation parameter should be 1 or -1 depending of the polarization.
- A and B correspond to the signals from horns Ant and Ref respectively.
- The on and off states correspond to the diodes states. To consider the off state in the relation (3.71), allows us to subtract from our analysis the basal noise of the instrument. This is achieved by subtracting the diodes voltages ($V_{A,B}$) from the expressions of the square modules (relations (3.35) to (3.42)).

In particular, the isolation parameter for KuPol instrument for both polarizations is:

$$\boxed{\gamma_{lcp} = \frac{(|E^{dh,1}_{l,out}|^2(on) - |E^{dh,1}_{l,out}|^2(off)) - (|E^{dh,2}_{l,out}|^2(on) - |E^{dh,2}_{l,out}|^2(off))}{(|E^{dh,1}_{l,out}|^2(on) - |E^{dh,1}_{l,out}|^2(off)) + (|E^{dh,2}_{l,out}|^2(on) - |E^{dh,2}_{l,out}|^2(off))}} \tag{3.72}$$

$$\boxed{\gamma_{rcp} = \frac{(|E^{dh,3}_{r,out}|^2(on) - |E^{dh,3}_{r,out}|^2(off)) - (|E^{dh,4}_{r,out}|^2(on) - |E^{dh,4}_{r,out}|^2(off))}{(|E^{dh,3}_{r,out}|^2(on) - |E^{dh,3}_{r,out}|^2(off)) + (|E^{dh,4}_{r,out}|^2(on) - |E^{dh,4}_{r,out}|^2(off))}} \tag{3.73}$$

Note that $E^{dh,1}_{l,out}$, $E^{dh,2}_{l,out}$, $E^{dh,3}_{r,out}$, and $E^{dh,4}_{r,out}$ are the 180° digital hybrid outputs.

Taking the square modules relations for 180° digital hybrid outputs from diodes injection when $\delta_{180} = 0$ (section 3.1.3.1), the isolation parameter for LCP and RCP is

$$\gamma_{lcp} = \frac{2\alpha_{lcp}(V_A^2 cos(\beta_{lcp}) - V_B^2 cos(\Delta\phi_l + \beta_{lcp}))}{(1+\alpha^2_{lcp})(V_A^2 + V_B^2)} \tag{3.74}$$

$$\gamma_{rcp} = \frac{2\alpha_{rcp}(V_A^2 cos(\beta_{rcp}) - V_B^2 cos(\Delta\phi_r + \beta_{rcp})}{(1+\alpha^2_{rcp})(V_A^2 + V_B^2)} \tag{3.75}$$

Note that for both polarizations, the isolation parameter is given by the same instrumental parameters that vary depending on the polarization under study, that is, instrumental balance parameters (α_{lcp} and β_{lcp} for LCP polarization and α_{rcp} and β_{rcp} for RCP polarization), balance parameters of 180° analog hybrid (in particular, phase parameter $\Delta\phi_{l,r}$), and noise diodes voltages (V_A and V_B).

3.2.1.1 Considerations for isolation parameter

1. **Ideal conditions for KuPol**
   If we consider that the 180° analog hybrid does not present imperfections and that KuPol receiver is balanced, the isolation parameter for LCP and RCP polarization is given as

$$\gamma_{lcp} = \frac{V_A^2 - V_B^2}{V_A^2 + V_B^2} \tag{3.76}$$

$$\gamma_{rcp} = \frac{V_A^2 - V_B^2}{V_A^2 + V_B^2} \tag{3.77}$$

Note that according to the operation of KuPol, if we inject a diode to the system at the same time:

- The isolation parameter will be 1 if we inject V_A to the system.
- The isolation parameter will be -1 if we inject V_B to the system.

Both previous values denote perfect isolation.

2. **Isolation parameter from diodes injection**
   If we consider the isolation parameter for KuPol for both polarizations (relations (3.74) and (3.75)) and the diodes ON and OFF states, the isolation parameter for LCP and RCP polarization is given as

   (a) V_A **ON;** V_B **OFF**

$$\gamma_{lcp} = \frac{2\alpha_{lcp} cos(\beta_{lcp})}{1 + \alpha_{lcp}^2} \tag{3.78}$$

$$\gamma_{rcp} = \frac{2\alpha_{rcp} cos(\beta_{rcp})}{1 + \alpha_{rcp}^2} \tag{3.79}$$

   (b) V_A **OFF;** V_B **ON**

$$\gamma_{lcp} = \frac{-2\alpha_{lcp} cos(\Delta\phi_l + \beta_{lcp})}{1 + \alpha_{lcp}^2} \tag{3.80}$$

$$\gamma_{rcp} = \frac{-2\alpha_{rcp} cos(\Delta\phi_r + \beta_{rcp})}{1 + \alpha_{rcp}^2} \tag{3.81}$$

From the previous relations, we can notice that according to our model, under real operating conditions of KuPol, the isolation parameter of the system will be given only by instrumental parameters. Here, it becomes relevant the noise diodes injection on the system, since it is possible to carry out all this analysis.

Chapter 4

Model analysis and future work

4.1 Considerations between complete and simplified analytical calibration model for KuPol receiver

From the relation (2.85) to (2.92), if we consider that the 180° analog hybrid does not present imperfections and that the KuPol receiver is balanced, the following values must be taken into account for the parameters involved:

- **Ideal** 180° **analog hybrid:** $\delta_{180} = \Delta\phi_{l,r} = 0$
- **KuPol receiver balanced:** For amplitude parameters $|g_1| = |g_3| = \alpha_{rl} = \alpha_{rcp} = \alpha_{lcp} = 1$. For phase parameters $\beta_{rl} = \beta_{rcp} = \beta_{lcp} = 0$

Thus, replacing this conditions in (2.85) - (2.92), the instrumental Stokes parameters are expresed by,

- **Horn Ant**

$$I_A = (A_l)^2 + (A_r)^2 + 2V_A^2 \tag{4.1}$$

$$Q_A = A_l A_r cos(2\theta_A + \delta_A) + V_A^2 \tag{4.2}$$

$$U_A = A_l A_r sin(2\theta_A + \delta_A) \tag{4.3}$$

$$V_A = (A_l)^2 - (A_r)^2 \tag{4.4}$$

- **Horn Ref**

$$I_B = (B_l)^2 + (B_r)^2 + 2V_B^2 \tag{4.5}$$

$$Q_B = B_l B_r cos(2\theta_B + \delta_B) + V_B^2 \tag{4.6}$$

$$U_B = B_l B_r sin(2\theta_B + \delta_B) \tag{4.7}$$

$$V_B = (B_l)^2 - (B_r)^2 \tag{4.8}$$

From (4.1) to (4.4), it is possible to note that this coincide with the simplified model Stokes parameters expressions (see (2.41) to (2.48)). Thus, it is possible to elucidate that considering ideal instrumental parameters, our model agrees with the simplified model of KuPol receiver.

4.2 Comments from analytical calibration model for KuPol receiver

4.2.1 Instrumental parameters from isolation parameter

From an analysis of the isolation parameter when the noise diodes are injected to the system, we will obtain relations to describe instrumental balance parameters.

For a particular case, from (3.78) and (3.79) relations, we can note:

- The isolation parameter is maximum when the cosine is maximum, i.e., $cos(\beta_{lcp}) = cos(\beta_{rcp}) = 1$. Thus, $\beta_{lcp} = \beta_{rcp} = 0$.
- The parameters β_{lcp} and β_{rcp} contain instrumental balance effects of the analog and digital instruments. In particular, for the digital instrument, this effect is on the *complex coefficients* that are obtained from the *digital calibration model*. The digital model calibration consists of the determination of complex coefficients for the digital instrument that provide optimal separation of the antenna and reference beams in the digital subchannels. These coefficients are measured with special observations performed at zenith by firing noise diodes. From data delivered by intermediate steps of this model, we can perform α_{lcp} and α_{rcp} sweep so that $cos(\beta_{lcp}) = cos(\beta_{rcp}) = 1$.
- We know that γ_{lcp} and γ_{rcp} are a real number that we have access from the system archive. To calculate the isolation parameter we work with KuPol data enableding it only for CAL procedures, chiefly aimed at monitoring isolation between beams when a *full track* source is being taken for the telescope.

Thus, from the previous points, we can to note that (3.78) and (3.79) given us a cuadratic relation for α_{lcp} and α_{rcp}.

1. α_{lcp} **from** γ_{lcp}

$$\alpha_{lcp}^2 - 2\frac{\alpha_{lcp}}{\gamma_{lcp}} + 1 = 0 \tag{4.9}$$

$$\Rightarrow \alpha_{lcp} = \frac{1 \pm \sqrt{1 - \gamma_{lcp}^2}}{\gamma_{lcp}} \tag{4.10}$$

2. α_{rcp} **from** γ_{rcp}

$$\alpha_{rcp}^2 - 2\frac{\alpha_{rcp}}{\gamma_{rcp}} + 1 = 0 \tag{4.11}$$

$$\Rightarrow \alpha_{rcp} = \frac{1 \pm \sqrt{1-\gamma_{rcp}^2}}{\gamma_{rcp}} \tag{4.12}$$

For our analysis, we only considerate α_{lcp} and α_{rcp} relations that consider the sum of parameters in their numerator, i.e., relations that give us $\alpha_s > 0$. If we consider a instrumental global effect souch that exist a relation between α_{lcp} and outputs signals from branches 1 and 2 for example, such that $\alpha_{lcp} = \frac{E_{l,out}^{bc,2}}{E_{l,out}^{bc,1}}$, and we assign values to the output signals, we can conclude that always $\alpha_{lcp} > 0$.
Using (4.10) and (4.12), and replacing in (3.80) and (3.81) respectively, we can obtain $\Delta\phi_l$ and $\Delta\phi_r$.

1. $\Delta\phi_l$ **from** γ_{lcp}

$$cos(\Delta\phi_l) = \frac{-2\alpha_{lcp}}{\gamma_{lcp}(1+\alpha_{lcp}^2)} \tag{4.13}$$

$$\Rightarrow \Delta\phi_l = arccos\left(\frac{-2\alpha_{lcp}}{\gamma_{lcp}(1+\alpha_{lcp}^2)}\right) \tag{4.14}$$

2. $\Delta\phi_r$ **from** γ_{rcp}

$$cos(\Delta\phi_r) = \frac{-2\alpha_{rcp}}{\gamma_{rcp}(1+\alpha_{rcp}^2)} \tag{4.15}$$

$$\Rightarrow \Delta\phi_r = arccos\left(\frac{-2\alpha_{rcp}}{\gamma_{rcp}(1+\alpha_{rcp}^2)}\right) \tag{4.16}$$

Note that $\Delta\phi_{l,r}$ is the phase balance of the two analog hybrid and that this instrumental value is fixed since it is characteristic of the component.

On the other hand, taking the previous $\Delta\phi_{r,l}$ and if we take the isolation paramater relations when the noise diodes are injected to the system, we can to obtain the instrumental balance parameters α_{lcp}, α_{rcp}, β_{lcp}, and β_{rcp}.
Now, dividing (3.78) for (3.80),

$$\begin{aligned}\frac{\gamma_{lcp}(V_A = ON)}{\gamma_{lcp}(V_B = ON)} &= \frac{1}{cos(\Delta\phi_l) - sin(\Delta\phi_l)tan(\beta_{lcp})} \\ \Rightarrow \beta_{lcp} &= arctan\left(cotan(\Delta\phi_l) - \frac{\gamma_{lcp}(V_B = ON)}{\gamma_{lcp}(V_A = ON)sin(\Delta\phi_l)}\right)\end{aligned} \tag{4.17}$$

So, we have obtained the phase balance of the instrument for polarization LCP. Note that the phase balance of the instrument for polarization RCP is is obtained after dividing (3.79) by

(3.81). Thus,

$$\beta_{rcp} = arctan\left(cotan(\Delta\phi_r) - \frac{\gamma_{rcp}(V_B = ON)}{\gamma_{rcp}(V_A = ON)sin(\Delta\phi_r)}\right) \tag{4.18}$$

Now if we take β_{lcp} and β_{rcp} values and replacing them in (3.78) and (3.79) (or (3.80) and (3.81)), the α_{lcp} and α_{rcp} are obtained.

Thus, from the previous relation we have shown that from an analysis of our analytical calibration model, and in particular, of the isolation parameter, it is possible to obtain the instrumental balance parameters (amplitude and phase) for both polarizations.

The numerical calibration of each of these parameters will be considered in the future scope of this thesis.

4.2.2 Instrumental parameters from Stokes parameters

4.2.2.1 β_{rl} parameter

In particular, if we take the Stokes parameters reductions from diodes injection (Section 3.1.3.2), and considering that $NOISE$ diode voltages are too large compared to the power of the signals that enter the instrument (A_l, A_r, B_l, B_r) [1], we can further reduce the relations (3.47) to (3.62). If we focus on Stokes parameters Q and U and we consider their states on and off, we take:

1. V_A **ON;** V_B **OFF**

   - **Horn Ant.**

$$\begin{aligned}\Delta Q_A &= Q_A(ON) - Q_A(OFF) \\ &= \frac{g_1 g_3 \alpha_{rl}}{2} V_A^2[(1 + \alpha_{lcp}cos(\beta_{lcp}))(cos(\beta_{rl}) + \alpha_{rcp}cos(\beta_{rl} + \beta_{rcp})) \\ &+ \alpha_{lcp}sin(\beta_{lcp})(sin(\beta_{rl}) + \alpha_{rcp}sin(\beta_{rl} + \beta_{rcp}))]\end{aligned} \tag{4.19}$$

$$\begin{aligned}\Delta U_A &= U_A(ON) - U_A(OFF) \\ &= \frac{g_1 g_3 \alpha_{rl}}{2} V_A^2[(1 + \alpha_{lcp}cos(\beta_{lcp}))(sin(\beta_{rl}) + \alpha_{rcp}sin(\beta_{rl} + \beta_{rcp})) \\ &- \alpha_{lcp}sin(\beta_{lcp})(cos(\beta_{rl}) - \alpha_{rcp}cos(\beta_{rl} + \beta_{rcp}))]\end{aligned} \tag{4.20}$$

   - **Horn Ref.**

[1] If we make a real comparison between these quantities, from the KuPol data we can say that the power of the $NOISE$ diodes is $\sim 10^6$ times larger than the signals of the astronomical sources that we used to make the calibration procedure of the telescope

$$\begin{aligned}\Delta Q_B &= Q_B(ON) - Q_B(OFF) \\ &= \frac{g_1 g_3 \alpha_{rl}}{2} V_A^2[(1 - \alpha_{lcp} cos(\beta_{lcp}))(cos(\beta_{rl}) - \alpha_{rcp} cos(\beta_{rl} + \beta_{rcp})) \\ &- \alpha_{lcp} sin(\beta_{lcp})(sin(\beta_{rl}) - \alpha_{rcp} sin(\beta_{rl} + \beta_{rcp}))]\end{aligned} \tag{4.21}$$

$$\begin{aligned}\Delta U_B &= U_B(ON) - U_B(OFF) \\ &= \frac{g_1 g_3 \alpha_{rl}}{2} V_A^2[(1 - \alpha_{lcp} cos(\beta_{lcp}))(sin(\beta_{rl}) - \alpha_{rcp} sin(\beta_{rl} + \beta_{rcp})) \\ &+ \alpha_{lcp} sin(\beta_{lcp})(cos(\beta_{rl}) - \alpha_{rcp} cos(\beta_{rl} + \beta_{rcp}))]\end{aligned} \tag{4.22}$$

2. V_A **OFF;** V_B **ON**

- **Horn Ant.**

$$\begin{aligned}\Delta Q_A &= Q_A(ON) - Q_A(OFF) \\ &= \frac{g_1 g_3 \alpha_{rl}}{2} V_B^2[(1 - \alpha_{lcp} cos(\Delta\phi_l + \beta_{lcp}))(cos(\beta_{rl}) - \alpha_{rcp} cos(\beta_{rl} + \Delta\phi_l + \beta_{rcp})) \\ &- \alpha_{lcp} sin(\Delta\phi_r + \beta_{lcp})(sin(\beta_{rl}) - \alpha_{rcp} sin(\beta_{rl} + \Delta\phi_r + \beta_{rcp})]\end{aligned} \tag{4.23}$$

$$\begin{aligned}\Delta U_A &= U_A(ON) - U_A(OFF) \\ &= \frac{g_1 g_3 \alpha_{rl}}{2} V_B^2[(1 - \alpha_{lcp} cos(\Delta\phi_l + \beta_{lcp}))(sin(\beta_{rl}) - \alpha_{rcp} sin(\beta_{rl} + \Delta\phi_l + \beta_{rcp})] \\ &+ \alpha_{lcp} sin(\Delta\phi_r + \beta_{lcp})(cos(\beta_{rl}) + \alpha_{rcp} cos(\beta_{rl} + \Delta\phi_r + \beta_{rcp}))]\end{aligned} \tag{4.24}$$

- **Horn Ref.**

$$\begin{aligned}\Delta Q_B &= Q_B(ON) - Q_B(OFF) \\ &= \frac{g_1 g_3 \alpha_{rl}}{2} V_B^2[(1 + \alpha_{lcp} cos(\Delta\phi_l + \beta_{lcp}))(cos(\beta_{rl}) + \alpha_{rcp} cos(\beta_{rl} + \Delta\phi_l + \beta_{rcp}))] \\ &+ \alpha_{lcp} sin(\Delta\phi_r + \beta_{lcp})(sin(\beta_{rl}) + \alpha_{rcp} sin(\beta_{rl} + \Delta\phi_r + \beta_{rcp})]\end{aligned} \tag{4.25}$$

$$\begin{aligned}\Delta U_B &= U_B(ON) - U_B(OFF) \\ &= \frac{g_1 g_3 \alpha_{rl}}{2} V_B^2[(1 + \alpha_{lcp} cos(\Delta\phi_l + \beta_{lcp}))(sin(\beta_{rl}) + \alpha_{rcp} sin(\beta_{rl} + \Delta\phi_l + \beta_{rcp})] \\ &- \alpha_{lcp} sin(\Delta\phi_r + \beta_{lcp})(cos(\beta_{rl}) + \alpha_{rcp} cos(\beta_{rl} + \Delta\phi_r + \beta_{rcp}))]\end{aligned} \tag{4.26}$$

From the theory, from the difference of the noise diode on and off spectra, we obtain the phase difference, β_{rl}, between the LCP and RCP channels as

$$\beta_{rl} = arctan\left(\frac{\Delta U}{\Delta Q}\right) \tag{4.27}$$

Then, taking for example, the relations (4.19) and (4.20), we have that β_{rl} is

$$\frac{\Delta U_A}{\Delta Q_A} = \frac{(1 + \alpha_{lcp} cos(\beta_{lcp}))(sin(\beta_{rl}) + \alpha_{rcp} sin(\beta_{rl} + \beta_{rcp})) - \alpha_{lcp} sin(\beta_{lcp})(cos(\beta_{rl}) - \alpha_{rcp} cos(\beta_{rl} + \beta_{rcp}))}{(1 + \alpha_{lcp} cos(\beta_{lcp}))(cos(\beta_{rl}) + \alpha_{rcp} cos(\beta_{rl} + \beta_{rcp})) + \alpha_{lcp} sin(\beta_{lcp})(sin(\beta_{rl}) + \alpha_{rcp} sin(\beta_{rl} + \beta_{rcp}))} \tag{4.28}$$

If we consider the values obtained for α_{lcp}, α_{rcp}, β_{lcp}, and β_{rcp} previously, and the relations (4.27) and (4.28), it is possible to get a β_{rl} parameter reduction from adjustments. This topic will be addressed in future works of this thesis.

4.2.2.2 α_{rl} parameter

If we consider the Stokes parameters relations after the $NOISE$ diodes were injected and we also take the considerations made in the previous section, we can observe that the parameter α_{rl} is conserved in all the relations for Q and U.
If we analyze the behavior of this parameter and the effect that this could have on the instrument, we see that within the instrumental calibration, it will be coupled to the gain terms g_1 and g_3 present in the expressions of Q and U. Therefore, we would expect that we only have a global effect of gain (amplitude) on our data, which makes it impossible to distinguish the term α_{rl} from the rest. The gain effects are going to get calibrated when carrying over the astronomical calibration of the system.
A deep analysis of this parameter and in particular, how it is relevant to KuPol polarization calibration will be considered as future work.

Chapter 5

Conclusion

The polarization study of astronomical sources is a challenge for astronomical instrumentation since it is a challenge for the instrumental developments that this implies.

The KuPol spectropolarimeter is a unique receiver in architecture, which to date has not been calibrated in polarization. Today, this topic takes importance since the polarization study of $AGNs$ for the scientific community becomes relevant.

The usual theorical calibration of this type of instrument is done through mathematical tools that do not ensure a complete and adequate instrumental characterization, which directly affects the instrument calibration. In particular for KuPol, today there is a proposed model (section 1.2.1.3) for its calibration from which very few results have been obtained, therefore more investigation is needed. Independent of this situation, this model does not provide an instance for the study of instrumental parameters relevant to the receiver. For this reason, an analytical calibration model that contributes to the characterization of parameters and instrumental diagnoses for KuPol was developed throughout this thesis.

The proposed analytical calibration model for KuPol provides unique opportunities and advantages so that from isolation parameter diagnosis of the system (to which we have access from the instrumental data) we can study and characterize the operation of the 180° analog hybrid. The model gives us the possibility of obtaining the balance component components (in amplitude and phase). This topic has not been studied until now for KuPol.

Another study advantage from the isolation parameter is the characterization of the system balance parameters (α_{lcp}, α_{rcp}, β_{lcp}, β_{rcp}). From the study and knowledge of these instrumental parameters, we should be able to study the stability of KuPol since it was installed (in 2014) and from this determine periods of time in which exist or not valid data for scientific analysis, i.e., determine what range of data are balanced or not. This topic to date has not been studied for KuPol.
Another important point of analysis and that the model gives us the opportunity to study is the

polarization leakage. For our model, the manifestation of this instrumental problem is related with α_{rl} and β_{rl}. For the α_{rl} we can conclude that it is coupled to the gain terms of branches 3 and 4 of the instrument (g_3) and that its calibration therefore depends on the obtaining and calibration of gain of the branch on analysis. On the other hand, the parameter β_{rl} is obtained from the ON and OFF states of the Stokes Q and U, and corresponds to the *instrumental polarization angle* of KuPol.
Thus, considering the α_{lcp}, α_{rcp}, β_{lcp}, β_{rcp}, α_{rl}, and β_{rl} from the model, we can be able to study the polarization impact on the Stokes parameters.

From all points previously exposed, from the challenge proposed by this thesis, and taking into account that the polarization study with astronomical instruments proposes a great challenge, we can say that this thesis establishes the basis for concrete and powerful instrumental studies in the area of polarimetry and spectropolarimetry astronomical.

Due to time issues related to the duration of this Master Program, it was not possible to carry out a numerical study of the parameters involved in the analytical model proposed for KuPol calibration. For this reason, it is important to say that we do not achieve all the objectives set out at the beginning of this thesis. So in the next section a series of future work related to it is proposed.

5.1 Future works

At this point of the investigation it is necessary to establish some future guidelines that contribute to meet the objectives set at the beginning of this thesis.

1. To obtain instrumental parameters $\Delta\phi_{l,r}$, α_{lcp}, α_{rcp}, β_{lcp}, β_{rcp}, α_{rl}, and β_{rl} from data.
2. To obtain instrumental Stokes parameters for KuPol receiver from data.
3. To contrast our results for Stokes parameter with existing previous results from the 40m collaboration.

Bibliography

[1] Aharonian, F., et al. An exceptional very high energy gamma-ray flare of PKS 2155-304. The Astrophysical Journal, **664**, L71–L74, 2007.

[2] Barres de Almeida, U., et al. Polarimetric tomography of blazar jets. Extragalactic jets from every angle. Proceedings IAU Symposium, **313**, 2014.

[3] Del Toro Iniesta, J. C., Introduction to Spectropolarimetry. *Cambridge University Press, Cambridge*, 2004.

[4] Fromm, C. Spectral Evolution in Blazars. The Case of CTA 102 Springer Theses, 2015.

[5] Hamaker J. P. and Bregman J. D. Understanding radio polarimetry. III. Interpreting the IAU/IEEE definitions of the Stokes parameters. Astron. Astrophys. Suppl. Ser. **117**, 161-165 (1996)

[6] Heiles, C., et al. Mueller matrix parameters for radio telescopes and their observational determination. Astronomical Society of the Pacific, **113**, 1274–1288, 2001.

[7] King, O. G. The KuPol Instrument. Manual, Septiembre 2014.

[8] King, O.G., et al. Astronomical Receiver Modelling Using Scattering Matrices. Monthly Notices of the Royal Astronomical Society **446**, 1252–1267 (2014)

[9] Krolik, J. H. Active galactic nuclei: from the central black hole to the galactic environment. Princeton University Press, 1999.

[10] Kuhn, J. R., et al. A new mechanism for polarizing light from obscured stars. The Astrophysical Journal. **668,1**, L63-L66 (2007).

[11] Manso Sainz, R & Trujillo Bueno, J. Zero-Field Dichroism in the Solar Chromosphere. Physical Review Letters. The American Physical Society. **91**, 11 (2003).

[12] Perlman, E. S., et al. A multiwavelength spectral and polarimetric study of the jet of 3C 264. The Astrophysical Journal, **708**, 171–187, 2010.

[13] Pozar D. M., Microwave Engineering. *Wiley*, 2005.

[14] Punch, M. et al. Detection of TeV photons from the active galaxy Markarian 421. Nature, **358**, 447-478, 1992.

[15] Richards, J., The Radio Variability of Gamma-Ray Blazars. Thesis, California Institute of Technology Pasadena, California. 2012.

[16] Snik, F., Astronomical Polarimetry. New concepts, new instruments, new measurements & observations. Thesis, Utrecht University. 1979.

[17] Socas-Navarro, H., et al. Characterization of telescope polarization properties across the visible and near-infrared spectrum. Astronomy & Astrophysics **531**, (2011)

[18] Tinbergen, J., Astronomical Polarimetry. *Cambridge University Press, Cambridge*, 1996.

[19] Urry, C. M. & Padovani, P. Unified Schemes for Radio-Loud Active Galactic Nuclei. Astronomical Society of the Pacific. **107**, 803-845, 1995.

[20] *https://www.ovro.caltech.edu/*

Appendix A

Polarimetry: Theorical background

A.1 Vector de Coherencia

An electromagnetic signal is polarized if there is any lasting relationship between the orthogonal modes of amplitude and phase [18].
The coherence vector captures this relationship, which is given by:

$$e = \left\langle \begin{bmatrix} E_x E_x^* \\ E_x E_y^* \\ E_y E_x^* \\ E_y E_y^* \end{bmatrix} \right\rangle =< E \otimes E^* > \tag{A.1}$$

where **E** is the complex vector of the orthogonal modes $E_x(t)$ and $E_y(t)$, $< ... >$ indicates the average in time, and $\otimes$ corresponds to the external product.

A.2 Stokes parameters on circular basis

Considering that the relation between linear and circular basis is: $E_x = \frac{1}{\sqrt{2}}(E_r + E_l)$ and $E_y = \frac{1}{\sqrt{2}}(E_r - E_l)$, the Stokes parameters on circular basis are given by

$$\begin{aligned} I =& < |E_x|^2 > + < |E_y|^2 > \\ &= \frac{1}{2}[(E_r + E_l)(E_r^* + E_l^*) + i(-i)(E_r - E_l)(E_r^* - E_l^*)] \\ &= \frac{1}{2}[2E_r E_r^* + 2E_l E_l^*] \\ =& < |E_r|^2 > + < |E_l|^2 > \end{aligned} \tag{A.2}$$

$$
\begin{aligned}
Q =& < |E_x|^2 > - < |E_y|^2 > \\
&= \frac{1}{2}[(E_r + E_l)(E_r^* + E_l^*) - i(-i)(E_r - E_l)(E_r^* - E_l^*)] \\
&= \frac{1}{2}[2E_r E_l^* + 2E_l E_r^*] \\
&= E_r E_l^* + E_l E_r^* \\
&= 2Re(E_l^* E_r)
\end{aligned} \tag{A.3}
$$

$$
\begin{aligned}
U &= 2Re(E_x E_y^*) \\
&=< E_x E_y^* > + < E_x^* E_y > \\
&= \frac{1}{2}[-i(E_r + E_l)(E_r^* - E_l^*) + i(E_r - E_l)(E_r^* + E_l^*)] \\
&= \frac{1}{2}[2iE_r E_l^* - 2iE_l E_r^*] \\
&= i(E_r E_l^* - E_l E_r^*) \\
&= i2iIm(E_l^* E_r) \\
&= -2Im(E_l^* E_r)
\end{aligned} \tag{A.4}
$$

$$
\begin{aligned}
V &= 2Im(E_x E_y^*) \\
&= -i[< E_x E_y^* > - < E_x^* E_y >] \\
&= \frac{-i}{2}[-i(E_r + E_l)(E_r^* - E_l^*) - i(E_r - E_l)(E_r^* + E_l^*)] \\
&= \frac{1}{2}[-2E_r E_l^* + 2E_l E_r^*] \\
&=< |E_l|^2 > - < |E_r|^2 >
\end{aligned} \tag{A.5}
$$

Appendix B

Simulink model of the receiver

Images of the most relevant stages for the polarization calibration model proposed for KuPol from its Simulink design developed by Dr. Oliver King [1].

[1] See Simulink file $rx\_29aug2014.slx$

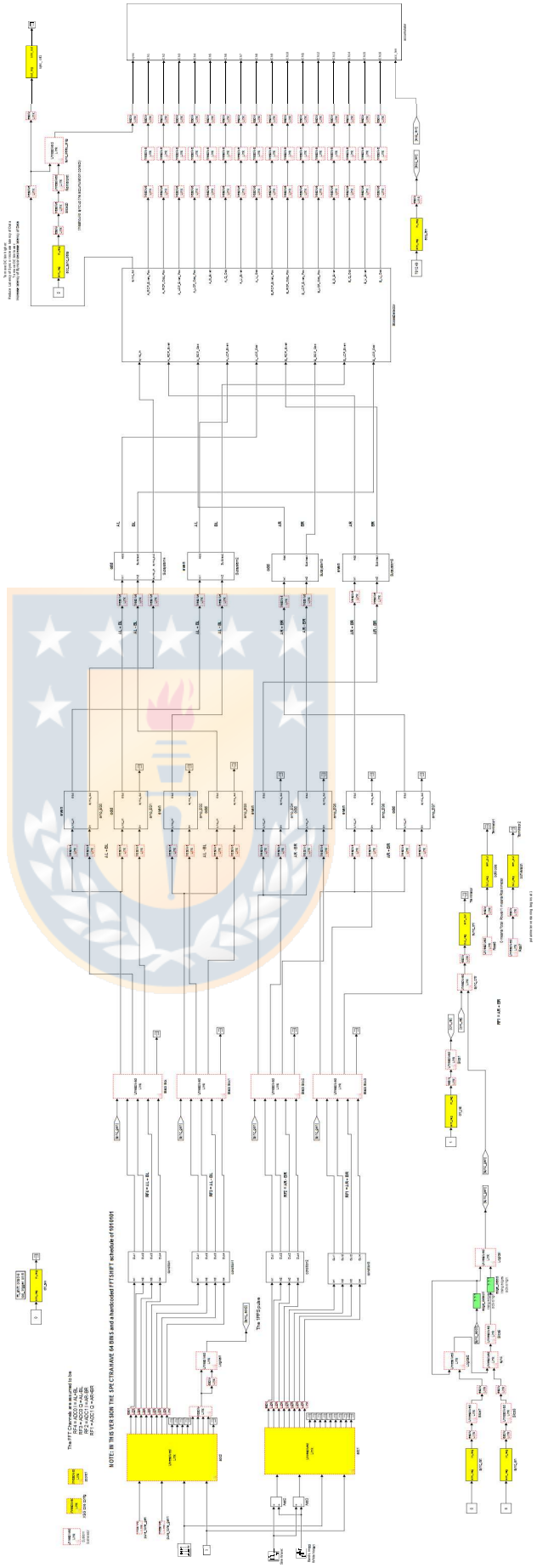

Figure B.1: General view of the KuPol simulink model.
In the image it is possible to see the *digitization and processing data*, and *data readout and archiving* processes are implemented in the KuPol roaches. Source: O. King ($rx\_29aug2014.slx$).

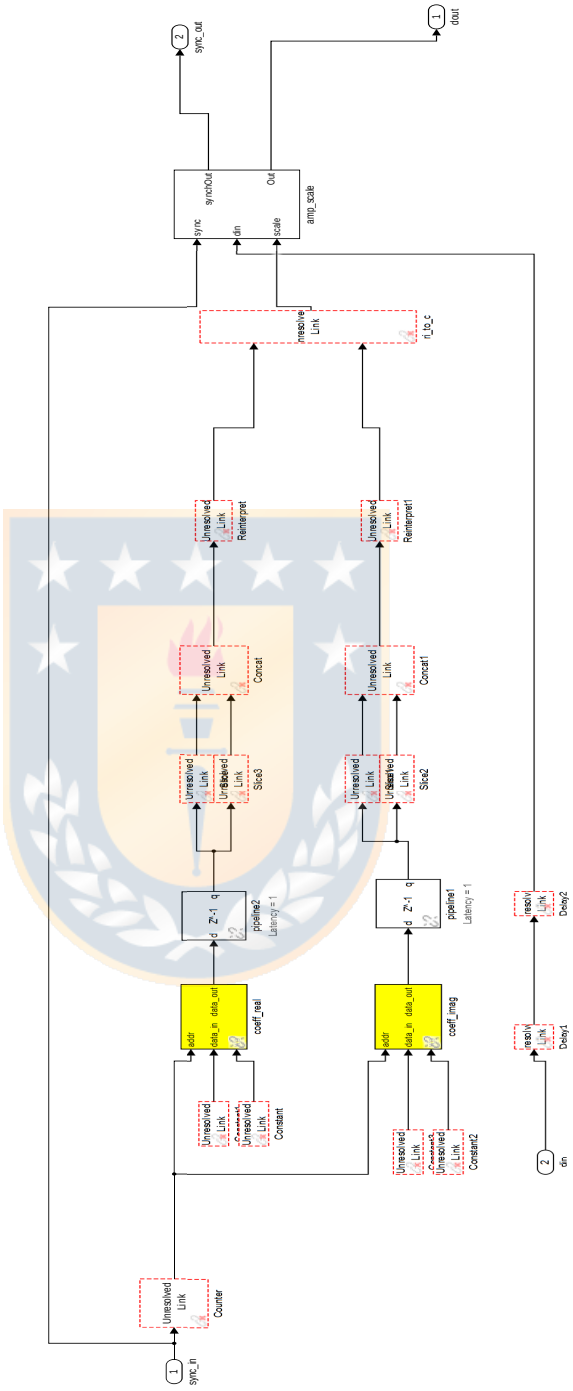

Figure B.2: Implementation of the complex coefficients determination.
The complex coefficients for the digital instrument that provide optimal separation of the antenna and reference beams in the digital sub-channels. Source: O. King ($rx\_29aug2014.slx$).

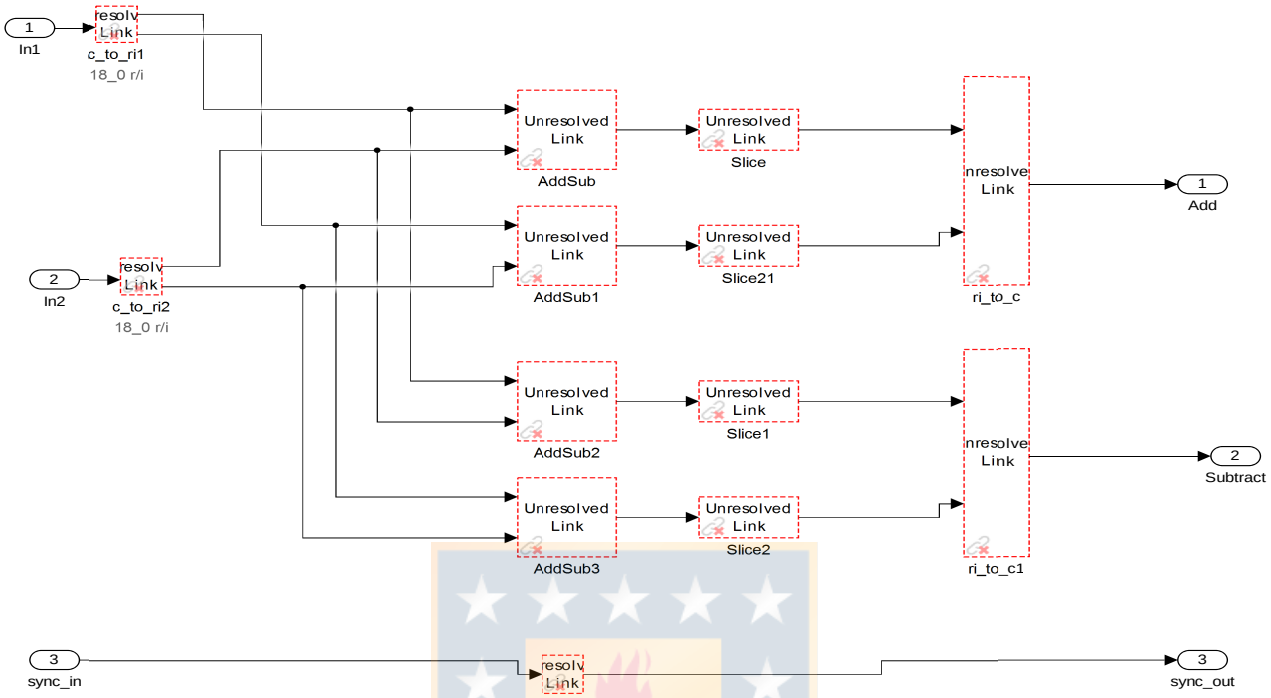

Figure B.3: Mathematical implementation of the digital hybrid on the roaches from Simulink model for KuPol.

Source: O. King (*rx_29aug2014.slx*).

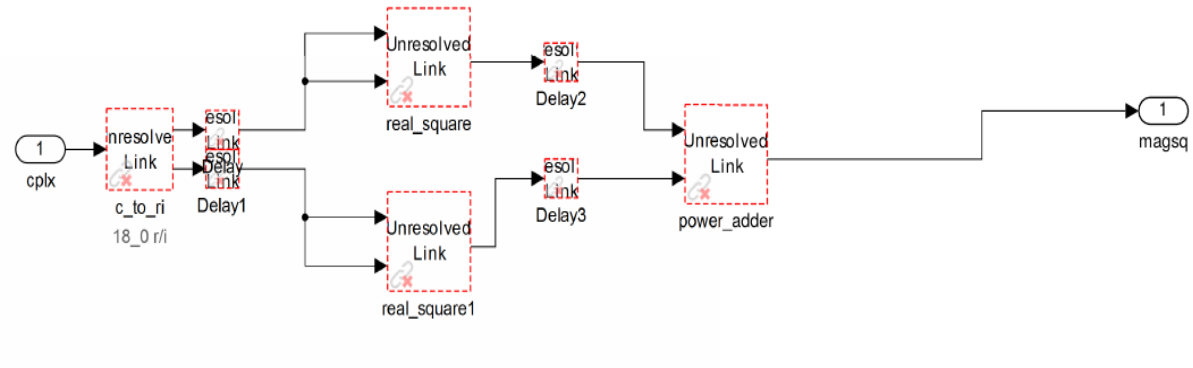

Figure B.4: Mathematical implementation of square module for digital hybrid outputs.
Source: O. King (*rx_29aug2014.slx*).

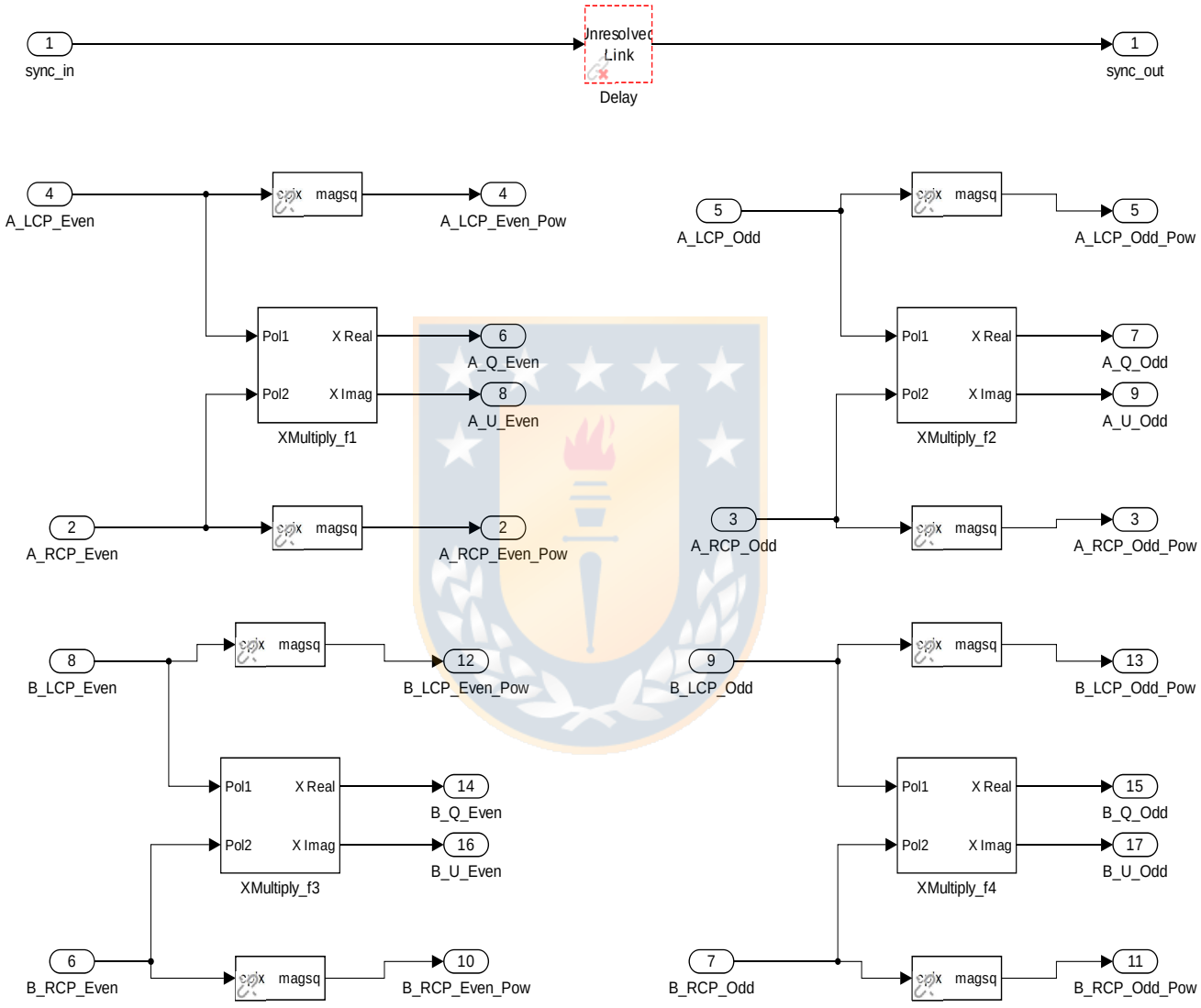

Figure B.5: Mathematical implementation of Q and U Stokes parameters of KuPol instrument. Source: O. King ($rx\_29aug2014.slx$).

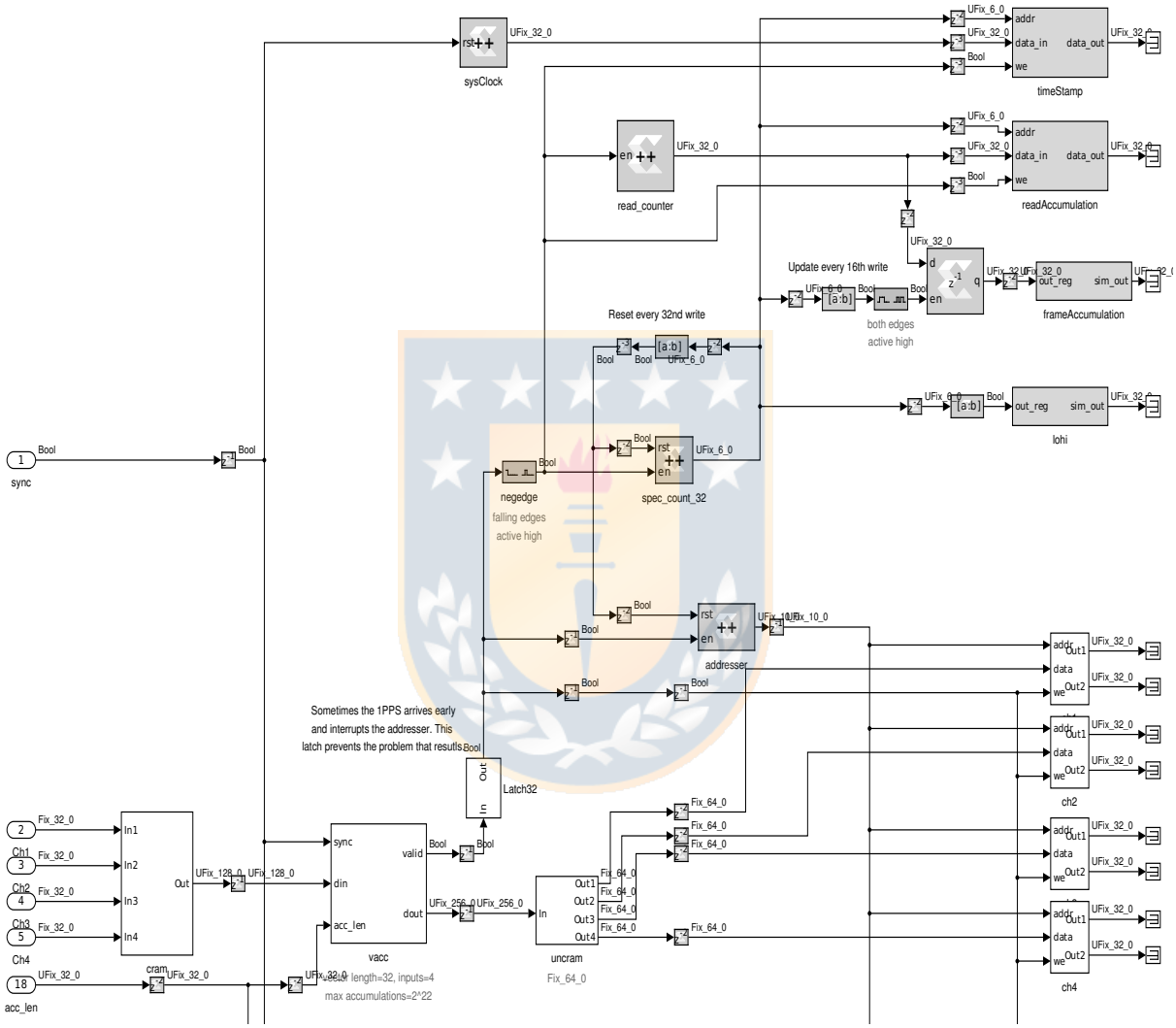

Figure B.6: Part of the Simulink accumulator model.
Here, the data readout and archiving processes are implemented. Source: O. King ($rx\_29aug2014.slx$).

Appendix C

Analog hybrid balance

Based on a series of measurements developed by Oliver King in 2016, it is possible to obtain the balance parameters (amplitude and phase) associated to the 4 hybrids present in the KuPol analogue instrument. These results are showed next,

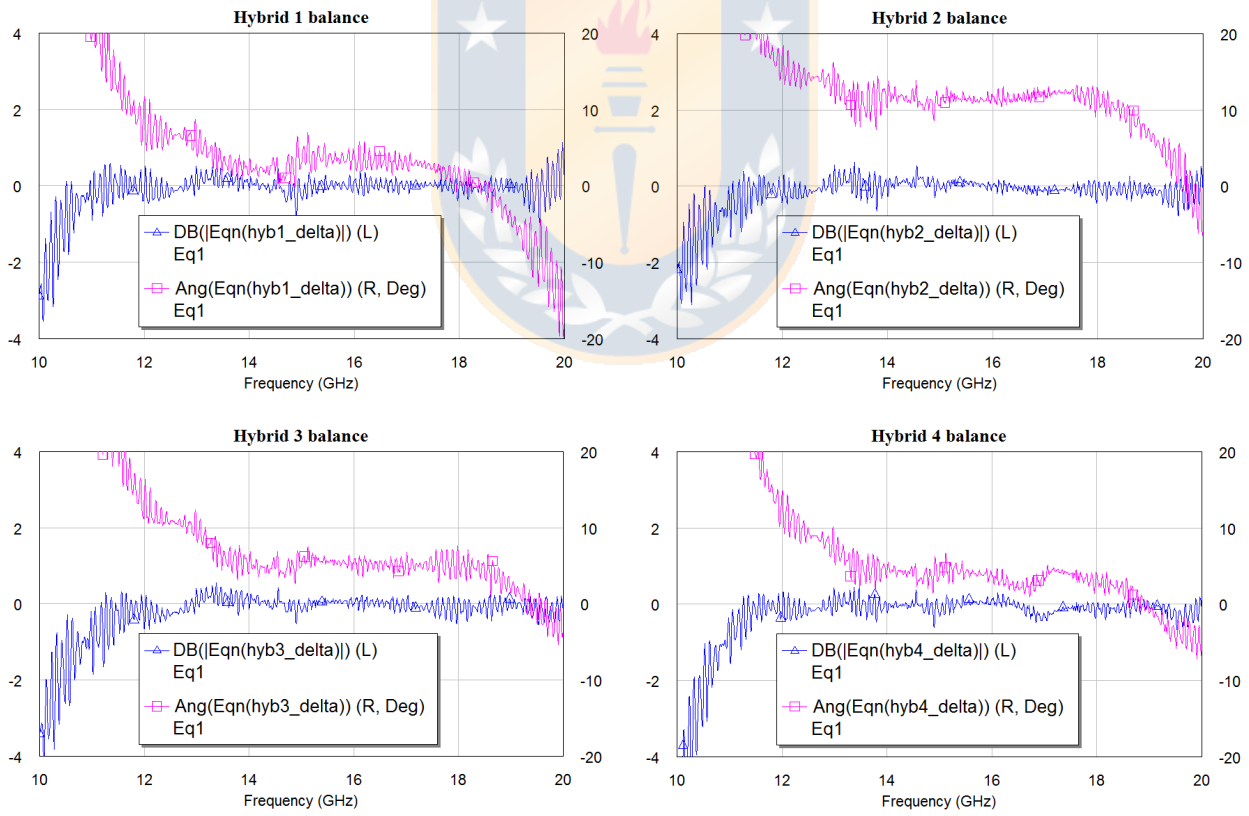

Figure C.1: Balance parameters analog hybrid.
The amplitude (blue) and phase (pink) parameters for hybrid balance are presented for the 4 hybrids located in the KuPol analogue instrument. Source: This plots have been developed by Rodrigo Reeves.

Note that for our analysis we considerate:

- Results between 13 and 18 GHz.
- Hybrids number 1 and 4. We assume that the highest gain hybrids have been located in the cryogenic stage and that the worst gain have been located in the cold plate stage. Therefore, we will consider for our analysis the highest gain hybrids.

From the figure C.1 we can be seen that the balance parameters for the analog hybrid (δ_{180} and $\Delta\phi$) that we consider in our model (see section 2.3.2.) are cero for both hybrids.

Appendix D

Actual KuPol instrument calibration

D.1 Correlation receiver errors

The Mueller matrix $M_{C_{L,R}}$, that describes the action of the correlation receiver, can be expressed by:

$$M_{C_{L,R}} = \begin{bmatrix} M_{CI_{L,R}} & 0 & 0 & 0 \\ 0 & M_{CP}cos(\theta_C) & M_{CP}sin(\theta_C) & 0 \\ 0 & -M_{CP}sin(\theta_C) & M_{CP}cos(\theta_C) & 0 \\ 0 & 0 & 0 & 0 \end{bmatrix} \tag{D.1}$$

where $M_{CI_{L,R}}$ is the gain experienced by the LCP or RCP signals[1], M_{CP} is the gain experienced by the polarized signal, and θ_C is the rotation induced by the instrument of the polarization vector.

It is important to mention that relation D.1 is variable in time as the gains of the amplifiers and response of the whole system changes with time and temperature. The noise diodes are using for to calculate them.

D.1.1 Instrumental calibration from noise diodes

The noise diode signal is described by a Stokes vector (e^{ND}) as

$$e^{ND} = \begin{bmatrix} T_{ND}(t) \\ T_{ND}(t) \\ 0 \\ 0 \end{bmatrix} = e_A^{ND} = e_B^{ND} \tag{D.2}$$

[1]Note that it is the same for horn A and B (balance of the instrument is assumed.

Note that:

- The noise diode Stokes vector is the same for signal from horn Ant and Ref.
- The noise diode is a purely linearly polarirized noise source aligned with $+Q$ in the instrument reference frame.

If we consider the previous relations and we take the difference between the noise diodes states ON and OFF, we get for horn Ant,

$$\begin{aligned}
\Delta e^{A_{L,R}} &= e^{A_{L,R}}(ON) - e^{A_{L,R}}(OFF) \\
&= \begin{bmatrix} A_{L,R} \\ A_Q \\ A_U \\ 0 \end{bmatrix} \\
&= M^A_{C_{L,R}} \Delta e^{ND_A} \\
&= \begin{bmatrix} M^A_{CI_{L,R}} & 0 & 0 & 0 \\ 0 & M^A_{CP} cos(\theta^A_C) & M^A_{CP} sin(\theta^A_C) & 0 \\ 0 & -M^A_{CP} sin(\theta^A_C) & M^A_{CP} cos(\theta^A_C) & 0 \\ 0 & 0 & 0 & 0 \end{bmatrix} \Delta e^{ND_A}
\end{aligned} \tag{D.3}$$

$$\Rightarrow \Delta e^{A_{L,R}} = \Delta T_{ND} \begin{bmatrix} M^A_{CI_{L,R}} \\ M^A_{CP} cos(\theta^A_C) \\ -M^A_{CP} sin(\theta^A_C) \\ 0 \end{bmatrix} \tag{D.4}$$

From D.4 we have for horn Ant the next relations,

$$\Delta A_{L,R} = \Delta T_{ND} M^A_{CI_{L,R}} \tag{D.5}$$

$$\Delta A_Q = \Delta T_{ND} M^A_{CP} cos(\theta^A_C) \tag{D.6}$$

$$\Delta A_U = -\Delta T_{ND} M^A_{CP} sin(\theta^A_C) \tag{D.7}$$

Using D.5, D.6 and D.7, we can to define:

1. **Intensity signal per polarization.**
   From (9),

$$m^A_{L,R} = \Delta T_{ND} M^A_{CI_{L,R}} = \Delta A_{L,R} \tag{D.8}$$

   or

$$\Rightarrow \boxed{m^A_L = \Delta T_{ND} M^A_{CI_L} = \Delta A_L} \tag{D.9}$$

$$\Rightarrow \boxed{m^A_R = \Delta T_{ND} M^A_{CI_R} = \Delta A_R} \tag{D.10}$$

Note that we will track $m_L^A = \Delta A_L$ and $m_R^A = \Delta A_R$ separately. These parameters will vary independently, and will allow us to calculate Stoke V.

2. **Degree of polarization.**
From D.6 and D.7, separately,

$$\Delta A_Q = \Delta T_{ND} M_{CP}^A cos(\theta_C^A)/()^2$$

$$(\Delta A_Q)^2 = (\Delta T_{ND})^2 (M_{CP}^A)^2 cos^2(\theta_C^A) \tag{D.11}$$

$$\Delta A_U = -\Delta T_{ND} M_{CP}^A sin(\theta_C^A)/()^2$$

$$(\Delta A_U)^2 = (\Delta T_{ND})^2 (M_{CP}^A)^2 sin^2(\theta_C^A) \tag{D.12}$$

Adding D.11 and D.12, we can calculate the degree of polarization m_p^A,

$$(\Delta A_Q)^2 + (\Delta A_U)^2 = (\Delta T_{ND})^2 (M_{CP}^A)^2$$

$$\Rightarrow \sqrt{\Delta A_Q)^2 + (\Delta A_U)^2} = \Delta T_{ND} M_{CP}^A$$

$$\Rightarrow \boxed{m_p^A = \sqrt{\Delta A_Q)^2 + (\Delta A_U)^2} = \Delta T_{ND} M_{CP}^A} \tag{D.13}$$

3. **Polarization angle.**
Dividing D.12 in D.11, we can calculate the polarization angle,

$$\frac{\Delta A_U}{\Delta A_Q} = \frac{-\Delta T_{ND} M_{CP}^A sin(\theta_C^A)}{\Delta T_{ND} M_{CP}^A cos(\theta_C^A)} = -tan(\theta_C^A)$$

$$\Rightarrow \boxed{\theta_C^A = -arctan\left(\frac{\Delta A_U}{\Delta A_Q}\right)} \tag{D.14}$$

For other hand, note that for the horn Ref, we have:

1. **Intensity signal per polarization.**

$$\boxed{m_L^B = \Delta T_{ND} M_{CI_L}^B = \Delta B_L} \tag{D.15}$$

$$\boxed{m_R^B = \Delta T_{ND} M_{CI_R}^B = \Delta B_R} \tag{D.16}$$

2. **Degree of polarization.**

$$\boxed{m_p^B = \sqrt{(\Delta B_Q)^2 + (\Delta B_U)^2} = \Delta T_{ND} M_{CP}^B} \tag{D.17}$$

3. **Polarization angle.**

$$\boxed{\theta_C^B = -arctan\left(\frac{\Delta B_U}{\Delta B_Q}\right)} \tag{D.18}$$

D.1.1.1 Noise diodes corrected data

We can filter bad values of m_L, m_R, m_p and θ_C, for horns A and B, and interpolated to apply the instrumental correction to any set of data.

We get corrected Stokes Q and U values, for horns Ant and Ref, by

$$\begin{bmatrix} Q^c \\ U^c \end{bmatrix} = \frac{1}{m_p}\begin{bmatrix} cos(\theta_C) & -sin(\theta_C) \\ sin(\theta_C) & cos(\theta_C) \end{bmatrix}\begin{bmatrix} \Delta Q \\ \Delta U \end{bmatrix} = \frac{1}{m_p}\begin{bmatrix} cos(\theta_C)\Delta Q - sin(\theta_C)\Delta U \\ sin(\theta_C)\Delta Q + cos(\theta_C)\Delta U \end{bmatrix} \tag{D.19}$$

Thus, the instrumentally-corrected values, for horns Ant and Ref, can be get by

1. **Horn Ant**

   (a) **Intensity signal for polarization LCP.**

$$A_L^c = \frac{\Delta A_L}{m_L^A} \tag{D.20}$$

   (b) **Intensity signal for polarization RCP.**

$$A_R^c = \frac{\Delta A_R}{m_R^A} \tag{D.21}$$

   (c) **Corrected Stokes Q.**

$$A_Q^c = \frac{1}{m_p}[cos(\theta_C)\Delta A_Q - sin(\theta_C)\Delta A_U] \tag{D.22}$$

   (d) **Corrected Stokes U.**

$$A_U^c = \frac{1}{m_p}[sin(\theta_C)\Delta A_Q + cos(\theta_C)\Delta A_U] \tag{D.23}$$

2. **Horn Ref**

   (a) **Intensity signal for polarization LCP.**

$$B_L^c = \frac{\Delta B_L}{m_L^B} \tag{D.24}$$

(b) **Intensity signal for polarization RCP.**

$$B_L^c = \frac{\Delta B_L}{m_L^B} \tag{D.25}$$

(c) **Corrected Stokes Q.**

$$B_Q^c = \frac{1}{m_p}[cos(\theta_C)\Delta B_Q - sin(\theta_C)\Delta B_U] \tag{D.26}$$

(d) **Corrected Stokes U.**

$$B_U^c = \frac{1}{m_p}[sin(\theta_C)\Delta B_Q + cos(\theta_C)\Delta B_U] \tag{D.27}$$

Now, if we use D.20 to D.27 expressions and the Stokes parameters relation on circular basis, we can form the *instrument-corrected data streams for horns Ant and Ref*, as

$$e^{A0} = \begin{bmatrix} A_L^c + A_R^c \\ A_Q^c \\ A_U^c \\ A_L^c - A_R^c \end{bmatrix} = \frac{1}{\Delta T_{ND}} M_A e^S \tag{D.28}$$

$$e^{B0} = \begin{bmatrix} B_L^c + B_R^c \\ B_Q^c \\ B_U^c \\ B_L^c - B_R^c \end{bmatrix} = \frac{1}{\Delta T_{ND}} M_B e^S \tag{D.29}$$